COMPETITION-INDUCED SELECTION OF LIGANDS FOR THE SCREENING OF DNA APTAMERS FOR GOLD SUBSTRATES

A Dissertation
Presented to
The Academic Faculty

By

Maeling Janelle Nicole Tapp

In Partial Fulfillment
Of the Requirements for the Degree
Doctor of Philosophy in the
School of Materials Science & Engineering

Georgia Institute of Technology

May 2015

COMPETITION-INDUCED SELECTION OF LIGANDS FOR THE IDENTIFICATION OF DNA APTAMERS FOR GOLD SUBSTRATES

Approved by:

Dr. Valeria T. Milam, Advisor
School of Materials Science and Engineering
Georgia Institute of Technology

Dr. Kenneth H. Sandhage
School of Materials Science and Engineering
Georgia Institute of Technology

Dr. Christopher J. Summers
School of Materials Science and Engineering
Georgia Institute of Technology

Dr. Vladimir V. Tsukruk
School of Materials Science and Engineering
Georgia Institute of Technology

Dr. Philip J. Santangelo
Wallace H. Coulter Department of Biomedical Engineering
Georgia Institute of Technology

Dr. Rajesh R. Naik
Air Force Research Laboratory,
Materials & Manufacturing Directorate,
Soft Matter Materials Branch
Wright Patterson AFB

Date Approved: December 19, 2014

Dedicated to my loving husband and parents

ACKNOWLEDGMENTS

I would like to express my sincere gratitude to my advisor, Dr. Valeria Milam for helping to make my graduate experience at Georgia Tech such a positive and meaningful one. From her guidance in my summer research experience abroad as a participant in the MSE SURF program before I started my first graduate semester to the preparation of this dissertation, she has been a tremendous source of inspiration, encouragement and knowledge. Her cheerful willingness while dedicating so much of her time to help me succeed in my academic pursuits is something I will always value and remember. I am extremely grateful to her for the opportunity to join her lab and the many learning experiences along the way that have made me a better scientist and engineer. I would also like to thank the MSE chair, Dr. Naresh Thadhani, for taking the time to speak with me about the MSE department at a conference during my undergraduate years, which ultimately led me to apply to Georgia Tech for my graduate studies. Thank you to Dr. Kenneth Sandhage, Dr. Christopher Summers, Dr. Philip Santangelo, Dr. Vladimir Tsukruk and Dr. Rajesh Naik for their willingness to serve on my dissertation committee and for providing their helpful feedback.

I thank my colleague, Rick Sullivan in the Milam lab for his upbeat attitude and for always being willing to lend a helping hand, whether it was discussing new research ideas or troubleshooting equipment in the lab. He helped to provide a positive and fruitful working environment, for which I am very grateful. I would also like to thank past group

members for their support and guidance: Blake Dunaway, Ngozi Eze, Bryan Baker and James Hardin. A special thank you to Susan Bowman, Jasmin Frett-Hodge and Mechelle Kitchings for helping me with numerous administrative tasks over the years to help everything run smoothly in my academic studies and in the lab. I would also like to thank Dr. Vonda Sheppard-Smith, formerly of the Kröger lab, for training me on bacterial transformation and agarose gel electrophoresis techniques. Thank you to Sidney Malak of the Tsukruk lab for his SEM analysis of my planar gold substrates. I would also like to thank my undergraduate mentors at the University of Maryland whose continued support and encouragement while at Georgia Tech has been truly cherished: MSE chair Dr. Robert Briber, Dr. Paige Smith and Dr. Kathleen Hart.

Our collaborators at the Air Force Research Laboratory were vital to my research progress. I would like to thank Dr. Rajesh Naik for his valuable input and allowing me the opportunity to spend several months learning in the Soft Matter Materials Branch over the course of my graduate tenure as a participant in the BIONIC program. I would especially like to thank Dr. Patrick Dennis for spending many hours training me on the many biological techniques that were used in this study and for his assistance in troubleshooting issues along the way. Thank you to Sharon Jones for her assistance in arranging my visits to AFRL. Thank you to Peter Mirau for his suggestion of using an aptamer he was investigating, which was very useful in troubleshooting and optimizing our CISL aptamer screening process during its development. Thank you to Kristi Singh for her AFM analysis of the planar gold substrates discussed in Chapter 6.

Finally, I would like to thank my amazing support system of family and friends whose love and encouragement has sustained me on this character-building journey. Thank you to my sisters for your impromptu visits to Atlanta that would always brighten my weekend. To my dad, thank you for your “right-on-time” words of wisdom. You always knew exactly what I needed to hear to keep me pushing forward. To my mother, your daily prayers and listening ear meant so much to me and helped me to keep things in perspective. To my husband, thank you for your undying love, patience and understanding throughout this journey. Having you by my side through this has meant everything to me. To my son, although we haven’t met face to face yet, witnessing your tiny flutters turn into full-fledged kicks while writing this dissertation has brought me much-needed smiles and laughs.

TABLE OF CONTENTS

LIST OF TABLES

LIST OF FIGURES

LIST OF SYMBOLS AND ABBREVIATIONS

DNA	deoxyribonucleic acid
ssDNA	single-stranded deoxyribonucleic acid
dsDNA	double-stranded deoxyribonucleic acid
SELEX	Systematic Evolution of Ligands by EXponential enrichment
PCR	polymerase chain reaction
A	adenine
T	thymine
C	cytosine
G	guanine
dNTP	deoxynucleotide triphosphate
dATP	deoxyadenosine triphosphate
dCTP	deoxycytidine triphosphate
dGTP	deoxyguanosine triphosphate
dTTP	deoxythymidine triphosphate
NTP	nucleoside triphosphate
ATP	adenosine triphosphate
CTP	cytidine triphosphate
GTP	guanosine triphosphate
UTP	uridine triphosphate
dNMP	deoxynucleoside monophosphate
dAMP	deoxyadenosine monophosphate
dCMP	deoxycytidine monophosphate
dGMP	deoxyguanosine monophosphate
dTMP	deoxythymidine monophosphate

Au	gold
AuNP	gold nanoparticle
PlanarAu	planar gold
RNA	ribonucleic acid
Exo I	Exonuclease I
LE	Lambda Exonuclease
PAGE	polyacrylamide gel electrophoresis
CTAB	cetyl trimethylammonium bromide
TEM	transmission electron microscopy
UV-Vis	ultraviolet-visible spectroscopy
CISL	Competition-Induced Selection of Ligands
AFM	atomic force microscopy
SEM	scanning electron microscopy
EDS	energy dispersive spectroscopy
NGS	Next Generation Sequencing

SUMMARY

This dissertation presents the development of an alternative aptamer screening process, Competition-Induced Selection of Ligands (CISL), and its use in screening for ssDNA aptamers for gold substrates. Gold substrates are presented as the nonnucleotide target for implementing CISL as a novel aptamer screening approach. Chapter 1 provides an overview of the *in vitro* selection of oligonucleotide aptamers, the polymerase chain reaction that is a key step in the aptamer screening process, the synthesis and properties of gold nanoparticles and the biomolecule-mediated formation of inorganic nanoparticles. Chapter 2 presents the goals and objectives of this thesis along with an organizational overview of the dissertation. Chapter 3 describes the experimental techniques and optimizations pertinent to the development of the CISL aptamer screening process. Chapter 4 investigates the effects of various nucleic acid additions during the seed-mediated growth of gold nanoparticles. Chapter 5 discusses the use of CISL in screening for ssDNA aptamer candidates for spherical gold nanoparticles (AuNPs) and the primary and secondary structure analysis of identified sequences. Chapter 6 presents the use of CISL in screening for ssDNA aptamer candidates for planar gold substrates (PlanarAu) and also includes primary and secondary structure analysis of identified sequences accompanied with an incubation study to provide a "frequency" ranking of aptamers as adsorbate species on PlanarAu. Chapter 7 offers concluding remarks and ideas for future expansion and applications of this work.

CHAPTER 1

INTRODUCTION

1.1 Introduction to Aptamers

Aptamers are single-stranded (ss) oligonucleotide sequences (DNA or RNA) that are characterized by their high affinity and specificity binding to their particular non-nucleotide targets. Using *in vitro* selection processes, aptamers have been identified for a wide variety of targets including but not limited to ions, small molecules, proteins and even whole cells.[1-7] Often treated as nucleic acid analogues to antibodies, the reported dissociation constants for aptamers typically fall within the micromolar to picomolar range.[8] As biomacromolecular ligands, however, aptamers offer several advantages over antibodies. Since aptamers are derived from synthetic libraries of DNA or RNA, their synthesis is well controlled and allows for easy chemical modifications at the sequence ends or within sequence backbone or base groups. The use of a synthetic library also enables an *in vitro* aptamer selection process that offers low costs and high reproducibility that is difficult to achieve in the animal-based generation of antibodies.[9] Aptamers also exhibit enhanced shelf life and stability when exposed to variations in temperature and solvent conditions.[9] These characteristics of aptamers have motivated research for their use in biosensing, therapeutics, cell tracking and diagnostic applications.[10-14]

Despite aptamers being identified for an array of targets, the nature of these aptamer-target binding interactions is not always well understood. Generally, the interactions are thought to be governed by a combination of van der Waals, hydrogen bonding, salt

bridges, hydrophobic or electrostatic interactions.[15] To date, only a few aptamers for targets including cocaine and theophylline have been thoroughly investigated as it relates to understanding the relationship between the aptamer structure and the binding affinity for its target.[16-19] Where initially, aptamers were thought to have a "lock-and-key" relationship with their target, more in-depth analysis has revealed that aptamers can bind to their target under various mechanisms such as conformational selection and induced fit models.[15, 20] These mechanisms are discussed in more detail in Chapter 5.

1.2 *In vitro* Selection of Aptamers

The idea of an *in vitro* selection process for the identification of nucleic acid ligands that exhibit binding for specific molecular targets is attributed to three separate groups that all published in 1990.[21] Robertson and Joyce used an *in vitro* selection process to identify variants of the *Tetrahymena* ribozyme that would cleave single-stranded DNA more efficiently than the wild type form of the enzyme.[22] Through repeated rounds of *in vitro* mutagenesis and selective amplification, they identified the first RNA sequence to be generated *in vitro* for the cleavage of single-stranded DNA specifically. Tuerk and Gold demonstrated that by randomizing an eight-base region of RNA that was known to bind to the bacteriophage T4 DNA polymerase followed by repeated rounds of selection and replication, that a new RNA sequence could be identified that exhibited improved binding affinity to the polymerase.[23] It was in this report that Tuerk and Gold coined the term 'Systematic Evolution of Ligands by Exponential Enrichment' (SELEX). In the same year, Ellington and Szostak reported their *in vitro* selection process for the selection of an RNA sequence from a completely randomized starting library of RNA that was found to exhibit high affinity binding to select organic dyes.[24] In this publication they

coined the term 'aptamers' from the Latin '*aptus*' to fit, to describe the RNA species they identified to have high specificity binding for the dyes. Since these reports over two decades ago, the SELEX process using a starting library of randomized oligonucleotides has become the conventional approach for the identification of high affinity single-stranded nucleic acid ligands, referred to as aptamers.

The conventional SELEX process begins with a large starting library of generally 10^{12}-10^{15} randomized single-stranded oligonucleotide sequences.[20, 25, 26] Template molecules are typically designed to have three main regions: an inner sequence of ~ 16-75 random nucleotides, and two constant sequence regions at both the 5'- and 3'- ends of the oligonucleotide.[27] These constant regions at both ends of the template sequence facilitate intermittent amplification steps in the process. For example, primers are designed to be complementary to these constant regions. Hybridization of the primers to these regions is necessary for amplification of the selected sequences during the polymerase chain reaction (PCR). These constant regions can also later be used to incorporate restriction enzyme sites that aid in the insertion of random regions of identified aptamers into the multi-cloning site of a bacterial vector for sequencing of the aptamer.[27] In the case of selection for RNA aptamers, a T7-promoter site must be incorporated in one of the constant regions of the template DNA to allow for transcription to RNA during PCR.

When selecting for DNA aptamers, the starting pool of random single-stranded DNA can be used directly. However, for the selection of RNA aptamers, it is necessary to first transcribe the DNA to RNA *in vitro*, using T7-RNA polymerase.[27, 28] DNA libraries have been useful for applications in which the chemical stability of oligonucleotides is

necessary, for biosensing, therapeutics and environmental monitoring.[26] This enhanced chemical stability is attributed to the absence in DNA of a 2'-hydroxyl on its sugar moiety, conferring more resistance to hydrolysis under alkaline pH and elevated temperature conditions compared to RNA.[29] However, in other cases, selection from RNA libraries tends to yield aptamers with higher affinities to their target due to RNA's ability to assume a wider variety of conformations compared to DNA.[26]

Where appropriate, a counter-SELEX step can precede the initial incubation step with the desired target in order to remove any sequences from the library that bind to non-targeted species such as the walls of the reaction vessels, impurities or other species that may be co-present with the desired target in the intended application (e.g. normal cells vs. targeted cancer cells).[6] During the incubation step, the pool of unique, randomized sequences is allowed to equilibrate with the specified target under buffer and temperature conditions that are favorable for binding (Figure 1.2.1). Following incubation, the next step of SELEX is partitioning, in which sequences that bind to the target are separated from unbound sequences using various separation and purification techniques that include but are not limited to the use of nitro-cellulose filter adsorption, magnetic beads, gel-shift separation and capillary electrophoresis.[12, 26, 27] The bound sequences are then eluted and amplified, in order to enrich the pool with sequences that bind to the target with high affinity. The RNA or DNA molecules eluted from the target are collected and amplified via reverse transcription - polymerase chain reaction (RT-PCR) or PCR, respectively.

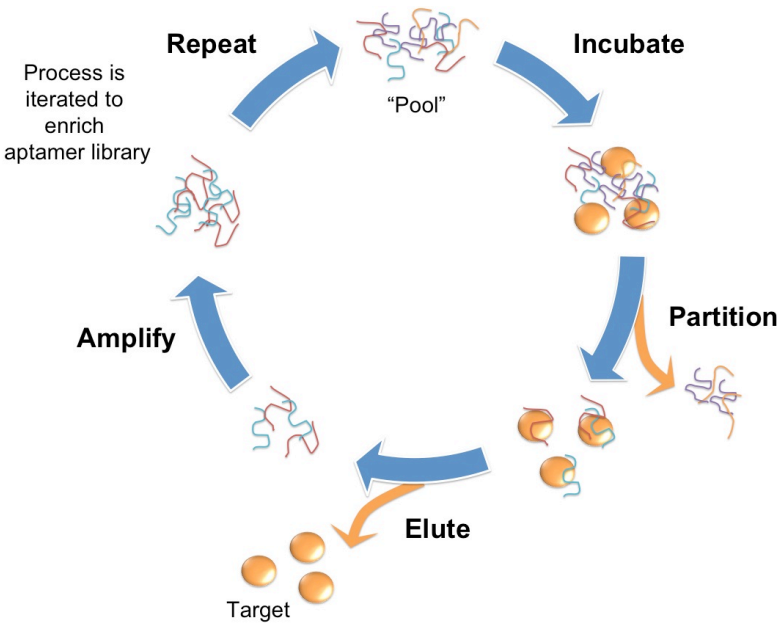

Figure 1.2.1. Schematic of the basic steps of the SELEX process, which consists of (1) incubation of a random nucleotide pool with the target (2) partitioning of the strands bound to the target from unbound strands (3) elution of the bound strands from the target surface and (4) amplification of the bound strands for use in the next cycle of the SELEX process. This process is iterated multiple times to enrich the pool of high affinity aptamers to the target. Adapted from Bouchard *et al*.[12]

This selection process is repeated iteratively since a single round of selection will initially only yield a small number of high affinity sequences from the pool. After multiple rounds of target-pool incubation, partitioning followed by repeated recovery and amplification of bound species, aptamers that survive this multi-round process are ultimately recovered, purified and sequenced.[10, 27] Depending on the nature of the target (e.g. immobilized molecules vs. soluble macromolecule) and the stringency of the solution conditions used during selection, this iterative selection process can involve between 7-15 rounds and can thus span the course of 2-3 months.[6, 9]

Post-SELEX processing and optimization can include identification of the minimal base segments and and/or structures of the aptamers that lead to high affinity binding. These conserved base segments within the random base segment are known as consensus motifs, and are often located in the stem-loop structures thought to mediate binding specificity.[27] Importantly, these consensus motifs should not be confused with primer-binding segments that are intentionally conserved. Variations of the basic SELEX procedure described do exist and include alternative methods for how the target is presented to the oligonucleotide pool (i.e. immobilized vs. free in solution), and how the target-complexes are partitioned and separated.[20, 26] In some instances, SELEX is carried out using a library of sequences with modified nucleotides in order to enhance nuclease resistance, increase binding affinity or to generate more stable aptamer secondary structures.[29-31] In a few studies, the SELEX protocol has even been abandoned for the adoption of an aptamer screening process that eliminates the repeated PCR amplification steps in between repeated partitioning steps that are characteristic to the conventional approach.[32-34] The benefits of these stated modifications is discussed in more detail in Chapter 5.

1.3 Introduction to Nucleic Acids

Nucleic acids can be described as chains of nucleotide-based units, which are comprised of nucleobases that are covalently linked together by phosphodiester bonds (Figure 1.3.1). The physico-chemical properties of these nucleic acids depend upon the composition of nucleotides (e.g. DNA vs. RNA) and their sequence (i.e. linear order of bases) also known as primary structure.[35]

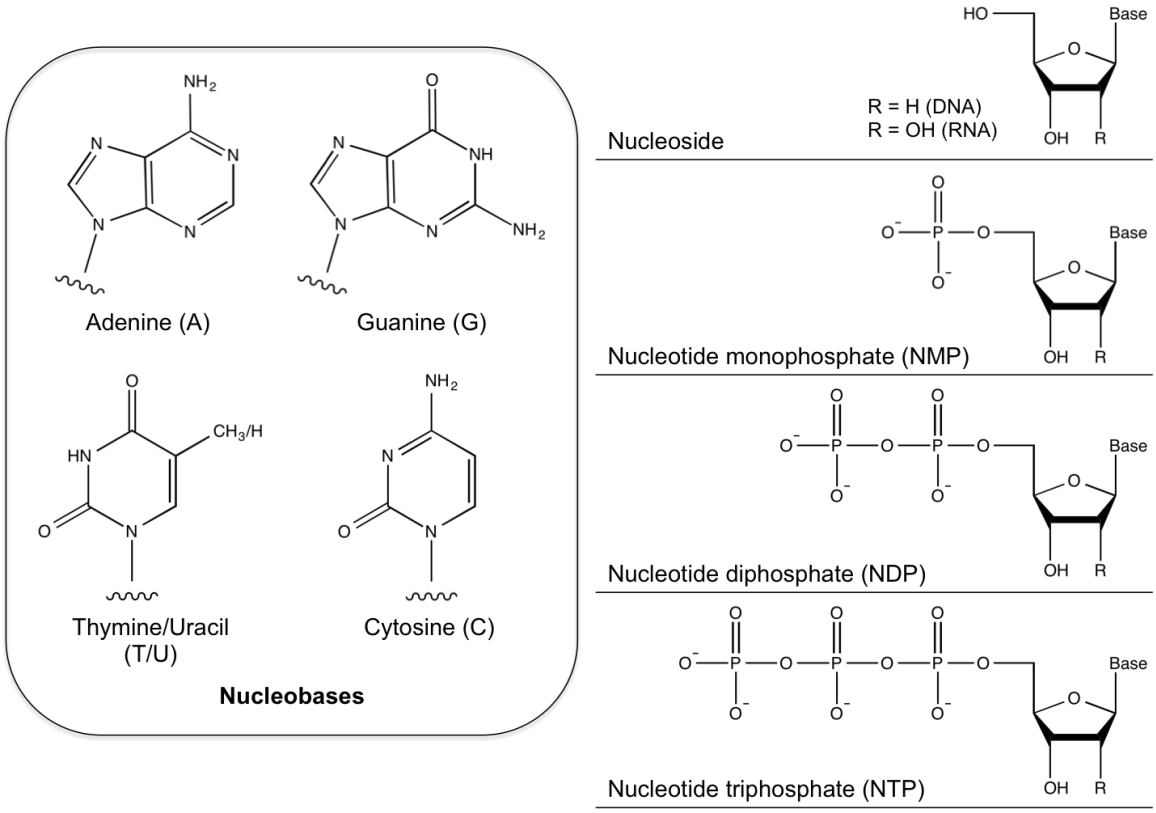

Figure 1.3.1. Nucleosides consist of a nucleobase [(A) Adenine, (G) Guanine, (T) Thymine, (U) Uracil, (C) Cytosine)] and a ribose (for RNA) or a 2'-deoxyribose (for DNA) sugar ring.

In living organisms, deoxyribonucleic acid (DNA) is the source of encoded genetic information in the cell and has a double helical structure. The double helix is maintained by the formation of hydrogen bonds between the bases of the two polynucleotide strands. Each strand of DNA is comprised of a specific ordering of the nucleobases (adenine (A), guanine (G), thymine (T) or cytosine (C)). The hydrogen bonds formed between the two complementary strands that create the duplex are governed by base pairings that are generally described by Watson-Crick base pairing (A with T and G with C) as shown in Figure 1.3.2. Although these are the most abundant base pairs in DNA, mismatched base pairs can occur in some instances as well.[36] In contrast to the double-stranded duplex

anticipated as the only secondary structure for two perfectly-matched DNA strands, these base pairings can also occur within single strands of DNA, where these interactions can form unique intrastrand secondary structures due to self-hybridization. Due to advancements in chemical syntheses, synthetic DNA can easily be produced via solid-phase DNA synthesis that allows for the tailoring of DNA sequence and length to explore a rich variety of intrastrand structures for a range of biotechnology applications.

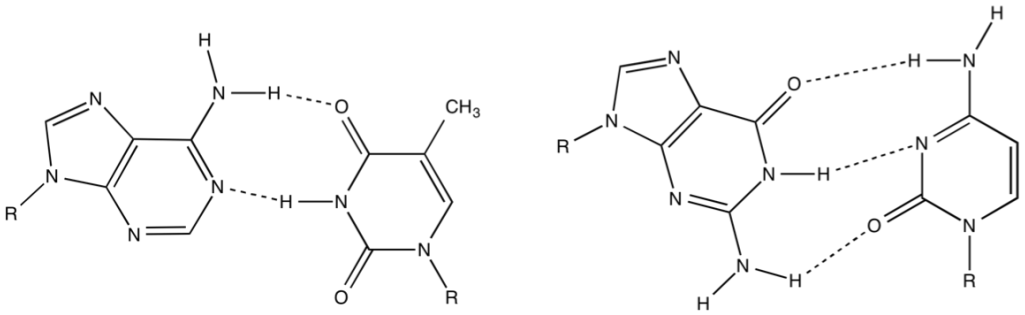

Figure 1.3.2. The two Watson-Crick base pairs.

1.4 Gold Nanoparticles Synthesis, Properties and Applications

Metal nanoparticles have been heavily studied throughout the years due to their size- and shape- dependent properties, particularly in the nanometer regime.[37] Since the formation of gold colloids reported by Faraday more than 100 years ago, much research has been dedicated to the study of the synthesis, properties and potential applications of gold nanoparticles.[38] Gold nanoparticles (AuNPs) are of great technological interest due to their unique size and shape-dependent optical properties such as localized surface plasmon resonance (LSPR).[38] The enhanced LSPR effects of gold nanoparticles stem from their scattering and absorption of visible light. These effects are apparent in the

variation of optical spectra that gold nanoparticles exhibit for different sizes and shapes ranging from spheres (strong extinction at ~520 nm) to nanorods (longitudinal plasmon bands at 600-1600 nm).[39-41]

The reason that AuNPs exhibit strong absorption and scattering of visible and near-infrared light can be explained by the coherent, collective oscillation of plasmons (conduction band electrons) in the particles when illuminated with light.[39] Aggregation of AuNPs can also tune the wavelength of the plasmon bands.[42-45] AuNP surfaces can additionally be modified to incorporate other moieties, such as oligonucleotides, proteins and antibodies due to their strong bonding to thiols, disulfides, phosphines and amines.[45-48] Gold nanoparticles are increasingly being used in a number of applications that involve DNA-functionalization of the gold surfaces for applications including colorimetric detection assays, cell-targeting for therapeutics and nanoscale directed assemblies.[45, 49-56] This demand for gold-based substrates has merited the need for further investigation into the nature of nucleic acid interactions with gold surfaces. Several studies have indicated that the affinities of nucleic acids for gold surfaces are affected by both base content and structure of the DNA (ssDNA vs. dsDNA).[46, 52, 57-60] These gold-DNA interactions will be discussed in more detail in Chapter 4.

AuNPs can be prepared using chemical, sonochemical or photochemical paths.[61, 62] However, AuNPs are most commonly synthesized through aqueous reduction of Au (III) derivatives.[47, 63] The citrate reduction method is the most widely used for the synthesis of spherical gold nanoparticles due to its simplicity as a procedure that yields stable and

reproducible monodisperse gold colloids.[47, 48] This method was pioneered by Turkevich *et al.* to synthesize 20-nm AuNPs by reducing chloroauric acid ($HAuCl_4$) with trisodium citrate ($Na_3C_6H_5O_7$).[64] This technique was further refined by Frens *et al.* to yield AuNPs of a variety of sizes by changing the relative concentrations of the chloroauric acid and trisodium citrate in the reaction.[65] Spherical AuNPs can also be synthesized using a seed-mediated approach, using CTAB as a stabilizing surfactant.[66, 67] In addition to forming spherical AuNPs, the gold nanoparticle seed used in this approach can also be used in conjunction with a growth solution to synthesize gold nanorods as shown in Figure 1.4.1.[66] This is the method that was used for the synthesis of AuNPs for the studies presented in this dissertation.

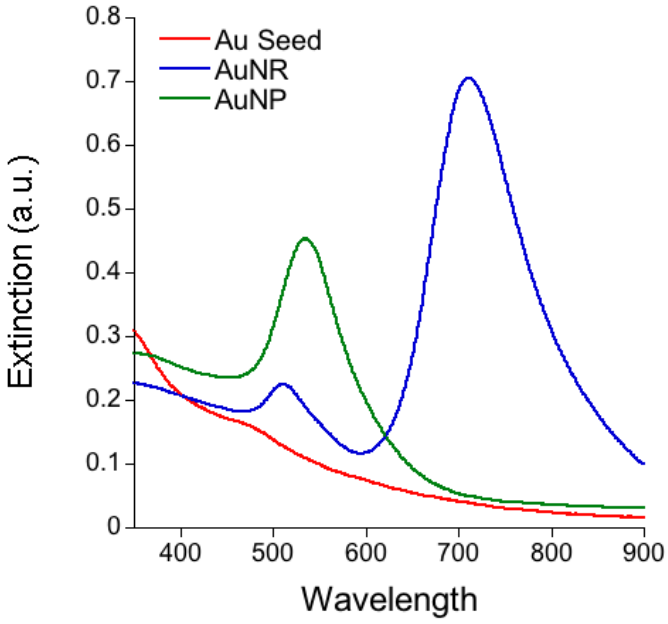

Figure 1.4.1. Representative extinction spectra from seed-mediated syntheses of spherical gold nanoparticles (AuNP) and gold nanorods (AuNR). The same Au seed was used to synthesize both AuNP and AuNR. Gold nanoparticles were synthesized according to the methods reported by Nikoobakht *et al.*[66]

Since the properties of AuNPs are strongly dictated by their size and shape, depending on the application it can be vital to choose a synthesis method that yields a high level of control of these features. Some approaches for controlling the shape and size of nanoparticles employ the use of capping agents such as surfactants, polymers, dendrimers and ligands to control growth. One synthesis method that has achieved success in shape control has been the use of templates, such as porous alumina, carbon nanotubes, polycarbonate membranes and micelles.[37, 68, 69] Templates act to constrain the growth of the nanoparticles, thereby tuning their shape in relation to the template itself.[37] Additionally, limited studies have examined the use of biomolecules to mediate the formation and shape of inorganic nanoparticles.[70-75]

1.5 Biomolecule-mediated Formation of Inorganic Nanoparticles

The physico-chemical properties of inorganic nanoparticles are highly size- and shape-dependent, resulting in the need to have their dimensions and dispersity controlled during synthesis. Although current synthesis methods ultimately yield fairly monodisperse populations, initial yields are often polydisperse populations that must be further separated to isolate the desired size range.[35] Looking to nature, the process of biomineralization has provided motivation for the use of biomolecules in the laboratory to assist in synthesizing and assembling materials.[70, 76, 77] Biomineralization is a natural process, by which living organisms can excrete inorganic materials in a manner that is guided by biological processes.[35] Mimicking the processes of biomineralization, biomolecules, such as proteins and peptides, have been shown to mediate the formation of inorganic nanoparticles in a controlled manner in laboratory settings.[70, 73, 78]

In a number of studies conducted by Sandhage *et al*., they employed the use of a combinatorial peptide display library to help identify peptides that exhibited strong binding to inorganic materials.[74, 75, 79] The goal of their studies was to use identified peptides to help promote the precipitation of inorganic nanoparticles. Using a "subtractive bacteriophage biopanning process", they were able to identify a select number of unique peptide sequences that bound and precipitated titania exclusively and not silica, which is a chemically similar oxide.[79] In a study conducted by Dickerson *et al*., rounds of selective panning were used to identify peptides that exhibited strong binding to germania.[75] By incubating these peptides in a germanium alkoxide-bearing solution at room temperature, they discovered that a select number of their most dominant peptides from selection could induce precipitation of germania nanoparticle networks. Peptides have also been discovered that are able to induce the precipitation of crystalline calcium molybdate phosphor microparticles, CdS nanoparticles, CoPt nanoparticles and a number of other inorganic materials.[73, 74, 80, 81]

In more recent studies, nucleic acids have been explored for use as templates for inorganic nanoparticle formation[35, 82-86]. In a series of studies conducted by Feldheim & Eaton and coworkers, researchers were able to identify RNA sequences that catalyzed the shape-controlled synthesis of palladium (Pd) particles using trisdibenzylideneacetone [$Pd_2(DBA)_3$] as a precursor complex.[76, 82, 87, 88] Using an *in vitro selection* process, distinct RNA sequences that were reported to help mediate the formation of both hexagonal and cubic Pd nanoparticles were identified. Using RNA to mediate the process,

the Pd nanoparticles were prepared under aqueous conditions, ambient temperature and with no need for an endogenous reducing agent.[82] In later studies, they also showed that the RNA sequences could be covalently attached to solid wafers in line or spot patterns using microcontact printing and still maintain their ability to be active in mediating Pd particle growth.[88]

Kelley *et al.* explored the use of transfer RNA (tRNA) as a template for the formation of CdS nanoparticles.[77] Using two different types of tRNA (folded wild type tRNA [WT tRNA] and unfolded mutant RNA [MT tRNA]), they discovered that both types of tRNA were able to mediate the precipitation of CdS from solution. It was noted that the average nanocrystal size and distribution was specific to the type of tRNA used, with CdS products synthesized in the presence of MT tRNA typically exhibiting a larger average size and a greater size dispersity.[77] Other studies conducted by the same group investigated using nucleic acids and nucleotides to stabilize CdS NPs. The ability of 5'-guanosine triphosphate to stabilize CdS NPs in their studies was attributed to the N7 electrons and pendant triphosphates as controlling factors in regulating the rate of nanocrystal formation.[89] RNA has also been studied for the mediation of iron oxide NPs and PbS quantum dots.[71, 90] Wang *et al.* has more recently investigated the effects of varying DNA sequence on the templated formation of gold nanoparticles in a seed-mediated approach that is discussed in Chapter 4.[91, 92]

Although a general model for nucleic acid/nucleotide-templated growth has not been established, a proposed mechanism has been developed which follows the general mechanism for nanoparticle formation and findings presented by Hinds *et al*.[72, 93, 94] The process begins with initiation, in which the nucleic acids/nucleotides bind to metal cations. This binding forms a nanoparticle precursor and initiates the nucleation event.[72] In the growth step, the nucleic acid/nucleotide molecules coat the small clusters formed during initiation with a negatively charged layer (capping). The thermodynamically favorable tendency towards cluster aggregation is counterbalanced by the negatively charged layer formed from the nucleic acids/nucleotides that must be overcome in order for aggregation to occur. Clusters reach a critical size and terminate growth once the magnitude of the electrostatic barrier becomes too large to overcome resulting in prevention of further aggregation and growth of the particles.

The nucleic acid/nucleotide-capping layer also serves to passivate the particles by minimizing defect states on the particle surface by saturating empty orbitals and dangling bonds. This passivation process also improves the physico-chemical properties of the particles. The nucleic acid/nucleotide molecules act to solubilize the NPs, helping them to remain homogeneously dispersed in an aqueous solution.[93] Though this model provides useful insight into biomolecule-mediated nanoparticle formation, it is clear that developing further understanding of how oligonucleotide sequence, composition, length and concentration affect nanoparticle synthesis is necessary to establishing a controllable and systematically modifiable synthesis process.

CHAPTER 2

RESEARCH GOALS, OBJECTIVES AND OVERVIEW

2.1 Goals

The goal of this research is to understand the interactions between DNA sequences and gold surfaces with the aim of developing a selection protocol that identifies ssDNA sequences that exhibit strong, but non-covalent binding to gold surfaces. The objective is to identify aptamer candidate sequences from a random single-stranded DNA (ssDNA) library that bind to spherical gold nanoparticles and planar gold surfaces and to develop a characterization scheme that highlights the sequence-gold interactions stemming from the primary structure and (predicted) secondary structure of the ssDNA.

2.2 Technical Objectives

The technical objectives of this study are summarized as follows:

1. Investigate the effects of nucleic acids on the seed-mediated growth of spherical gold nanoparticles through incubation studies that evaluate the base-specific and structure-specific effects of these nucleic acid additions through UV-Vis spectroscopy and TEM analysis.
2. Optimize the polymerase chain reaction for the amplification of a random ssDNA library to be used in the aptamer screening process.
3. Develop and optimize an aptamer screening process that identifies ssDNA sequences that bind to spherical gold nanoparticles and planar gold surfaces and minimizes errors in ssDNA library generation due to PCR amplification.

4. Develop a scheme for correlating primary and predicted secondary structure similarities across identified aptamer sequences to elucidate the nature of aptamer-gold binding.

2.3 Organization and composition of dissertation

Chapter 1 provides a critical review of foundational and current techniques related to the *in vitro* selection of oligonucleotide aptamers. In addition, this chapter gives an overview of aptamers and their target interactions and applications. One of the key techniques used in the aptamer screening process, the polymerase chain reaction, will also be described in detail. Since the nonnucleotide target of interest in the presented research is gold nanoparticles, background on gold nanoparticle synthesis, properties, applications and their interactions with nucleic acids is also provided. Finally, since select studies also investigated aptamer as well as non-aptamer sequence effects on gold seeded-mediated nanoparticle growth, relevant literature on biomolecule-mediated formation of inorganic nanoparticles is also covered.

Chapter 2 details the goals and technical objectives of this research. Furthermore, this chapter provides an organizational overview of the dissertation with a brief synopsis of each chapter.

Chapter 3 describes the experimental techniques and optimizations pertinent to the studies presented in this dissertation. It includes the synthesis of the gold nanoparticles used in this study along with characterization techniques, including UV-Vis spectroscopy

and transmission electron microscopy. Characterization of the planar gold substrates used in this study are detailed, including SEM (with EDS) and XRD. This chapter also covers the methods used to characterize and analyze the DNA used in this study including gel electrophoresis to determine molecular weight of the DNA, spectrophotometry to evaluate DNA concentration and purity, flow cytometry to measure duplex densities on bead surfaces, as well as a variety of primary and secondary structure characterization techniques. Finally, the development and optimization of the aptamer screening process (Competition-Induced Selection of Ligands (CISL)) is presented.

Chapter 4 investigates the effects of adding various nucleic acids to gold seeds during the growth stage of nanospheres using UV-Vis spectroscopy to reveal any oligonucleotide base or structure-specific effects on plasmonic signatures. Spectral data indicate that the presence of DNA duplexes during seed ageing drastically accelerated nanosphere growth while the addition of single-stranded polyadenine at any point during seed ageing induces nanosphere aggregation. Monomeric forms of the nucleic acids, however, do not yield discernable spectral differences in any of the gold suspensions studied.

Chapter 5 demonstrates the use of the developed Competition-Induced Selection of Ligands (CISL) approach to identify ssDNA aptamer candidates for spherical gold nanoparticles (AuNPs). This approach differs from conventional SELEX-based approaches by eliminating repeated elution and PCR amplification steps of bound candidate sequences between each round of selection to continually enrich the candidate

aptamer pool with prior adsorbate species. Instead, a new pool of unenriched oligonucleotides is adding during each incubation round to compete with the existing adsorbate species. In this study, 24 aptamer candidates for AuNPs were identified using the CISL approach and then compared to reveal similarities in their primary structures and their predicted secondary structures. Consensus in individual bases (position-dependent) and segments of bases (independent of position) were not prevalent among the identified sequences. Shared motifs, on the other hand, were present in subgroups of seemingly unrelated sequences as revealed by a systematic classification and enumeration of distinct secondary structure features including hairpins, duplex regions, single-stranded segments, interior loops, bulges and multi-branched loops.

Chapter 6 demonstrates the use of the CISL aptamer screening process to identify ssDNA aptamer candidates for planar gold (PlanarAu) surfaces. In this study, 25 aptamer sequences for PlanarAu were identified using the CISL approach and then classified according to similarities in their primary structures and predicted secondary structures. Similar to the results in Chapter 5, consensus in individual, position-dependent bases were not prevalent; however, shared secondary structure feature motifs were revealed. An "ultimate" incubation study involving simultaneous exposure of the PlanarAu substrate with all 25 identified aptamer candidates provided a possible ranking of relative binding affinities arising from corresponding next generation sequencing analysis.

Chapter 7 offers general conclusions for the research presented in this dissertation and also discusses the significance of this work and its potential for broader impact.

CHAPTER 3

EXPERIMENTAL DETAILS

3.1 Gold Nanoparticle Synthesis and Characterization

3.1.1 Synthesis of gold nanoparticles (AuNPs)

The gold nanoparticles used in this research were synthesized using a seed-mediated method reported by Nikoobakht *et al.*[66] The synthesis begins with the preparation of a gold nanoparticle seed solution. To prepare the seed solution, a 0.2 M CTAB solution is mixed with a 0.5 mM gold (III) chloride trihydrate ($HAuCl_4 \bullet 3H_2O$) solution and mixed on a stir plate for at least 30 min. The CTAB in this reaction is a surfactant that serves to stabilize the final gold nanoparticle suspension. This mixture produces a solution that is dark orange in color. The next step involves the addition of chilled 0.01 M sodium borohydride ($NaBH_4$) to the mixture with continued stirring for an additional 2 min. The sodium borohydride acts as the reducing agent to reduce the Au^{3+} ions to Au^0. This final solution appears light brown in color and corresponds to the gold nanoparticle seed solution. Gold nanospheres were prepared by aging the gold nanoparticle seed solution under mixing on a rotomixer. During this aging process, the solution color changes over time from light brown to reddish in color.

3.1.2 UV-Vis spectroscopy of AuNPs

UV-Vis spectroscopy was used to characterize the spectral behavior of the gold nanoparticles used in the presented studies. Due to the localized surface plasmon resonance (LSPR) behavior exhibited by AuNPs, an extinction spectrum is produced that is affected by the size, shape and aggregation of the AuNPs.[95] The LSPR of AuNPs produces a strong absorbance band in the visible region (500 nm - 600 nm), which allows

for detection by UV-Vis. UV-Vis analysis was conducted on a Biotek Synergy H1 Hybrid Reader with a sweeping scan at a 1 nm wavelength resolution.

Figure 3.1.1 shows the evolution of the UV-Vis spectra at various timepoints throughout the gold seed aging process. The spectra for the freshly prepared gold seed solution remains featureless at this early timepoint (< 30 min after gold seed preparation) due to the small size (~4 nm) of the seeds.[66] By day 4 of the aging process, the characteristic extinction peak (531 nm) associated with spherical gold nanoparticles can be observed.

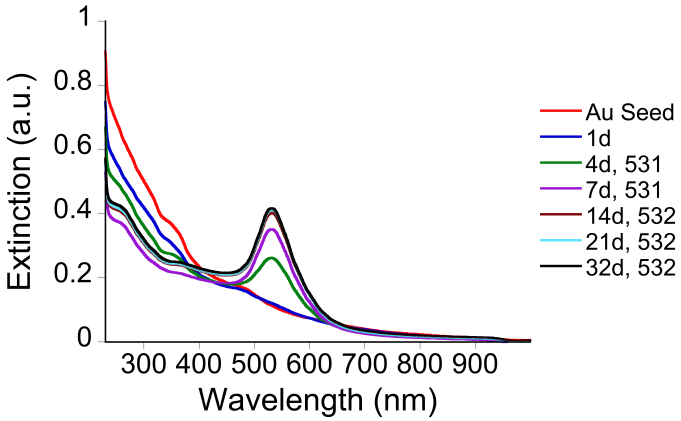

Figure 3.1.1. UV-Vis spectra of freshly prepared gold nanoparticle seed solution (< 30 min) aged over time for up to one month. The resulting peak wavelength values are included in the legend.

3.1.3 Transmission electron microscopy (TEM) of AuNPs

Select gold nanoparticle samples were also analyzed via transmission electron microscopy to obtain information on size and morphology. TEM images were acquired with a JEOL 100CX II transmission electron microscope at 100 kV. Samples for TEM were centrifuged (14,000 rpm x 15 min) twice to remove surfactant and redispersed in nanopure water. After redispersion, a small volume of the sample was drop-cast onto a carbon-coated copper TEM grid and allowed to dry at room temperature. The

concentration of gold nanospheres was estimated in these studies by using the absorbance values from UV-Vis measurements, TEM measurements and the Beer-Lambert law for absorption ($A=\varepsilon lc$, where c is the concentration of solution, l is the pathlength and ε is the extinction coefficient. The extinction coefficient was estimated using the equation ($\ln \varepsilon = k \ln D + a$) based on work by Liu *et al*., where ε is the extinction coefficient in M^{-1} cm^{-1}, D is the core diameter of the nanoparticles, and k = 3.32111, a = 10.80505.[38]

3.2 Characterization of Planar Gold (PlanarAu) Substrates

The planar gold (PlanarAu) substrates used in the incubation study presented in Chapter 6 were purchased from Sigma Aldrich (product 643246). They are reported to have a 99.999% Au 1000 Å layer thickness. An underlying 99.9% Ti adhesion layer is used to adhere the Au film to a glass microscope slide. Sidney Malak of Dr. Tsukruk's lab kindly carried out for his SEM characterization of the gold substrates.

3.2.1 Scanning Electron Microscopy (SEM) with Energy Dispersive Spectroscopy (EDS)

SEM with EDS analysis confirmed that the exposed surface area on the PlanarAu was 100% Au as shown in Figure 3.2.1. SEM was conducted on a Hitachi-3400SN with an Oxford EDX utilized with an operating voltage of 5-10 keV.

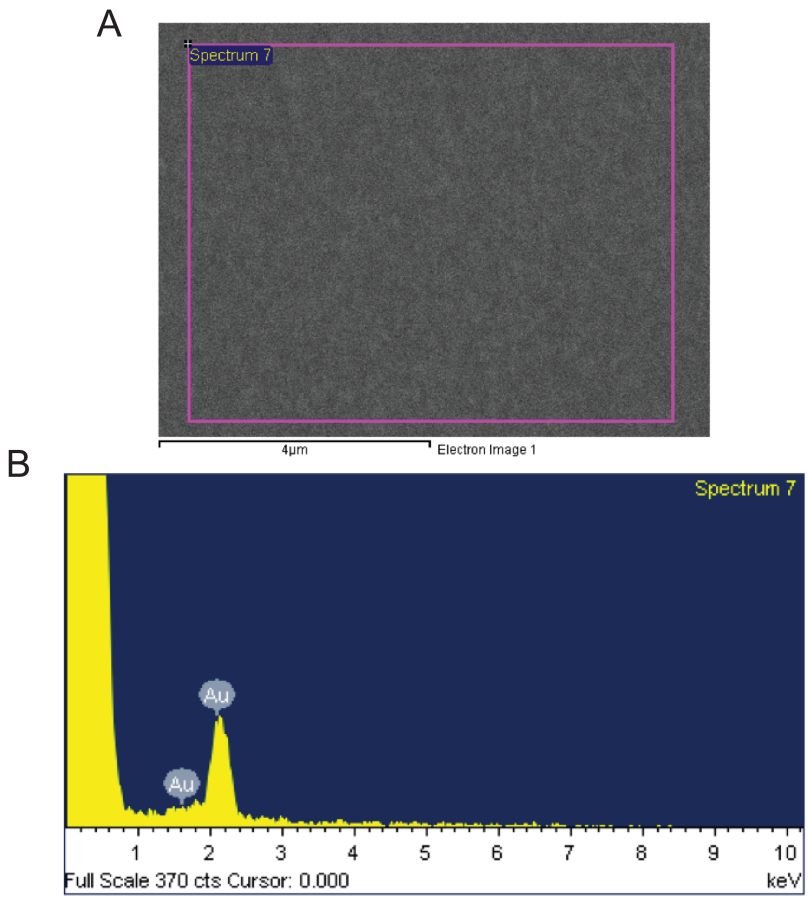

Figure 3.2.1. (a) SEM micrograph of the PlanarAu surface with an accompanying scale bar (4 µM) below with (b) corresponding EDS spectrum exhibiting characteristic Au peaks.

3.2.2 X-ray Diffraction (XRD)

The Sigma Aldrich PlanarAu substrates are reported by the manufacturer to be polycrystalline with a tendency towards the <111> orientation. Separate XRD analysis shown in Figure 3.2.2 verified the presence of 2θ=38° which corresponds to the (111) crystalline plane according to the JCPDS 00-004-0784 standard for gold. XRD was conducted using a PANalytical X'Pert Pro x-ray diffractometer (Almelo, The Netherlands).

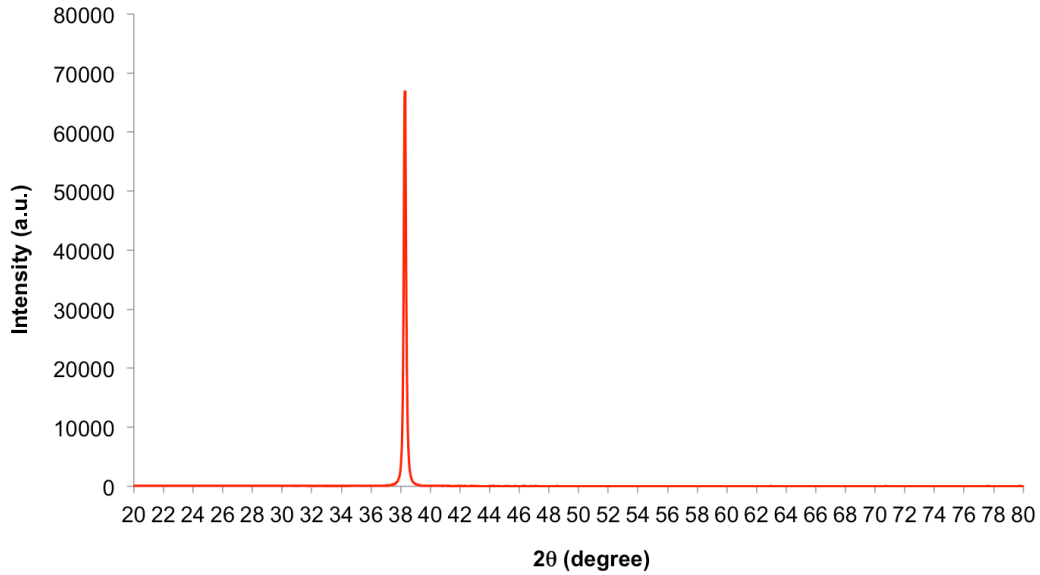

Figure 3.2.2. XRD analysis of the PlanarAu surface.

3.3 Characterization of DNA

3.3.1 Gel Electrophoresis

Gel electrophoresis is a commonly used technique for the separation of charged molecules. Since DNA is a negatively charged macromolecule due to its sugar-phosphate backbone, gel electrophoresis is widely used for the separation of DNA based on size differences (i.e. sequence base length). By running DNA products on a gel with a DNA ladder (mixture of DNA fragments of known base length) serving as a standard, the length of a DNA segment can be determined. Typically, shorter sequences travel faster down the length of the gel though ssDNA and dsDNA of the same base length may possess different migration times due to differences in conformation. In this work, gels for electrophoresis were primarily made using polyacrylamide (13 wt%) with methylenebisacrylamide as the crosslinker. In a select study, 2% agarose gels were used for electrophoretic analysis.

For the preparation of PAGE (polyacrylamide gel electrophoresis) gels, 3.25 mL of 40% acrylamide (w/bisacrylamide) was mixed with 2 mL 5X TBE buffer (Tris/Borate/EDTA) (1.1M Tris, 900 mM Borate, 25 mM EDTA, pH 8.0) and 4.75 mL nanopure water. Thermal initiators were then added (50 µL 20% (w/v) ammonium persulfate and 10 µL tetramethylethylene diamine) and the solution was inserted into gel cassettes with lane dividers (Invitrogen, Life Technologies, Grand Island, NY) and allowed to form a cross-linked network. DNA products were loaded into the gel wells after being mixed with the BlueJuice™ gel loading buffer and a separate lane for a companion DNA ladder was always included to allow for comparative base length evaluation. Gels were run for 30 min at 50 V followed by 1 h 30 min at 70 V. For imaging, gels were then stained with ethidium bromide (DNA intercalator dye) and imaged using a UV transluminator (BioDoc-IT, UVP, Inc., Upland, CA).

3.3.2 Spectrophotometry

Spectrophotometry is a technique that is used to measure the amount of light that a sample absorbs. Due to the participation of the aromatic bases of nucleic acids in light absorption events at 260 nm, spectrophotometry can be used in conjunction with the Beer-Lambert law to convert absorbance values to DNA concentration.[96] By comparing the absorption values of a DNA sample at 260 and 280 nm (A260/A280 ratio), the purity of a DNA sample can also be assessed with a value above 1.8 indicating a high purity solution of DNA.[96] In the presented studies, DNA concentrations were estimated using the NanoVue™ Plus spectrophotometer (GE Healthcare Life Sciences, USA).

3.3.3 Estimation of ssDNA size

For the aptamer screenings conducted in Chapters 5 and 6, an excess of ssDNA relative to the exposed surface areas of the gold targets was desired to promote competition between the candidate ssDNA sequences to bind to limited target surface. The length of the ssDNA used in these studies is 69 bases and a simple random coil conformation was used to estimate the size of ssDNA in terms of the radius of gyration (R_g). The R_g of ssDNA consisting of N segments is generally given by $R_g{}^2 = \frac{1}{6}Na^2$, in which a is the segment length of the ssDNA (1.5 nm).[97] The number of segments is given by N=(contour length)/(segment length), in which the contour length, L, is estimated by $L=b_0N_b$. N_b is the number of bases and the value of b_0 (i.e. the unit length of each base) is estimated to be around 6.4 nm for ssDNA.[98] Based on the above criteria, 69-base long ssDNA is estimated to have a R_g of ~ 3.32 nm.

3.3.4 Primary and Secondary Structure Analysis

The primary structure of DNA refers to the specific linear order of bases (A, C, G, T) in a given DNA sequence. For primary structure analysis in Chapters 5 and 6, the conservation of the base type by numerical position (in which base 1 starts at the 5' end) was assessed using Geneious software (Biomatters, Available from http://www.geneious.com) in multiple sequence alignments and pairwise sequence comparisons. By aligning the sequences, it was possible to identify the specific base types that were conserved across the same positions across the various sequence lengths.

Pairwise sequence comparisons are similar to multiple sequence alignments, but involve the comparison of only two sequences yielding an overall % primary sequence similarity. Online software MEME 4.9.1 was used to identify sequence motifs (specific ordering of bases repeated in 2 or more sequences) that could occur at any position throughout the length of the central 40 base variable region of the candidate sequences.[99] By taking into account the total percentage of each base (e.g. 25% A,T,C,G) across the sequences being analyzed, MEME assigns a statistical significance to identified motifs amongst a grouping of sequences, described by the E-value (E-value > 0.01 not statistically significant). The difference between a sequence alignment and sequence motif is visually demonstrated in Figure 3.3.1.

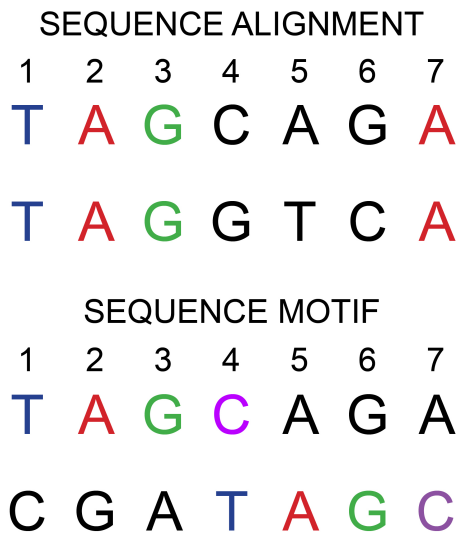

Figure 3.3.1. Schematic illustration of two pairs of DNA sequences to compare sequence alignment vs. sequence motif analysis. In sequence alignments, bases are marked or highlighted if that particular base is conserved in terms of base type and position in several (typically, 50%) of all sequences. In sequence motifs, a specific ordering of a series of bases that is conserved is marked or highlighted, but this conserved base segment can occur throughout any position along the sequence.

The UNAFOLD server[100] (also know by its older nomenclature as Mfold) was used to predict thermodynamically favorable secondary structures for all candidates. UNAFOLD predictions take into account Watson-Crick base-pair matches as well as occasional G-T wobble base pairs that are flanked by Watson-Crick base pair matches. It also takes into account the temperature and ionic conditions for the final predicted structures. Additional methods that were developed for specifically evaluating secondary structure similarities of identified aptamer candidates will be discussed in detail in Chapter 5.

3.4 Development and Optimization of the Competition-Induced Selection of Ligands (CISL) Screening Process

In the development of a new aptamer screening process, special steps were taken to thoroughly characterize each step of the process. The random ssDNA library used in the aptamer screening process is especially vital to the process as it is the pool from which aptamers are selected, yet throughout the literature very few groups report characterization details on their generated random ssDNA libraries. With this in mind, details of the development of the Competition-Induced Selection of Ligands (CISL) aptamer screening process are covered below from the amplification of random single-stranded libraries to the sequencing techniques used to identify the final aptamer candidates.

3.4.1 Polymerase Chain Reaction for Amplification of Random Single-stranded DNA Libraries

One of the key steps during the *in vitro* selection of aptamers is generation of the amplified random ssDNA library used for incubation with the target. In the studies described in Chapters 5 and 6, an exponential polymerase chain reaction (PCR) was used to amplify the initial random ssDNA template library, which produces final amplified PCR product in dsDNA form. A schematic illustrating how an exponential PCR reaction proceeds differently when using a starting library of ssDNA vs. dsDNA is shown in Figure 3.4.1.

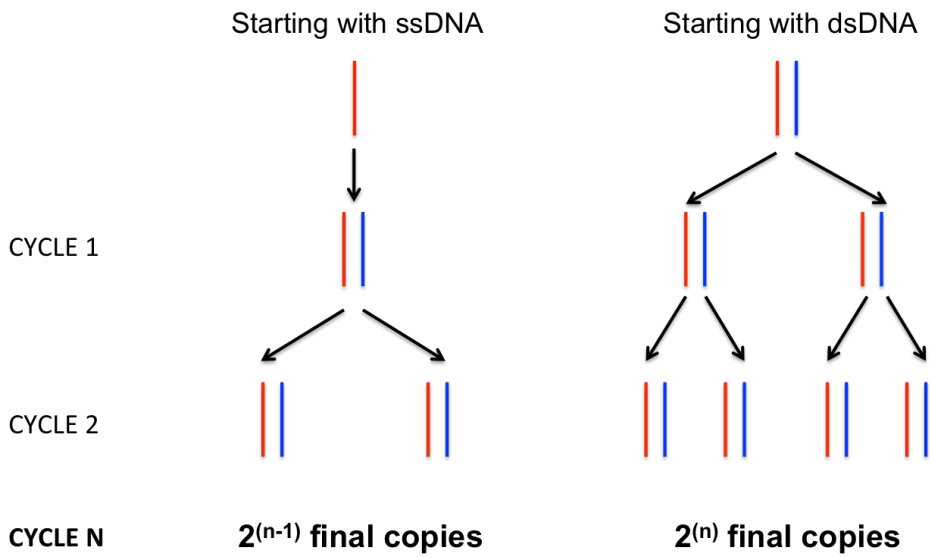

Figure 3.4.1. Schematic illustrating how many copies of DNA are achieved after an exponential amplification of the original template strands following PCR for a certain number of cycles (n), using a ssDNA starting library vs. a dsDNA starting library. For simplicity, details regarding the addition of reagents (e.g. primers, dNTPs, polymerase) are omitted.

PCR conditions were carefully optimized in the current work since it was observed that amplification of a random sequence population proceeds differently from that of a

homogeneous sequence population. In particular, the formation of unwanted byproducts is sensitive to differences in the initial template concentration and total number of PCR cycles.[101]

In order to optimize the exponential PCR reaction, PCR was conducted with a random ssDNA template library with variations in the number of initial template molecules and the number of PCR cycles. The remaining PCR reagents were kept constant at the following concentrations: 200 μM dNTPs, 60 nM forward primer, 60 nM phosphorylated reverse primer, 0.05 unit/μL GoTaq polymerase and 1X colorless GoTaq buffer. Cycle number was varied (15, 20, and 25 cycles) with denaturation (95 °C, 30 s), annealing (47 °C, 30 s), and extension (72 °C, 30 s). Final products were analyzed on a 2 wt% agarose gel stained with ethidium bromide and imaged using a UV transluminator (BioDoc-IT, UVP, Inc., Upland, CA). Analysis of the PCR products via agarose gel electrophoresis indicated that exceeding the optimal number of initial template molecules and cycle number can lead to an increase in the production of undesired side-products accompanied by a decrease in desired PCR product as shown in Figure 3.4.2. The highest yield of desired PCR product with no apparent side-product formation was achieved using 10^7 initial template molecules and 25 cycles (Group B, lane 3). It was observed that increasing the number of initial template molecules to 10^8 with a cycle number of 25 led to the formation of undesired side-products and a relative decrease in the desired PCR product formation. To maximize desired amplified dsDNA product yield while minimizing the formation of unwanted byproducts, exponential PCR reactions conducted in Chapters 5 and 6 were conducted with 10^7 initial random ssDNA template molecules and 25 total PCR cycles.

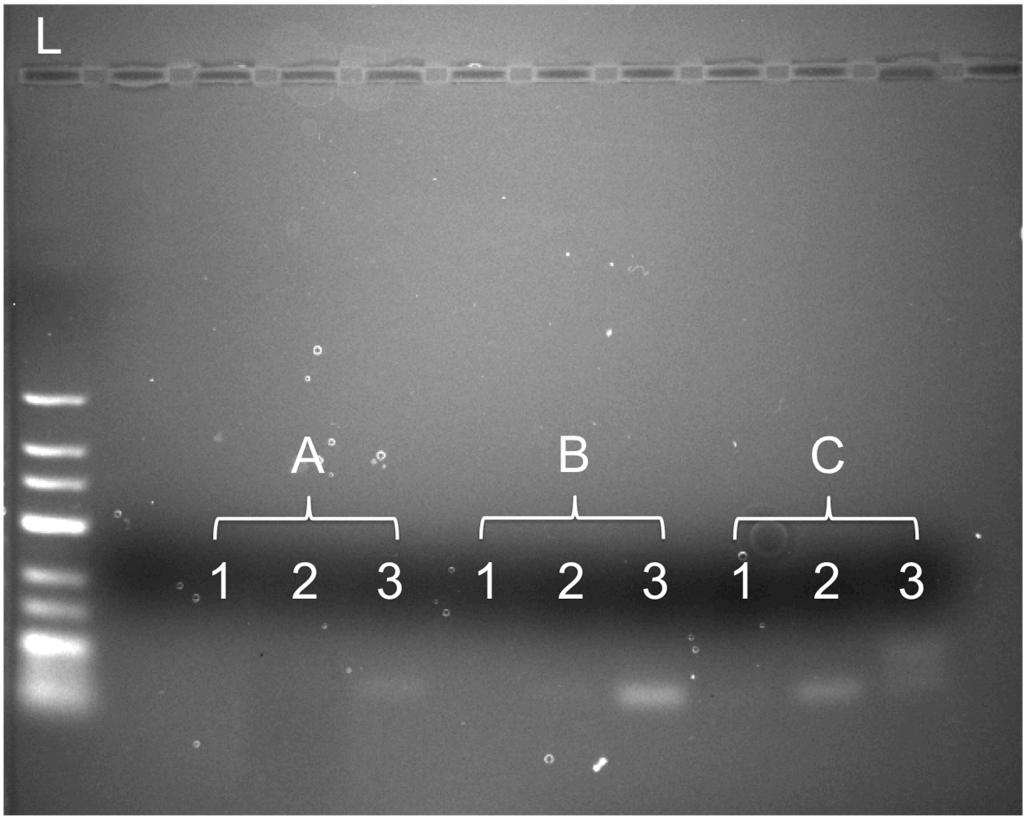

Figure 3.4.2. PCR product analysis on 2% agarose gel electrophoresis. L: 25 bp DNA ladder; Group A = 10^6 initial template molecules (1: 15 cycles, 2: 20 cycles, 3: 25 cycles); Group B = 10^7 initial template molecules (1: 15 cycles, 2: 20 cycles, 3: 25 cycles); Group C = 10^8 initial template molecules (1: 15 cycles, 2: 20 cycles, 3: 25 cycles).

3.4.2 Generation of Single-stranded DNA from Exponentially Amplified Double-stranded DNA

In order to proceed with aptamer selection, the amplified random dsDNA product must first be converted to ssDNA. In order to be able to convert the dsDNA PCR product to ssDNA, the initial PCR amplification reaction (using optimized formulation above) with the initial random ssDNA template library was conducted with a phosphorylated reverse primer in order to allow for lambda exonuclease digestion of the final phosphorylated

strands (i.e. complementary partner strands of template strands) of dsDNA from the 5' to 3' end as lambda exonuclease exhibits 20 times more affinity for phosphorylated 5'-ends than hydroxylated 5'-ends.[102, 103] A schematic describing the lambda exonuclease digestion process for the generation of ssDNA from dsDNA is shown in Figure 3.4.3.

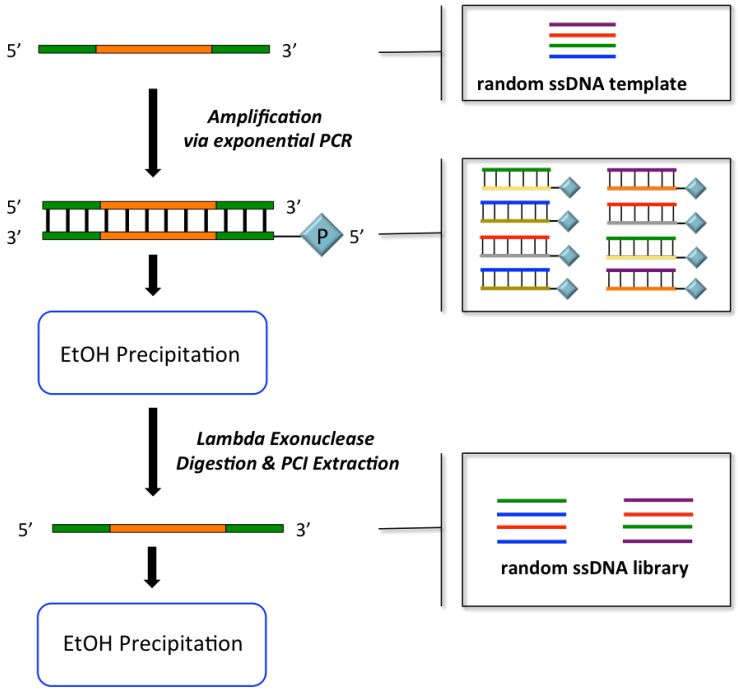

Figure 3.4.3. Schematic of the lambda exonuclease digestion process for the generation of ssDNA from dsDNA PCR product. Adapted from Marimuthu *et al*.[103]

Generation of ssDNA from dsDNA via lambda exonuclease digestion was confirmed by exposing dsDNA PCR product and lambda exonuclease-generated ssDNA product to Exonuclease I (Exo I), which selectively degrades ssDNA in the 3' to 5' direction.[104] Initial dsDNA PCR product and lambda exonuclease generated ssDNA product were mixed with Exo I (1U/1 µL DNA) and 1X Exo I reaction buffer. These mixtures were incubated at 37 °C for 30 min followed by a 20 min incubation step at 80 °C. Final

products were analyzed on a 13 wt% polyacrylamide/bis gel stained with ethidium bromide and imaged using a UV transluminator (BioDoc-IT, UVP, Inc., Upland, CA).

Figure 3.4.4 shows analysis of lambda exonuclease-digested PCR products before (Figure 3.4.4A) and after (Figure 3.4.4B) incubation with Exo I, which selectively cleaves ssDNA, but not dsDNA.

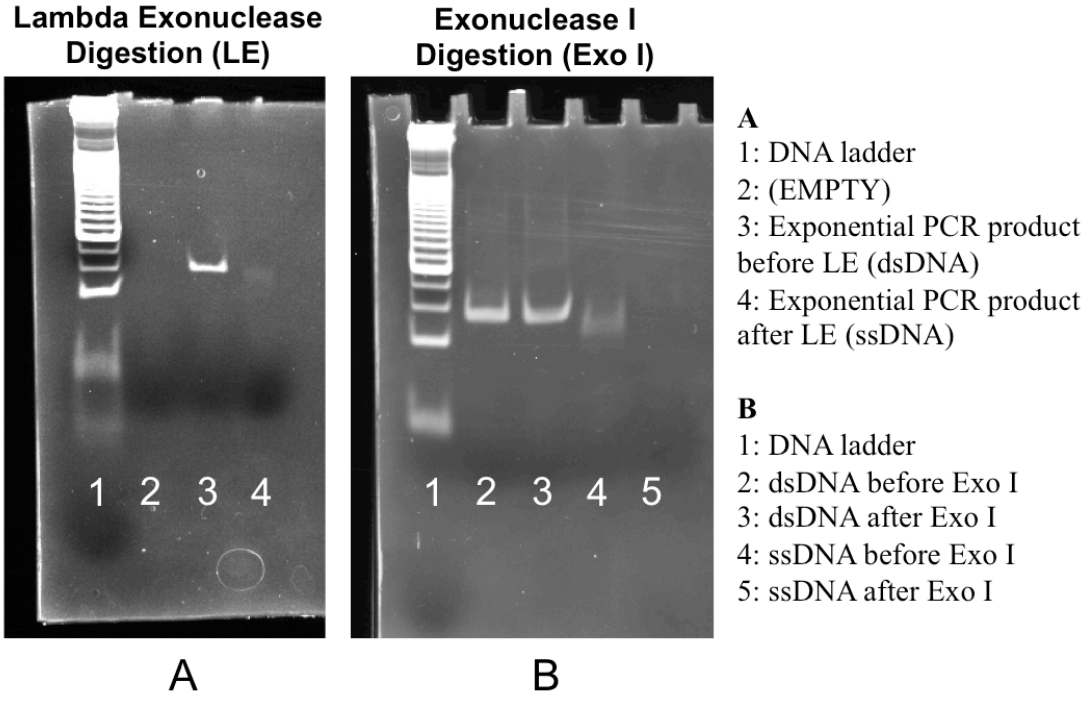

Figure 3.4.4. PAGE analysis of a (A) random ssDNA library generated for aptamer selection using an exponential PCR reaction followed by lambda exonuclease digestion and (B) confirming the ssDNA nature of the lambda exonuclease digested PCR product using exonuclease I digestion. The dsDNA used was generated from an exponential PCR reaction while the ssDNA was generated through a lambda exonuclease digestion of the exponential PCR generated product.

In Figure 3.4.4A, the bright band in Lane 3 becomes noticeably dimmer in Lane 4 due to loss in DNA conversion of dsDNA to ssDNA. While no differences in the dsDNA bands

occur in Lanes 2 and 3 in Figure 3.4.4B following Exo I exposure, the ssDNA product in Lane 4 disappears in Lane 5 following Exo I digestion.

3.4.3 Bacterial transformation and sequencing of DNA

In order to retrieve sequence information from the random ssDNA aptamer candidates identified in this study, it was necessary to conduct a bacterial transformation. Bacterial transformations are common procedures that are used for making copies of DNA. In the studies described in Chapters 5 and 6, upon completion of the final panning incubation round, the target is washed several times with a PCR optimized buffer solution (Invitrogen). Exponential PCR is then conducted directly on the target using unmodified forward and reverse primers. Following the PCR reaction, the PCR product is purified using the Qiagen MinElute PCR Purification Kit (Qiagen) to prepare for the subsequent bacterial transformation steps.

The purified PCR product is cloned into the pCR 2.1® TOPO® TA vector by mixing it with a salt solution and the vector provided in the TOPO® TA kit for subcloning (Invitrogen). The reaction is mixed gently and incubated for 15 minutes at room temperature. Once the reaction is complete, it is placed on ice. The ligation mixture is then transformed into One Shot TOP10 chemically competent E. coli cells (Invitrogen) by adding the ligation mixture to one vial of the thawed E. coli cells. This transformation reaction is allowed to proceed for 2 hours on ice, followed by a heat shock treatment for 30 seconds at 42°C. The vials are then placed on ice for 2 minutes followed by an addition of S.O.C medium (Invitrogen) to each vial to aid in obtaining maximal transformation efficiency. The vials are then placed in a shaking incubator at 37°C for 1 hour at 225 rpm.

Transformed cells are plated on Luria broth (LB) plates containing ampicillin and X-gal for blue/white screening of the cells. The plates are incubated for 16 hours after which colonies are picked that contain the vector insert which appear white due to the X-gal based blue/white screening. The colonies are then incubated in a solution of LB and ampicillin for 16 hours in a shaking incubator at 37°C at 225 rpm.

Plasmid DNA from the cultures is isolated and purified using an "in-house" protocol used by Dr. Patrick Dennis at the Wright Patterson Air Force Research Lab (Soft Matter Materials Branch) that proved to be more successful than initial trials with commercial kits. After overnight incubation, the culture vials are centrifuged and the liquid from the cultures is decanted. Solution I (50 mM glucose, 50 mM Tris-HCl, 10 mM EDTA pH 8) with 100 μg/mL lysozyme is then added to the cells in the culture vial and mixed to aid in breaking down the cell walls. After mixing, the cells are lysed by incubating with a solution of 0.2N NaOH/1% SDS for 5 minutes. A solution of 3M potassium acetate (pH 5.2) is then added to neutralize the reaction. The solution is then mixed which yields a precipitate that is then centrifuged and the supernatant is saved and transferred to a clean vial. 2-propanol is then added to the recovered supernatant and placed at 4°C for at least 3 hours to allow for precipitation of the plasmid DNA. The solution is then centrifuged and the resultant pellet is washed with 80% EtOH. The pellet is then resuspended in TE pH 8 and treated with RNAse A at 37°C for 1 hour to degrade bacterial RNA. The solution is then mixed with 7.5M ammonium acetate and PCI, after which the solution is centrifuged and the extracted plasmid DNA is collected in the upper layer. This is followed by a final precipitation step with 2-propanol at -20°C and wash steps with 80% EtOH. The final plasmid DNA product is resuspended in Nanopure H_2O (Barnstead, 18.2

MΩ cm). Purified plasmid DNA is sent to Genewiz, Inc. (South Plainfield, NJ) for Sanger sequencing using their standard M13R primer. For select experiments in Chapter 6, samples were also sent to GENEWIZ for next generation sequencing (NGS) analysis, which provides both sequence information and relative counts of each sequence. In contrast to Sanger sequencing which is more of a low throughput technique (~ 20-100 sequenced colonies from population), NGS allows for direct sequencing from the amplified PCR product step, bypassing the lengthy bacterial transformation process and provides high throughput analysis (millions of reads from population).[105]

3.5 Conclusions

The studies presented in this chapter highlight the importance of characterizing the DNA products at each step of the ssDNA generation process since ssDNA preparation from dsDNA amplified PCR products is not trivial. The characterization of ssDNA generation for libraries in aptamer screening processes is not typically reported for SELEX. In contrast to SELEX, the CISL aptamer screening process does not involve intermittent PCR cycles. This is important to note since intermittent PCR would require that each population of eluted sequences (of unknown concentration) undergo PCR optimization for every selection round in efforts to avoid introducing undesirable PCR by-products during aptamer screening.

CHAPTER 4

SPECTROSCOPIC STUDIES OF NUCLEIC ACID ADDITIONS DURING SEED-MEDIATED GROWTH OF GOLD NANOPARTICLES[1]

4.1 Introduction

This chapter focuses on a series of spectroscopic studies of gold-nucleic acid suspensions to inform our later design approaches of random libraries (e.g. equimolar base content vs. adenine-rich, etc.) as well as provide some insight into base (e.g. A vs. T) and secondary structure (e.g. ssDNA vs. dsDNA) effects on oligonucleotide-gold binding. Gold nanoparticles (AuNPs) have been heavily investigated for their unique size- and shape-dependent optical properties. These effects are apparent in the variation of optical spectra that gold nanoparticles exhibit for different sizes and shapes ranging from spheres (plasmon band at ~520 nm) to nanorods (transverse and longitudinal plasmon bands at ~520 and 600-1600 nm, respectively).[39, 40, 106] These signature spectral bands correspond to a localized surface plasmon resonance effect caused by the coherent, collective oscillation of conduction band electrons in AuNPs illuminated with light.[39] In addition to the effects of size and shape on the resulting absorption and scattering of light, changes in the spatial arrangement of AuNPs can shift the position of the plasmon bands.[43-45, 107-109] AuNP surfaces can be conveniently modified to incorporate other moieties such as oligonucleotides, proteins and antibodies due to the strong binding interaction between gold and chemical moieties such as thiols.[45-48, 110] As a result of these practical optical properties and conjugation possibilities, gold nanoparticles have been studied in biosensing, molecular imaging, therapeutic and medical diagnostic applications.[44, 48, 111]

[1] Much of the experimental work presented in this chapter is taken from the following

Synthesis of gold nanoparticles of various shapes is typically performed via reduction of Au(III) ions in an aqueous solution with a capping agent present to stabilize formed particles. Common capping agents include citrate or cetyltrimethylamonium bromide (CTAB). [38, 47, 48, 66, 106, 112, 113] While synthesis protocols can vary[61, 114] once gold seeds have nucleated, gold nanospheres can be formed by simply allowing the solution to sufficiently age.[115]

Over the past several years, numerous studies have focused on using grafted oligonucleotides to induce recognition-based assembly of gold nanoparticles as highlighted in recent reviews.[116-119] The studies typically conjugate single-stranded thiol-modified, complementary oligonucleotides on one or more populations of nanoparticles and then induce nanoparticle aggregation as hybridized duplexes bridge nanoparticle surfaces.[108, 120, 121] As opposed to employing DNA as a nanoparticle assembly tool, select studies have explored the use of oligonucleotides and nucleotides as templates for the synthesis of inorganic nanoparticles. Similar to prior work using peptide-based templates[72, 122-126], the goal of these bio-inspired approaches was to efficiently control particle shape and size during particle nucleation events, or more commonly, during the growth stage following seed preparation.[35] Some studies reveal, for example, that variation in physical size and fluorescence characteristics of CdS nanoparticles can be achieved by adding specific homopolymer sequences during nanoparticle synthesis.[127] DNA has also been used as a template to create Ag nanoring structures which could not be achieved using conventional direct growth methods.[84, 128]

Select studies by Wang *et al.* have specifically investigated the effect of incubating soluble oligonucleotides (i.e. not intentionally conjugated to material surface) with gold seeds during the growth stage. Their studies involved incubating solutions of 30 base-long (polyadenine, polythymine, or polycytosine)[91, 92] or 20 base-long (polyguanine)[44] homopolymers with CTAB-stabilized gold nanoprism seeds. They reported a variation occurs in particle morphology and topography ranging from rough (polyadenine) and smooth (polycytosine) surfaces to star-shaped (polythymine) and hexagonal (polyguanine) nanoparticles.[92] Depending on sequence compositions, binary mixtures of the homopolymers resulted in intermediate morphologies and surface roughness in the resulting nanoparticles.

While few studies[91, 92] have investigated particle growth in the presence of nucleic acids, base-specific and structure-specific interactions of oligonucleotides with gold surfaces have been reported. SPR and FTIR analysis on gold surfaces can provide information on relative differences in the timing and extent of oligonucleotide adsorption events.[59, 129, 130] Notably, while bare planar gold serves as a convenient sample geometry for characterizing surface binding events, the nature of these binding events on colloidal gold may be significantly affected by additional materials parameters ranging from curvature to additional surface moieties (e.g. citrate).[130] For gold nanoparticles initially stabilized by citrate ions, bridging of nanoparticle surfaces via single-stranded homopolymers of DNA has been assessed using colorimetric analysis and UV-Vis spectroscopy.[52, 131] Collectively, these studies indicate that homopolymer sequences do not have equivalent

affinities for gold substrates with purines adsorbing more strongly than pyrimidines to gold in the following order: G>A>C>T.[129, 131] Among these studies, the secondary structure of DNA (single-stranded chains vs. double-stranded helix) has been shown to affect the propensity for gold nanoparticles to aggregate.[52, 59]

In the current spectroscopy study, base-specific and structure-specific effects of single-stranded DNA (ssDNA) and double-stranded DNA (dsDNA) added during seeded growth are investigated to reveal if the presence of various nucleic acids directs the shape evolution of resulting gold nanoparticles. In an effort to directly compare results of adding various nucleic acids ranging from individual nucleotides to mixtures of polynucleotides in the current study, a common gold seed approach involving CTAB was chosen based on the work of Nikoobakht and El Sayed.[66, 112] The effects of various nucleic acids on gold nanoparticle formation under seed-mediated growth is primarily investigated using UV-Vis spectroscopy. Due to its widespread and practical use as a characterization tool for gold nanoparticle suspensions, UV-Vis spectroscopy was chosen as our primary analytical tool in order to quantitatively assess differences in the spectral signatures of the resulting nanoparticle suspensions from numerous nucleic acid incubation conditions. In order to identify base specific effects, 20 base-long homopolymer (**A20**, **T20**, **C20**, **G20**) and random (**R20**) sequences alone and as mixtures are employed in these studies. Structure-specific effects (ssDNA vs. dsDNA) were also investigated by incubating gold seeds with mixtures of complementary homopolymer sequences as well as with specific sequences (**S20**, **S20'**) that were shown to be capable of duplex formation (**S20**:**S20'**) under the nanoparticle growth conditions explored. Pure

and mixed monomeric forms of nucleic acids were also investigated as additives during nanoparticle growth.

4.2 Materials and Methods

4.2.1 Materials

All oligonucleotide sequences were purchased from Integrated DNA Technologies and were HPLC purified (Integrated DNA Technologies, Inc., Coralville, IA). Hydrogen tetrachloroaurate (III) hydrate ($HAuCl_4 \bullet 3H_2O$), hexadecyltrimethylammonium bromide (CTAB), hydrochloric acid (HCl), and deoxynucleoside monophosphates (dNMPs: dAMP, dTMP, dGMP, and dCMP) were purchased from Sigma Aldrich, St. Louis, MO. Sodium borohydride ($NaBH_4$) was purchased from Fluka Analytical, Bushs, Switzerland. Tris HCl (pH 7.5) was purchased from Amresco, Solon, OH. Deoxynucleoside triphosphates (dNTPs: dATP, dTTP, dGTP, dCTP, dNTP Mix) were purchased from Invitrogen, Grand Island, NY. All buffers were prepared using 0.2 μM filtered water from a Barnstead Nanopure ultrapure water purification system. 1 mM stock solutions of nucleic acids were prepared using 1 mM Tris HCL, pH 7.5.

4.2.2 Preparation of gold nanoparticle seed solution and gold nanospheres

Gold nanoparticle seeds were synthesized according to the methods described by Nikoobakht and El Sayed.[66] CTAB solution (20 mL, 0.2 M) was mixed with a solution of $HAuCl_4 \bullet 3H_20$ (20 mL, 0.5 mM) on a stir plate with a magnetic stir bar. After 30 min of stirring, a freshly prepared solution of ice-cold $NaBH_4$ (2.4 mL, 0.01 M) was then added to the stirred seed solution and mixed for an additional 2 min. Gold nanospheres were

allowed to form (in the absence or presence of various nucleic acids) by allowing the gold seed solution to age for up to seven days while mixing on a rotomixer.

4.2.3. Incubation of nucleic acids with aging gold nanoparticle seed solution

For all seed suspensions incubated with nucleic acids, each oligonucleotide or nucleotide was incubated at a final concentration of 2 μM in a 1 mL total volume of the gold seed solution (to be aged). For cases involving mixtures of oligonucleotides or nucleotides, each oligonucleotide or nucleotide was added to yield a final concentration of 2 μM for each individual species. Select experiments were also conducted at a nucleic acid concentration of 0.1 μM. Sequence **A20** was also selectively investigated at concentrations of 2, 1, 0.1 and 0.01 μM. The nucleotides used in this incubation study were dNTP mix, dATP, dCTP, dGTP, dTTP, ATP, GTP, CTP, UTP, dCMP, dGMP, dAMP, dTMP. A list of the oligonucleotide sequences used in the incubation studies is provided in Table 4.2.1.

Table 4.2.1. List of 20-base long DNA oligonucleotide sequences incubated with gold seeds.

Nomenclature	Sequence (5'→3')
A20	AAA AAA AAA AAA AAA AAA AA
T20	TTT TTT TTT TTT TTT TTT TT
C20	CCC CCC CCC CCC CCC CCC CC
G20	GGG GGG GGG GGG GGG GGG GG
R20	25% (A,T,C,G) in random order
S20	TTT TTT GGA TTG CGG CTG AT
S20'	ATC AGC CGC AAT CCA AAA AA

4.2.4 UV-Vis spectroscopy and TEM analysis

Following the addition of seed solutions to a particular nucleic acid solution, suspensions

were mixed on a rotomixer and examined at various timepoints using UV-Vis analysis. For the 2 h and 7 d timepoints, UV-Vis spectra were gathered at 1 nm intervals using a Biotek Synergy H1 Hybrid Reader. After data collection, spectra for each set of samples were first normalized against a water blank. Next, each sample was normalized to the same relative absorbance value of 0.3 at 400 nm as has been done in previous studies.[132] Select samples were additionally characterized via transmission electron microscopy. TEM images were acquired with a JEOL 100CX II transmission electron microscope at 100 kV. Samples for TEM were centrifuged (14,000 rpm x 15 min) twice to remove surfactant and redispersed in nanopure water. After redispersion, 0.3 μL of the sample was drop-cast onto a carbon-coated copper TEM grid and allowed to dry at room temperature.

4.2.5 Confirmation of DNA duplex formation in presence of gold nanoparticle seed solution

To prepare gold nanoparticle seed solution, 10 mL of 0.5 mM $HAuCl_4$ and 10 mL of 0.2 M CTAB were mixed on a stir plate for 50 min. After mixing, 1.2 mL of chilled 0.01 M $NaBH_4$ was added to the solution and mixed for 2 min. This solution was then used as the incubation buffer for the primary hybridization study carried out with 1.1 μM carboxylated polystyrene beads (PS) (Bangs Laboratories, Inc., Fishers, IN). Beads were coupled to aminated **S20*** and primary hybridization was conducted with fluorescently tagged complementary and non-complementary targets, following the protocol described by Hardin and Milam[133] using sequences listed in Table 4.2.2 for the suspension conditions listed in Table 4.2.3. Duplex densities were evaluated by measuring the

average fluorescence of the microsphere population and converting these average fluorescence intensities to duplex densities using calibration standards (Bangs Laboratories) in conjunction with BD FACSDiva software on a BD-LSR II flow cytometer as detailed by Hardin and Milam.[133]

Table 4.2.2. List of sequences used for flow cytometry study with probe-functionalized polystyrene microspheres to verify duplex formation is possible in gold nanoparticle seed solution conditions.

Function	**Sequence**
Probe	**S20*=** 3'-TAG TCG GCG TTA GGT TTT TT /NH_2/-5'
Complementary Target	**S15'**= 3'-ACC TAA CGC CGA CTA/ FITC/- 5'
Noncomplementary Target	**NC14**= 3'-GGA TTG CGG CTG AT/ FITC/- 5'

Table 4.2.3. Tabulated description of polystyrene suspensions analyzed via flow cytometry to verify duplex formation between complementary **S20** and **S15′** sequences in gold nanoparticle seed conditions.

Sample	**Description**
Bare Beads (BB)	Bare Polystyrene (PS) Bead
BB + S20*	Bare PS bead + **S20*** probe functionalized with amine
BB+NC14	Bare PS bead incubated with **NC14**
BB+S15'	Bare PS bead incubated with **S15'**
CB	**S20***-conjugated PS bead alone
CB+NC14	**S20***-conjugated PS bead incubated with noncomplementary **NC14**
CB+S15'	**S20***-conjugated PS bead incubated with complementary **S15'**

4.3 Results and Discussion

4.3.1 Effects of 20 base-long homopolymer additions to aging gold seed suspensions

Gold nanoparticle seed solutions were prepared following methods reported by Nikoobakht *et al*. which yields seeds that are less than 4 nm in size.[66] Figure 4.3.1 shows the visible spectra of the gold nanoparticle seed solution which does not feature the distinct characteristic extinction spectra associated with gold nanoparticles that are larger in size due to the localized surface plasmon resonance effect.[61]

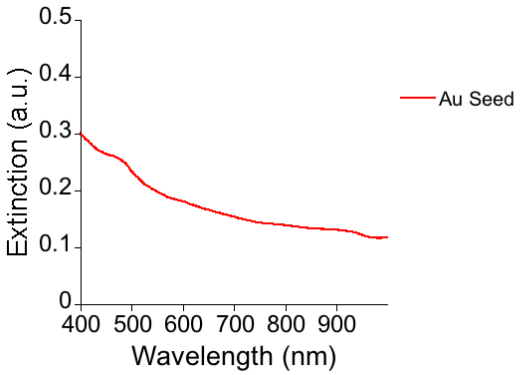

Figure 4.3.1. UV-vis spectra of freshly prepared gold nanoparticle seed solution.

20-base long homopolymer sequences (**A20**, **T20**, **C20**, or **G20**) as well as random oligonucleotide sequences (**R20**) were incubated with freshly prepared gold nanoparticle seed solution and were evaluated via UV-Vis spectroscopy at 2 h and 7 d timepoints. Following a 2 h incubation period, there are no noticeable spectral differences between any of the aging gold nanoparticle suspensions in the presence or absence of the single-stranded oligonucleotide sequences as shown in Figure 4.3.2 (a). As described earlier, the featureless spectra seen here is also due to the relatively small gold nanoparticle seed size (~4 nm) at this early timepoint. After a 7 d incubation period as shown in Figure 4.3.2 (b), an extinction peak appears in all incubation cases associated with the formation of larger gold nanoparticles over time. All of the controls and DNA cases, with the exception of

A20, exhibit a characteristic extinction peak around 525 nm. In the case of **A20**, a red-shift (571 nm) and an overall broadening of the characteristic peak is observed.

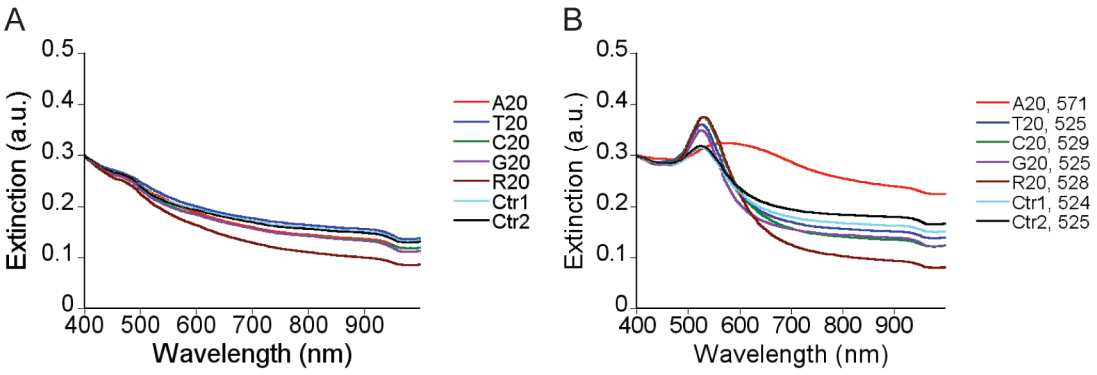

Figure 4.3.2. UV-Vis spectra of gold seed following incubation with various 20 base-long homopolymers (**A20**, **T20**, **C20**, **G20**) and random (**R20**) sequences at 2 μM for (a) 2 h and (b) 7 d. Controls involve the addition of 2 μL of 1 mM Tris HCl (Ctr1) or 2 μL of nanopure water (Ctr2) in the absence of DNA. The resulting peak wavelength values are included in the legend.

It was also visually observed that nanoparticle sedimentation occurred in the presence of **A20**, which was unlike the other suspensions as shown in Figure 4.3.3. It has been shown that the aggregation of gold nanoparticles in solution leads to a change in solution color from red (stable) to blue (aggregated).[50, 108]

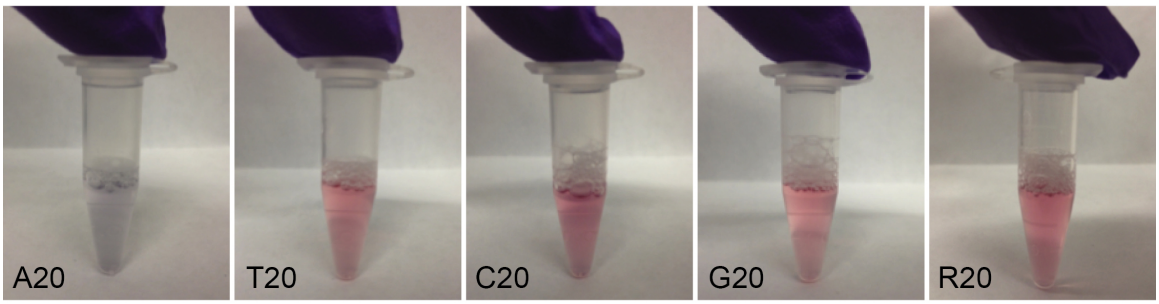

Figure 4.3.3. Photographs of gold nanoparticle seed suspensions at 7 d following incubation with **A20**, **T20**, **C20**, **G20** and **R20** at 2 μM.

The observed sedimentation behavior and spectral differences seen in the **A20** suspension indicate that polyadenine (**A20**) induces particle aggregation that was not observed with

any of the other homopolymer or random oligonucleotide sequences. This aggregation behavior is most likely caused by polyadenine bridging of the nanoparticles into disordered clusters as indicated in a TEM micrograph in Figure 4.3.4.

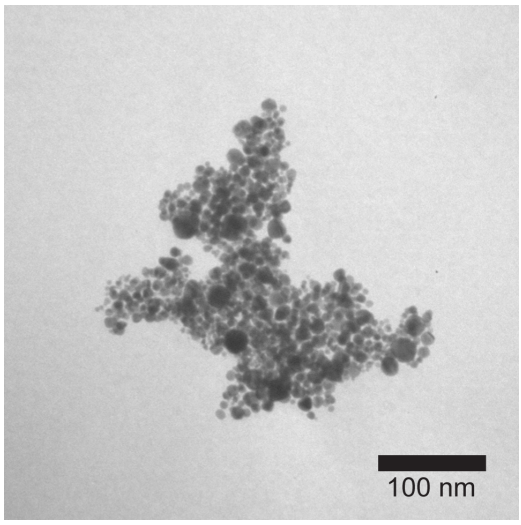

Figure 4.3.4. TEM micrograph of gold seed aged for 7 days in the presence of added **A20** at 2 μM.

In prior work by Wolf *et al.*, it was reported that 25-base long polyadenine exhibits the strongest and fastest binding activity to gold surfaces compared to polycytosine and polythymine.[129] Although the gold nanoparticles used in this study are synthesized in the presence of CTAB surfactant, prior work[134] indicates that the CTAB association with the nanoparticle surface is very weak. Thus, it is possible that polyadenine is effective in displacing the associated CTAB layer to reduce the stability of the colloid suspension by inducing bridging between nanoparticle surfaces. In prior studies, it has been shown that relatively short DNA strands (20 bases or less) can form duplex bridges between nanoparticles.[108, 135] Thus, bridging induced by the 20-base long **A20** sequences is plausible. Storhoff *et al.* has also investigated the nucleobase-dependent agglomeration of gold nanoparticles and reported that deoxynucleosides (dA, dG, dC) induced

significant red-shifts in the surface plasmon band frequency due to agglomeration, while dT induced only slight changes.[131] The 20-base oligonucleotides were also incubated with aging gold seed at 0.1 μM. Even at this lower concentration of DNA, **A20** was still observed to induce a red-shift and peak broadening effect, although to a lesser extent as shown in Figure 4.3.5.

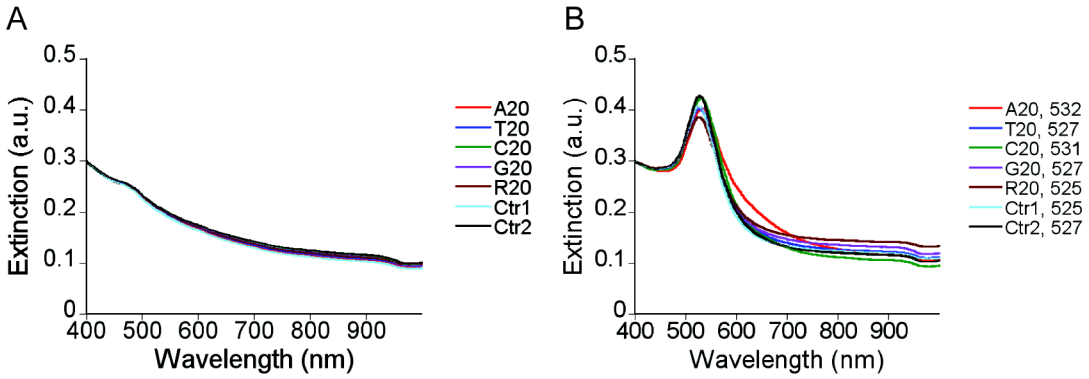

Figure 4.3.5. UV-Vis spectra of gold seed following incubation with various 20 base-long homopolymers (**A20**, **T20**, **C20**, **G20**) and random (**R20**) sequences at 0.1 μM for 2 h (left) and 7 d (right). Controls involve the addition of Tris HCl (Ctr1= 2 μL Tris HCl) or nanopure water (Ctr2= 2 μL 18 MΩ-cm water) in the absence of DNA. The resulting peak wavelength values are included in the legend.

To further investigate the effects of **A20** on gold nanoparticle aging effects, the incubation of **A20** at other concentrations (1 μM, 0.01 μM) was also studied at the 7 d timepoint. As shown in Figure 4.3.6, as the concentration of **A20** increases, the extent of the red-shift in the surface plasmon band frequency and peak broadening effect increases as well. The degree to which agglomeration of the gold nanoparticles occurred at the various **A20** concentrations could also be observed visually in the shift of the solution color from red to blue with an increase in **A20** concentration as shown in Figure 4.3.7.

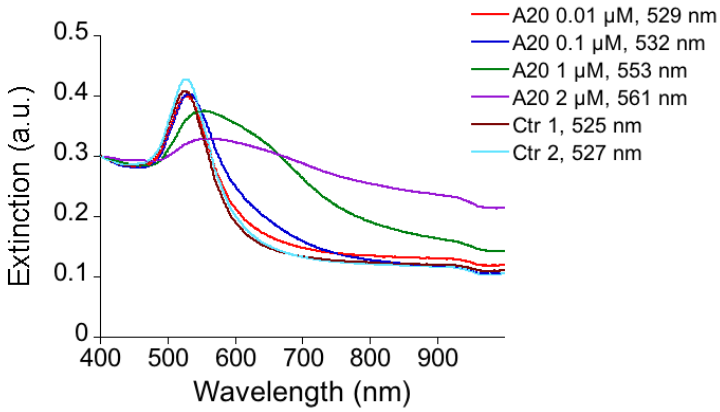

Figure 4.3.6. UV-Vis spectra of gold seed following incubation with **A20** at various concentrations for 7 d. Controls involve the addition of Tris HCl (Ctr1= 2 µL Tris HCl) or nanopure water (Ctr2= 2 µL 18 MΩ-cm water) in the absence of DNA. The resulting peak wavelength values are included in the legend.

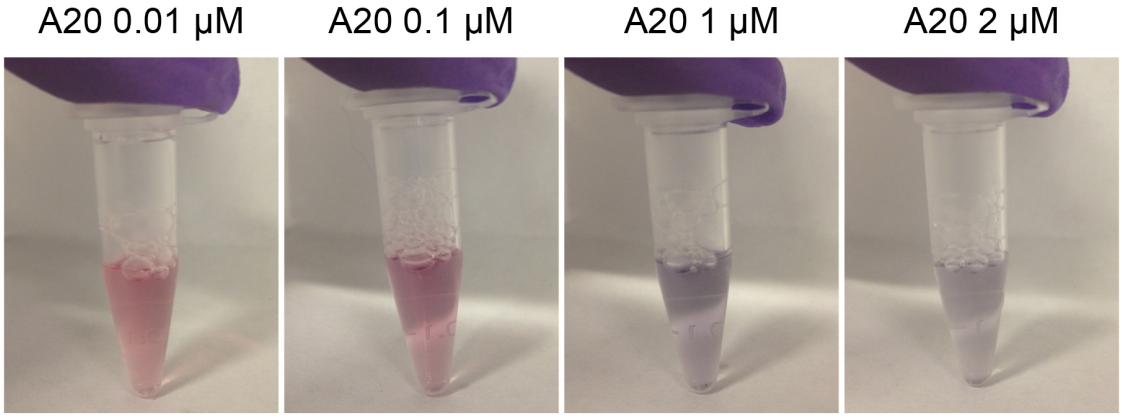

Figure 4.3.7. Photographs of gold nanoparticle seed suspensions at 7 d following incubation with **A20** at 0.01, 0.1, 1 and 2 µM.

For all incubation studies described to this point, the oligonucleotides were added to freshly-prepared (within 30 min) gold seeds. However, it was observed that the addition of **A20** even after the gold nanoparticle seed solution was aged for 7 d still resulted in a

red-shift and overall broadening of the characteristic peak as shown in Figure 4.3.8. Thus, the destabilizing effects of **A20**, likely due to bridging is not limited to the initial stages of nanoparticle growth.

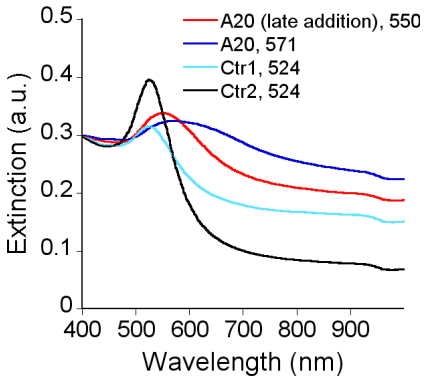

Figure 4.3.8. UV-Vis spectra of gold nanoparticle suspensions in which (i) the gold nanoparticle seed solution was aged for 7 d prior to the addition and brief incubation of the aged seed solution with **A20** (2 μM) (**late addition**) or (ii) following a 7 d incubation in which **A20** (2 μM) was immediately added to a freshly prepared gold nanoparticle seed solution. Controls involve the addition of Tris HCl (**Ctr1**= 2 μL Tris HCl) or water (**Ctr2**= 2 μL 18 MΩ-cm water) in the absence of DNA. The resulting peak wavelength values are included in the legend.

4.3.2 Effects of various nucleotide additions to aging gold seed suspensions

The effects of individual bases alone were investigated by conducting analogous 7 d incubation studies with the monomeric derivatives of oligonucleotides (e.g. NTPs, dNTPs, dNMPs). In these studies however, no significant spectral differences were observed (Figure 4.3.9) which indicates that it is the polymeric nature of polyadenine that plays a key role in affecting spectral behavior, which is most likely due to polyadenine-induced gold nanoparticle bridging.

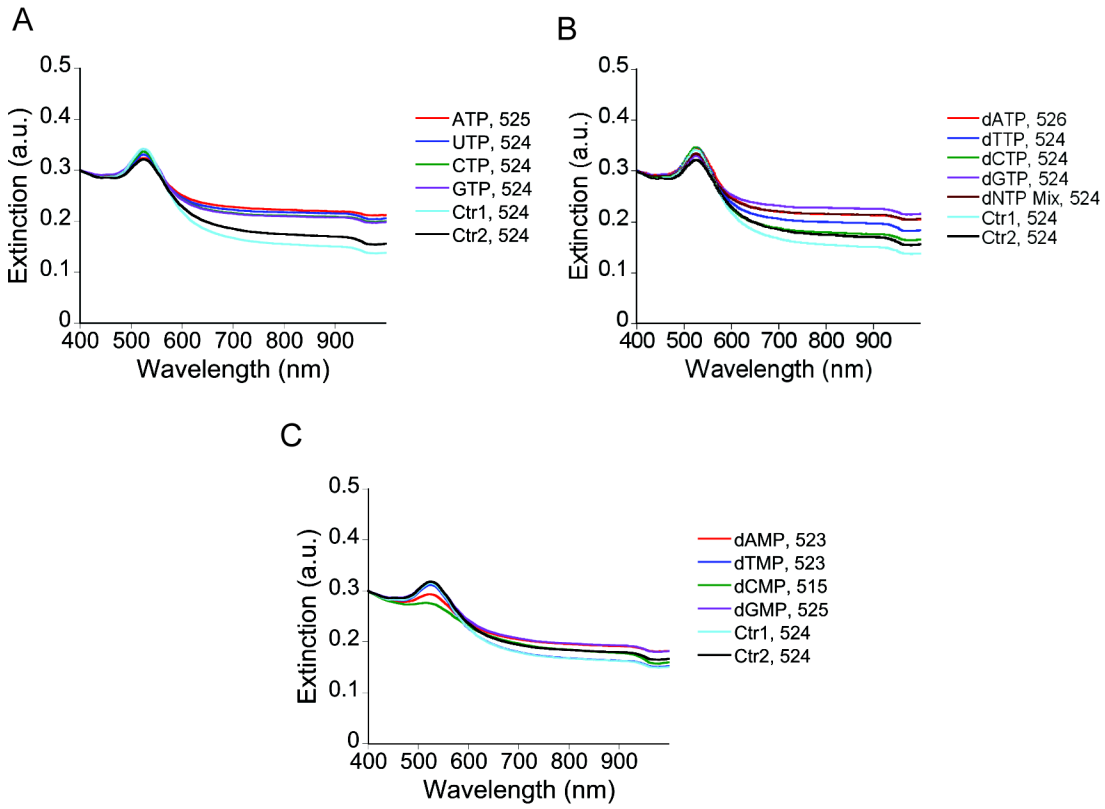

Figure 4.3.9. UV-vis spectra of aged gold seed following incubation with various (a) NTPs (ATP, UTP, CTP, GTP), (b) dNTPs (dATP, dTTP, dCTP, dGTP, dNTP Mix) and (c) dNMPs (dAMP, dTMP, dCMP, dGMP) at 2 µM for 7 d. Controls involve the addition of Tris HCl (Ctr1= 2 µL Tris HCl) or water (Ctr2=2 µL 18 MΩ-cm water) in the absence of DNA. The resulting peak wavelength values are included in the legend.

4.3.3 Effects of homopolymer mixture additions to aging gold seed suspensions

In the next series of studies, mixtures of homopolymers are added to the gold nanoparticle seed suspensions and are examined at 2 h and 7 d timepoints. In order to investigate if the **A20**-induced aggregation effect on aged gold nanoparticle seeds is mitigated by the presence of other homopolymer sequences, **A20** is first mixed with one other homopolymer (**T20**, **C20**, or **G20**) and then added to the seed solution for a 7 d aging time period. Figure 4.3.10 (b) shows that the peak broadening effect induced by **A20** at the 7 d timepoint is increasingly mitigated by the copresence of one other

homopolymer in the following order: **C20**<**G20**<**T20** as well as by the copresence of all four homopolymers (**ATCG:20**). In competitive adsorption studies conducted by Kimura-Suda *et al*., the relative adsorption affinities of 5-mer ssDNA oligonucleotides on gold surfaces was reported to be T (weakest) < G < C < A (strongest).[59]

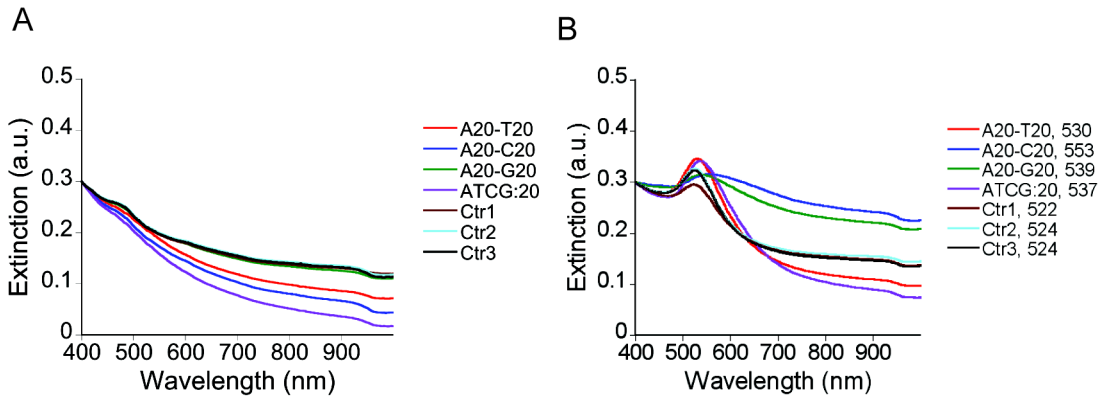

Figure 4.3.10. UV-Vis spectra of gold seeds after a (a) 2 h incubation and (b) 7 d incubation in the presence of various homopolymer mixtures of two or four sequences at 2 µM total concentration. Controls involve the addition of Tris HCl (Ctr1= 4 µL Tris HCl, Ctr2= 8 µL Tris HCl) or water (Ctr3= 4 µL nanopure water) in the absence of DNA. The resulting peak wavelength values are included in the legend.

This trend is comparable to our results in which one can infer that the homopolymer (**A20**) causing nanoparticle aggregation (see Figure 4.3.2) is likely to be the strongest adsorbate. Furthermore, when incubated in the presence of two homopolymers with increasingly weaker binding affinity for the gold substrate (**C20** (strongest adsorbate) > **G20** > **T20** (weakest adsorbate)), the degree of **A20**-induced aggregation also diminishes in the same order as shown in Figure 4.3.10 (b). In the case of these homopolymer mixtures, however, one must consider both the DNA-nanoparticle interactions as well as the DNA-DNA interactions. The **A20-T20** mixture is a particular case in which polythymine has the weakest apparent affinity for the nanoparticles, but the strongest

affinity for polyadenine due to Watson-Crick base pairing. Compared to all other homopolymer combinations, the dual mixture of **A20**-**T20** promotes the smallest differences in the peak location (530 nm) and breadth compared to the controls. Given the complementarity between strands and the distinctive spectroscopic effect compared to the other homopolymer additions, it is likely that a mixture of **A20** and **T20** strands leads to the formation of partially hybridized duplexes that inhibit single-stranded overhangs or unhybridized segments of a polyadenine "tail" from forming bridges between nanoparticles and causing the aggregation evident in the **A20** case shown in Figure 4.3.2. Notably, spectra at an early time (2 h) remain featureless indicating that mixtures of homopolymers, even **A20**-**T20**, do not promote any significant, immediate differences in the spectra (see Figure 4.3.10 (a)).

4.3.4 Effects of 20 base-long complementary strands alone and mixed together on aging gold seeds

The next series of DNA incubation studies involves the addition of two complementary sequences (**S20** and **S20'**) consisting of 50% thymine and 50% adenine bases, respectively, as shown in Table 4.2.1 and capable of forming **S20:S20'** duplexes under the incubation conditions explored for gold seed formation and nanoparticle growth explored here. Similar to the ssDNA incubation studies discussed in the previous section, here the effects of double-stranded DNA (dsDNA) additions on gold nanoparticle formation are explored using UV-Vis spectroscopy as shown in Figure 4.3.11. As before, gold seeds here are aged with various DNA solutions. Figure 4.3.11(a) shows that by the 2 h timepoint, the spectra remain featureless for the ssDNA cases of **S20** or **S20'** alone;

however, a peak at 531 nm does appear if both complementary strands are present. The emergence of this peak at this early timepoint indicates that rapid nanoparticle growth occurs in the presence of the duplexes. Moreover, it is clear that this result is due to the presence of **S20:S20'** duplexes and not the single-stranded sequences since no characteristic peaks appear at the 2 h timepoint if gold seeds are incubated with the individual single-stranded **S20** or **S20'** oligonucleotide strands. The early emergence of this peak is also observed at the lower concentration (0.1 µM) of **S20:S20'** duplexes as shown in Figure 4.3.12.

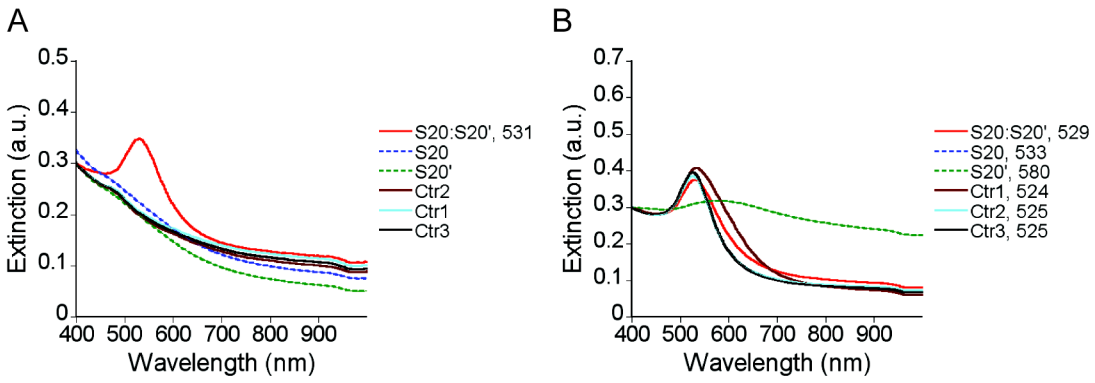

Figure 4.3.11. UV-Vis spectra of gold following incubation with various complementary ssDNA alone (**S20** or **S20'**) and mixed together (**S20:S20'**) at 2 µM for (a) 2 h and (b) 7 d. Controls involve the addition of Tris HCl (Ctr1= 4 µL Tris HCl, Ctr2= 2 µL Tris HCl) or water (Ctr3= 2 µL nanopure water) in the absence of DNA. The resulting peak wavelength values are included in the legend.

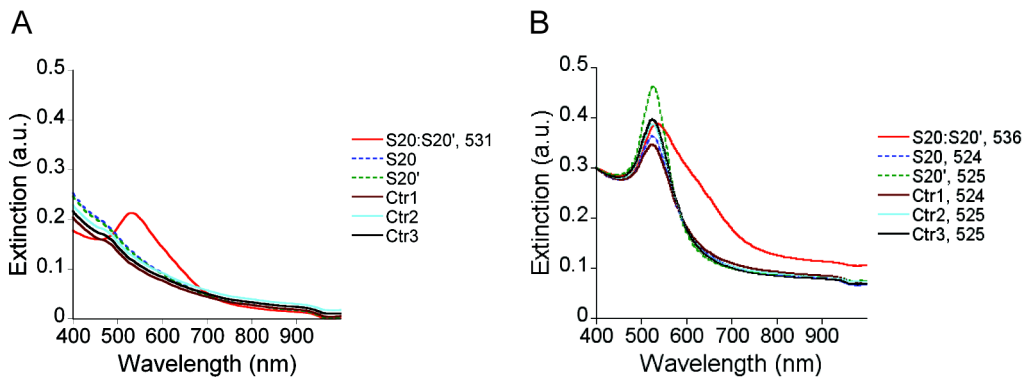

Figure 4.3.12. UV-Vis spectra of gold seeds following incubation with various complementary ssDNA alone (**S20** or **S20'**) and mixed together (**S20:S20'**) at 0.1 μM for (a) 2 h and (b) 7 d. Controls involve the addition of Tris HCl (Ctr1= 4 μL Tris HCl, Ctr2= 2 μL Tris HCl) or water (Ctr3= 4 μL 18 MΩ-cm water) in the absence of DNA. The resulting peak wavelength values are included in the legend.

Notably, this characteristic peak was not evident at early timepoints for the complementary **A20-T20** mixtures (see Figure 4.3.10(a)). The differences between these two mixtures may be attributed to differences in the duplex structure since the primary structure or specific sequence of bases in **S20** and **S20'** strands promotes the formation of duplexes with blunt ends while a rich range of partially hybridized duplexes with single-stranded overhangs of varying base lengths are possible for an **A20-T20** mixture. As shown in Figure 4.3.11(b) following a 7 day incubation, similar spectra occur in all cases with and without DNA present, with one exception. Similar to the **A20** case shown previously in Figure 4.3.2(b) the adenine-rich **S20'** also causes a peak broadening effect as evidenced by a red-shift of the characteristic peak from 524 nm (for the controls) to 580 nm (see Figure 4.3.11(b)). Separate TEM micrographs confirm the formation of gold nanospheres in the presence of the **S20:S20'** duplexes at 2 μM and 0.1 μM as shown in Figure 4.3.13.

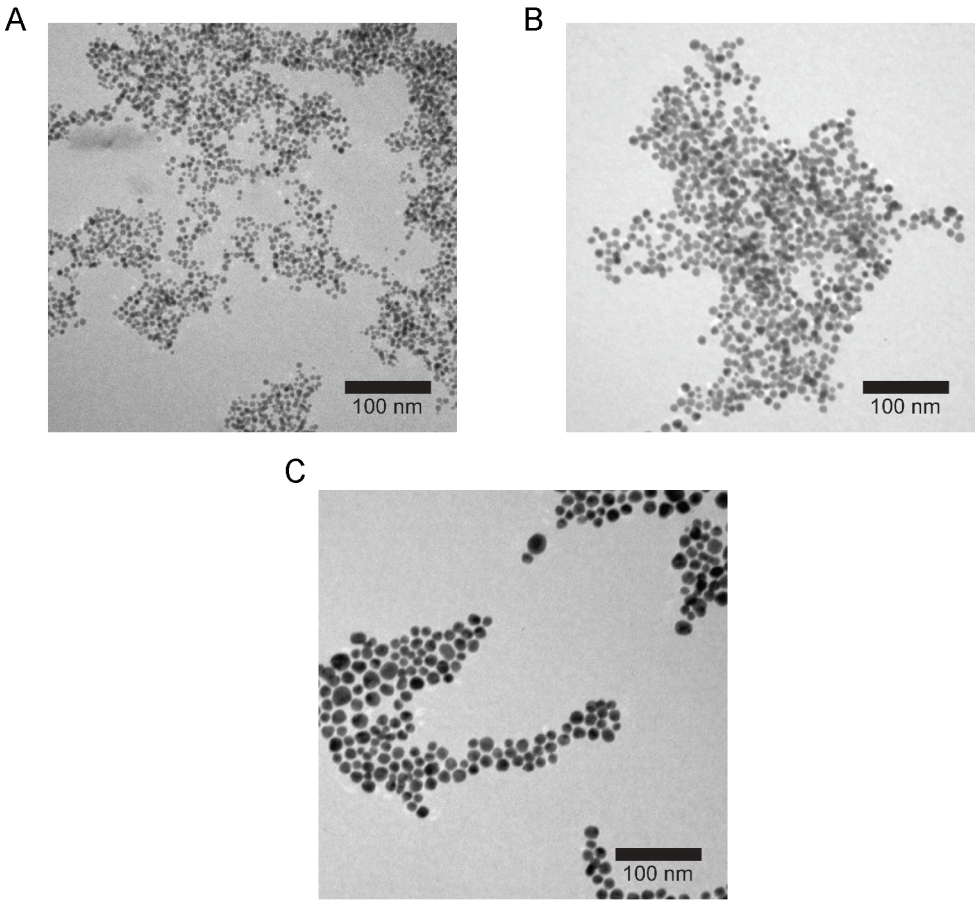

Figure 4.3.13. TEM micrographs of gold seed aged for 7 days in the presence of added (a) **S20:S20′** at 2 μM (b) **S20:S20′** at 0.1 μM and (d) 4 μL Tris HCl (**Ctr2**).

The ability to form duplexes in the presence of gold nanoparticle seed solution was confirmed by conducting primary hybridization experiments with 1.1 μM **S20*-**coupled polystyrene beads and fluorescently tagged complementary sequences in the presence of the as-synthesized gold nanoparticle seed solution (See Tables 4.2.2 and 4.2.3). Flow cytometry analysis of these suspensions after primary hybridization was allowed to occur indicates that primary hybridization between **S20***-coupled beads (CB) and complementary **S15'** strands were successful as shown by high duplex densities as compared to controls in Figure 4.3.14.

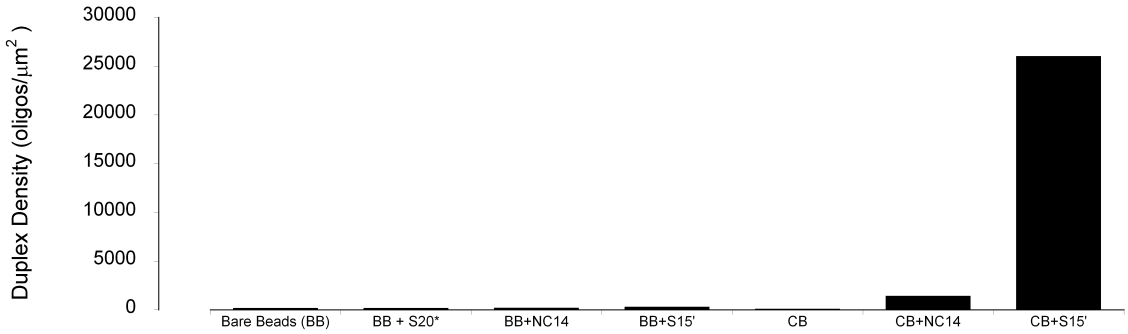

Figure 4.3.14. Duplex density per μm^2 of polystyrene microspheres for controls (**BB**, **BB+20***, **BB+NC14**) and complementary target cases (CB+**S15'**). See Table 4.2.3 for tabulated description of samples analyzed via flow cytometry.

4.4 Conclusions

In this study, monomeric forms of the nucleic acids do not appear to affect the spectral evolution in the seed-mediated growth of spherical gold nanoparticles. In contrast, base-specific and structure-specific effects of 20 base-long oligonucleotides are evident in several cases involving seed-mediated growth of gold nanoparticles. Moreover, while the distinctive and likely dynamic role of the cationic CTAB species is not clear, separate washing studies indicate that although CTAB does remain on the particle surface, it is only weakly bound to the gold surface. Thus, displacement by a stronger adsorbate such as polyadenine to cause aggregation in the aged gold nanoparticle seed is possible. However, the copresence of the complementary homopolymer **T20** lessens the effect of the homopolymer **A20**. In fact, the secondary structure of the DNA appears to play a key role in the evolution of the nanoparticle spectra since the presence of blunt-end duplexes (**S20:S20'**) has a marked effect on accelerating nanoparticle growth from an aging gold seed solution. This accelerated growth, however, was not observed for mixtures of

complementary homopolymers (**A20:T20**), which can likely form a heterogeneous population of short hybridized segments (of varying base length) flanked by single-stranded segments. Collectively, the interactions between complementary oligonucleotides involving Watson-Crick base pair matching appears to either completely overcome (for blunt-ended duplexes) or at least reduce (for duplexes with single-stranded overhangs) interactions between oligonucleotides and nano-sized gold particles during their growth.

CHAPTER 5

COMPETITION-INDUCED SELECTION OF LIGANDS TO SCREEN FOR SSDNA APTAMERS FOR GOLD NANOPARTICLES[2]

5.1 Introduction

The most commonly used screening technique for identifying aptamers is widely known as Systematic Evolution of Ligands by EXponential Enrichment (SELEX) which was first reported in 1990 by two groups and revolutionized the aptamer field.[23, 24] In brief, the traditional SELEX approach is an iterative process with each selection round consisting of three main stages: incubation of random oligonucleotide library with target, partitioning and finally elution and amplification of the bound aptamers.[10, 20, 136] A detailed description of the SELEX process is provided in Chapter 1.

Since the initial reporting of the SELEX method nearly twenty-five years ago, there have been many variations to this approach, including the use of oligonucleotide libraries with modified nucleotides for enhanced resistance against chemical and nuclease-mediated degradation as well as improved separation technologies to shorten the involved cycles of enrichment and partitioning native to the SELEX process.[29, 137] For example, the incorporation of modern analytical tools such as capillary electrophoresis (CE-SELEX) and microfluidics (M-SELEX) into the SELEX process have allowed for aptamer screening in only 1-4 selection rounds, significantly reducing the time needed for the overall selection process.[138-140] These techniques also avoid the need to immobilize small target species to a substrate or colloidal carrier during the screening process. While practical for purposes of separation, target immobilization can impose additional steric

[2] Manuscript in preparation for publication.

hindrances to binding or additional sources of nonspecific binding events to species other than the intended target. In addition to these modified SELEX methods for aptamer selection, there have been select reports of a non-SELEX approach for the selection of aptamers. In 2005 Berezovski *et al.* reported implementing a nonequilibrium capillary electrophoresis of equilibrium mixtures (NECEEM) method to select for aptamers for the h-RAS protein.[32] Their non-SELEX selection involved three rounds of partitioning using NECEEM without intermittent steps involving PCR amplification and re-introduction of amplified ssDNA between each selection round. With this modified approach, they were able to achieve aptamer screening in 1 hour and reduce the sequence propagation error associated with PCR of heterogeneous sequence populations by avoiding intermittent amplification steps inherent to SELEX. Tok *et al.* also used this non-SELEX approach in 2010 to identify aptamers for signal transduction proteins with dissociation constants in the low micro- to nanomolar range.[33]

Although aptamers or oligonucleotide-based ligands have been identified for a number of diverse targets, the binding mechanisms supporting these aptamer-target interactions are not always well understood or with few exceptions, experimentally interrogated.[17, 19, 141] Further investigations into the structures of aptamers in their free vs. bound states has revealed that the formerly held lock-and-key analogy is too simplistic for some aptamer-target systems in which the nature of binding appears to be a combination of conformational selection and induced fit.[15, 18] For example, structural investigations of the cocaine-binding aptamer initially reported by Stojanovic *et al.* in 2000 describe the aptamer secondary structure to consist of three helical stems centered around a three-way junction.[142] Ten years later, a study conducted by Neves *et al.* reported that the secondary

structure and resulting binding of the same aptamer sequence could actually vary depending on as little as one base difference in the hybridization segment of one of the stems.[17] Depending on the stem length, they reported the aptamer could either undergo a transition from an unstructured state (in the absence of cocaine target) to a well-structured state if bound to its target or, alternatively, could return to a completely structured conformation that is maintained in both the free and bound states.

While aptamers have been identified for a number of biologically-based targets[143-146], few studies have investigated nonbiological materials as targets.[83, 88] In 2010, Liu *et al.* investigated the precipitation of Pd nanoparticles in the presence of RNA sequences identified from an *in vitro* selection process that were hypothesized to catalyze Pd nanoparticles from a precursor complex.[82, 88] Bawazer *et al.* recently reported the use of Single round Enrichment of Ligands by deep Sequencing (SEL-Seq) to identify a DNA aptamer that promotes the formation of ZnO nanoparticles from solution.[83] Gold nanoparticles (AuNPs) are presented as a target of interest due to their unique optoelectronic properties that are size- and shape-dependent and thus provide advantages for use as biological sensors and in therapeutic and medical diagnostic applications.[48, 147] Specifically, interactions between oligonucleotides and AuNPs have become a great area of interest, as DNA-functionalized AuNPs have provided even greater flexibility for their use in the development of controlled nanoassemblies, biodiagnostics and cellular imaging.[55, 56, 135, 148] In the majority of these vast studies, ssDNA is generally conjugated to the surface of AuNPs through thiol linkers and duplex formation follows to bridge AuNPs together. [46, 48] Separate studies and our own study in Chapter 4, however, indicate that there are certain base-specific interactions between the DNA sequences and the

underlying gold surface.[52, 59, 130, 131, 149] As described in Chapter 4, it was observed that the addition of single-stranded polyadenine during seed-mediated gold nanoparticle growth induced nanoparticle aggregation. Based on this observation, one set of CISL screening involved an adenine-rich library (40% A; 20% C,T,G) to promote selection of higher affinity aptamers. Interestingly, it was also seen that the presence of dsDNA promoted the rapid formation of AuNPs in the same study, in contrast to ssDNA, which did not induce the same effect.

In the current study and in contrast to conventional SELEX, a modified aptamer selection approach, referred to as Competition-Induced Selection of Ligands (CISL) is presented to screen through random ssDNA libraries to recover and identify aptamer candidates for spherical gold nanoparticles. In contrast to the traditional SELEX approach, CISL intentionally promotes intense competition between candidate ssDNA ligands or aptamers by continually introducing unenriched pools of random ssDNA during each selection round followed by partitioning with no intermittent amplification steps between each round. By eliminating intermittent elution of PCR amplification steps, some of the potential benefits of using the CISL approach for aptamer screening include (1) avoiding library bias towards "early winners" that may ultimately outnumber better candidates introduced at later selection rounds; (2) reducing amplification errors (e.g. partially elongated duplexes) associated with repeated PCR of heterogeneous sequence populations[101]; (3) intentional promotion of competition between existing and potential adsorbates to reveal the strongest affinity candidates; and finally (4) a significant reduction in time for aptamer screening. Identified aptamer sequences were then analyzed to determine similarities in their primary structures and their predicted secondary

structures. To the best of our knowledge, the work in this chapter is the first report of an aptamer screening process with a colloidal gold target.

5.2 Materials and Methods

5.2.1 Materials

The normal (25% A, 25% C, 25% T, 25% G) and A-rich (40% A, 20% C, 20% T, 20% G) random single-stranded DNA template libraries were purchased from Integrated DNA Technologies. The 69-base random template strands consisted of a 40-base randomized central region flanked on either end by primer binding sites (5'-GGG ACA GGG CTA GC-[40N]-GAG GCA AAG CTT CCG -3'). The random libraries were synthesized via hand mixing and were PAGE-purified. The reverse primer (5'-CGG AAG CTT TGC CTC-3'), phosphorylated reverse primer (5'-Phos-CGG AAG CTT TGC CTC-3') and forward primer (5'-GGG ACA GGG CTA GC-3') were purchased from Integrated DNA Technologies and were HPLC purified.

GoTaq DNA polymerase and 5X colorless GoTaq reaction buffer were purchased from Promega (Madison, WI). The 10 mM dNTP mix, phenol:chloroform:isoamyl alcohol (25:24:1), ethidium bromide, TOPO TA Cloning Kit for Subcloning, One Shot TOP10 Chemically Competent E. coli and X-gal were purchased from Invitrogen (Grand Island, NY). HEPES, $MgCl_2$, $CaCl_2$, and KCl were purchased from BDH Chemicals (VWR Scientific, Radnor, PA). Ethanol and Tris EDTA pH 7.4 were purchased from Fisher Scientific (Pittsburgh, PA). NaCl, hexadecyltrimethylammonium bromide (CTAB) hydrogen tetrachloroaurate (III) hydrate ($HAuCl_4 \bullet 3H_2O$), sodium borohydride ($NaBH_4$), ammonium persulfate (98%), tetramethylethylene diamine, ampicillin sodium salt,

dimethylformamide were purchased from Sigma Aldrich (St. Louis, MO). Glycogen, Acryl/Bis 29:1 40% w/v solution, Acryl/Bis 37.5:1 40% w/v solution, agar (bacteriological), LB broth (Luria-Bertani) were purchased from Amresco (Solon, OH). Lambda exonuclease enzyme and 10X lambda exonuclease reaction buffer were purchased from New England Biolabs (Ipswich, MA). The MinElute PCR Purification Kit was purchased from Qiagen (Gaithersburg, MD). The aptamer incubation buffer (AIB) used for selection consisted of 20 mM HEPES, 2 mM $MgCl_2$, 150 mM NaCl, 2 mM $CaCl_2$, 2 mM KCl at pH 7.4 All buffers were prepared using 0.2 μM filtered water from a Barnstead Nanopure ultrapure water purification system (Barnstead, Thermo Fisher Scientific, Inc., USA).

5.2.2 Random Library Amplification and ssDNA Generation

To prepare for selection, amplified pools of template DNA were generated via exponential PCR reactions on libraries of ssDNA template strands that were 69 bases in length with a 40-base central randomized region. This randomized region consisted of 25% of each base for the "normal" (N) random library and 40% adenine (20% each of cytosine, guanine, thymine) for the "A-rich" (A) random library.

The normal and A-rich libraries were prepared separately. The PCR reaction mix for each library amplification was prepared in nanopure water and consisted of 0.17 pM ssDNA template, 200 μM dNTPs, 60 nM forward primer, 60 nM phosphorylated reverse primer, 0.05 unit/μL GoTaq polymerase and 1X colorless GoTaq buffer. Twenty-five cycles of denaturation (95 °C, 30 s), annealing (47 °C, 30 s), and extension (72 °C, 30 s) were conducted. The PCR formulation and cycling process was carefully optimized to

minimize the formation of unwanted byproducts as described in Chapter 3. Amplified PCR products, now in dsDNA form, were purified via ethanol precipitation with glycogen and resuspended in Tris EDTA pH 7.4.

The purified dsDNA PCR products were then digested with lambda exonuclease in order to generate a ssDNA library from the amplified products as described in Chapter 3. Purified dsDNA PCR product was mixed with lambda exonuclease enzyme (10U lambda exonuclease/ 2 μg dsDNA) and lambda exonuclease reaction buffer to yield 1X from a 10X buffer stock. Immediately after mixing, the solution was incubated at 37 °C for 1 h, followed by a 10 min incubation step at 80 °C to halt the enzymatic reaction. The digested ssDNA was then purified with a phenol/chloroform/Isoamyl alcohol extraction followed by ethanol precipitation with glycogen. Purified ssDNA was resuspended in aptamer incubation buffer (20 mM HEPES, 2 mM $MgCl_2$, 150 mM NaCl, 2 mM $CaCl_2$, 2 mM KCl pH 7.4) to prepare for aptamer selection.

5.2.3 Preparation and Growth of Spherical Gold Nanoparticles (AuNPs)

Gold nanoparticle seeds were synthesized based on methods described by Nikoobakht *et al.*[66] A CTAB solution (10 mL, 0.2 M) was mixed with a solution of $HAuCl_4 \bullet 3H_20$ (10 mL, 0.5 mM) for 3 h. A fresh solution of ice-cold $NaBH_4$ (1.2 mL, 0.01 M) was then added to the mixture after 30 min and allowed to stir for an additional 2 min. Gold nanospheres were formed by allowing the gold seed solution to age for 11 days in amber glass vials under rotation mixing. Gold nanoparticle seeds were characterized with UV-Vis spectroscopy using a Biotek Synergy H1 Hybrid Reader (Biotek, Winooski, VT). Gold nanospheres were characterized with UV-Vis spectroscopy and transmission

electron microscopy (JEOL 100CX II 100 kV, JEOL USA, Inc., Peabody, MA) at the 11 day aged timepoint. Average nanoparticle diameter was estimated using ImageJ software (http:// rsbweb.nih.gov/ij/) by measuring the diameter of ca. 150 particles.

To prepare for use in aptamer selection, gold nanospheres on day 11 post-synthesis were centrifuged and resuspended in nanopure water (pH 7.4) after supernatant removal.

5.2.4 Competition-Induced Selection of Ligands (CISL)

The aptamer selection processes for the normal and A-rich random ssDNA libraries were separate and individual screening experiments but the same procedure was followed for both cases and sequence results for both CISL screening sessions were combined for subsequent analysis. An aliquot was taken from the washed gold nanospheres stock that was equal to approximately 10^{11} gold nanospheres and placed in a PCR tube. Gold nanosphere concentration was estimated using the average particle diameter based on TEM measurements, absorbance values from UV-Vis measurements and the use of Beer-Lambert's law where the extinction coefficient was estimated using the equation ($\ln \varepsilon = k \ln D + a$) based on work by Liu *et al*., where ε is the extinction coefficient in M^{-1} cm^{-1}, D is the core diameter of the nanoparticles, and k = 3.32111, a = 10.80505 (See Figure 5.3.1).[38] This aliquot of gold nanospheres was centrifuged for 15 min at 14,000 rpm, the supernatant was removed and the nanospheres resuspended in the equivalent volume of nanopure water. This wash step was repeated 2 additional times and the final resuspension was in 100 µL of a 2 µM dNTP solution in aptamer incubation buffer. The washed gold nanospheres were incubated in this 2 µM dNTP solution for 30 min at room

temperature on a shaking thermomixer (1200 rpm) and then the supernatant was removed (Eppendorf AG, Hamburg, Germany).

Before selection, each 3.5 μM random ssDNA library aliquot (100 μL) in aptamer incubation buffer was heated to 90 °C for 10 min, 4 °C for 15 min and 24 °C for 5 min. After cooling, the aliquot was added to the gold nanospheres and allowed to incubate at room temperature for 30 min on a shaking thermomixer (1200 rpm). After incubation, the supernatant was removed and the next denatured random ssDNA library aliquot was added. These steps were repeated for a total of 10 incubation rounds. After the 10^{th} round, the supernatant was removed and the gold nanospheres were washed six times with 100 μL of incubation buffer. Following the final wash, a PCR mix was added to the gold nanospheres and an exponential PCR reaction with unmodified primers was conducted to amplify the ssDNA that remained bound to the gold nanosphere surface (200 μM dNTPs, 60 nM forward primer, 60 nM reverse primer, 0.05 unit/μL GoTaq polymerase, 1X colorless GoTaq buffer). Twenty-five cycles of denaturation (95 °C, 30 s), annealing (47 °C, 30 s), and extension (72 °C, 30 s) were conducted. Final PCR product was purified using the Qiagen MinElute PCR Purification Kit with the manufacturer's protocol (Qiagen, Inc., Gaithersburg, MD).

5.2.5 Cloning and Sequencing of Aptamer Candidates

Purified PCR product was cloned into *Escherichia coli* using the TOPO TA Cloning Kit (Invitrogen, Life Technologies, Grand Island, NY). Transformed bacteria were plated on LB-agar medium supplemented with ampicillin and X-gal, followed by overnight growth in a 37 °C incubator. Sanger sequencing was then carried out as described in Chapter 3.

Twenty positive bacterial colonies out of several hundred colonies from both aptamer selection cases (normal & A-rich random ssDNA libraries) were randomly picked and sequenced at Genewiz Inc. (South Plainfield, NJ). Identified sequences were labeled as aptamer candidates since dissociation constants have not been attained through binding affinity analysis.

5.2.6 Primary and Secondary Structure Analysis of Aptamer Candidates

The identified aptamer candidates were analyzed and aligned using Geneious 7.1.2 (Biomatters Ltd., Auckland, New Zealand). Focusing on the 40 base variable segment of the candidates (bases 15-54 of the 69 base-long sequences), Geneious 7.1.2 was used to perform a multiple sequence alignment across all identified aptamer candidates for the gold nanospheres and to generate a distance matrix for pairwise similarity comparisons between sequences (Biomatters, Available from http://www.geneious.com). Online software MEME 4.9.1 was used to identify sequence motifs that could occur at any position throughout the length of the 40 base variable region of the candidate sequences.[99, 150]

UNAFOLD (also known by its older nomenclature as Mfold) software[100] was used to predict and analyze the thermodynamically favorable secondary structures of the candidates under the given salt conditions ($[Na^{+}]$ = 152 mM, $[Mg^{++}]$ = 4 mM). Base-pair maps were constructed based on the base pairs indicated in the Mfold-predicted secondary structures for each candidate. Aptamer candidates were also grouped by their secondary structure similarities by noting the presence of the following structural features in their predicted secondary structures: single-stranded segments, duplex regions (not

associated with a hairpin), hairpins, interior loops, bulges and multi-branched loops. Structures sharing the same number of these specific features were grouped together.

5.2.7 Aptamer Candidate Incubation with Gold Nanoparticle Seed Solution

Gold nanoparticle seeds were synthesized as previously described. Immediately after synthesis, the aptamer candidate was incubated at a final concentration of 2 μM in a 1 mL total volume of the seed solution. The suspension was then mixed on a rotomixer and examined at 2 h and 7 d timepoints using UV-Vis analysis. For the 2 h and 7 d timepoints, UV-Vis spectra were gathered at 1 nm intervals using a Biotek Synergy H1 Hybrid Reader. Spectra for each set of samples were first normalized against a water blank and the reported spectra for all samples were normalized to the same relative absorbance value of 0.3 at 400 nm as others have done in previous studies.[132] Samples were additionally characterized via transmission electron microscopy. TEM images were acquired with a JEOL 100CX II transmission electron microscope at 100 kV. Samples for TEM were centrifuged (14,000 rpm x 15 min) twice to remove surfactant and redispersed in nanopure water. After redispersion, the sample was drop-cast onto a carbon-coated copper TEM grid and allowed to dry at room temperature.

5.3 Results and Discussion

5.3.1 Preparation and growth of spherical gold nanoparticles (AuNPs)

Spherical gold nanoparticles (AuNPs) were analyzed via TEM and UV-vis spectroscopy at 11 days post-aging from gold nanoparticle seeds as shown in Figure 5.3.1. Average nanoparticle diameter was estimated to be 15.8 ± 5.5 nm.

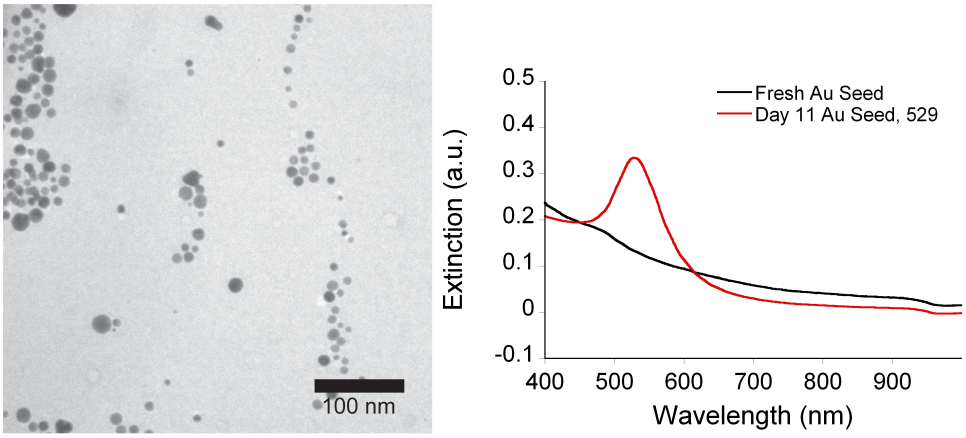

Figure 5.3.1. TEM micrograph of gold seed aged for 11 days (AuNPs) with accompanying UV-Vis spectra with resulting peak wavelength value included in the legend.

5.3.2 Competition-Induced Selection of Ligands (CISL)

Aptamer selection was performed in two separate CISL-based screening sessions for a target of gold nanospheres (AuNPs) using normal and A-rich random ssDNA libraries in separate cases under otherwise identical selection conditions. As stated previously, the choice of employing an A-rich library is based on the previous study reported in Chapter 4 that indicated both adenine-rich ssDNA and pure polyadenine induce aggregation of gold nanoparticles during their seeded growth as evidenced by a red-shift and overall broadening in the characteristic extinction peak. As detailed previously, the key differences between the competition-induced selection of ligands (CISL) approach used in the current work and the widely implemented "Systematic Evolution of Ligands by Exponential Enrichment" (SELEX) process for the selection of aptamers stems from the elimination of intermittent oligonucleotide elution and amplification steps.

As illustrated in Figure 5.3.2, the CISL process begins with the preparation of the amplified random ssDNA library. Each random ssDNA library consisted of sequences that are 69 bases in length that contain a 40-base central randomized region flanked by two primer binding regions. The random ssDNA template libraries were exponentially amplified via PCR with a phosphorylated reverse primer which ultimately enabled selective digestion of the resulting hybridization partners in the dsDNA product with lambda exonuclease to yield the amplified ssDNA (~10^7 copies of each unique template strand from starting library).[102] Generation of ssDNA from dsDNA via lambda exonuclease digestion was confirmed by exposing dsDNA PCR product and lambda exonuclease-generated ssDNA product to Exonuclease I (Exo I), which selectively degrades ssDNA and not dsDNA in the 3' to 5' direction.[104]

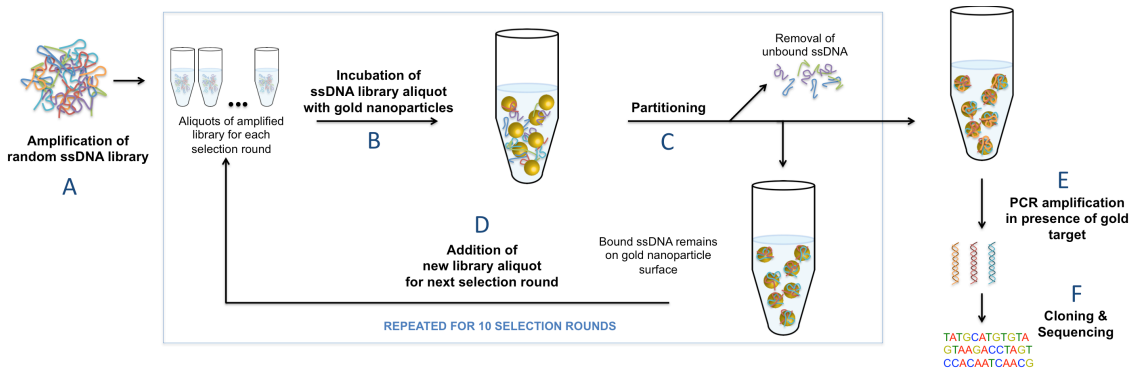

Figure 5.3.2. Schematic overview of the competition-induced selection of ligands (CISL) aptamer screening process that involves the following steps: (A) preparation of the random ssDNA library by PCR amplification and lambda exonuclease digestion; (B) incubation of the amplified random ssDNA library with a suspension of the AuNPs target; (C) removal of unbound ssDNA after incubation round; (D) addition of new aliquot of amplified random ssDNA library for the next selection round. After steps (A) - (C) have been repeated for a total of 10 rounds, then the next steps are (E) PCR amplification of bound ssDNA in presence of AuNPs target; and finally the AuNPs are removed and the sequences in the supernatant undergo (F) cloning and sequencing of identified aptamer candidates.

An aliquot of the amplified random ssDNA library (3.5 μM) was incubated with a solution of AuNPs within a PCR tube (~ 10^{11} AuNPs, avg. diameter = 15.8 ± 5.5 nm). This concentration of ssDNA was chosen in order to ensure an excess of ssDNA with a simple random coil conformation are available for monolayer coverage (~ 2D hexagonal packing density) of the AuNPs ($R_{g,69\text{ base ssDNA}}$ ~ 3.32 nm) compared to the total surface area of the AuNPs in solution (total surface area ~ 784.3 nm^2). After each incubation round, non-binding sequences are removed and a new aliquot of random ssDNA library is added to the suspension of AuNPs for the next selection round in the presence of any existing sequence adsorbates. After the 10^{th} and final incubation round, non-binding sequences are removed and PCR amplification is performed in the presence of the gold nanospheres to amplify the bound sequences and allow for cloning and sequencing of the identified aptamer candidates. In total, 24 aptamer sequences were identified from two CISL screening sessions using normal or A-rich random ssDNA libraries for each session.

5.3.3 Primary Structure Analysis of Aptamer Candidates

The 24 sequences were analyzed to identify both position-dependent and position-independent similarities in their primary structures. For primary structure analysis, the conservation of the base type by numerical position was assessed using Geneious software. Figure 5.3.3 shows the resulting multiple sequence alignment of the central 40-base variable segment (bases 15-54). The highlighted bases indicate specific positions that are conserved in at least 50% of all 24 sequences. In light of this potentially rich variety of sequence candidates, Figure 5.3.3 reveals that there are still 6 base positions conserved in at least 50% of the 24 sequences. Assuming the ideal conditions in which the initial unamplified ssDNA template libraries possess only unique sequences, we

estimate that the target is ultimately exposed to as many as 10^{15} sequences following 10 selection rounds.

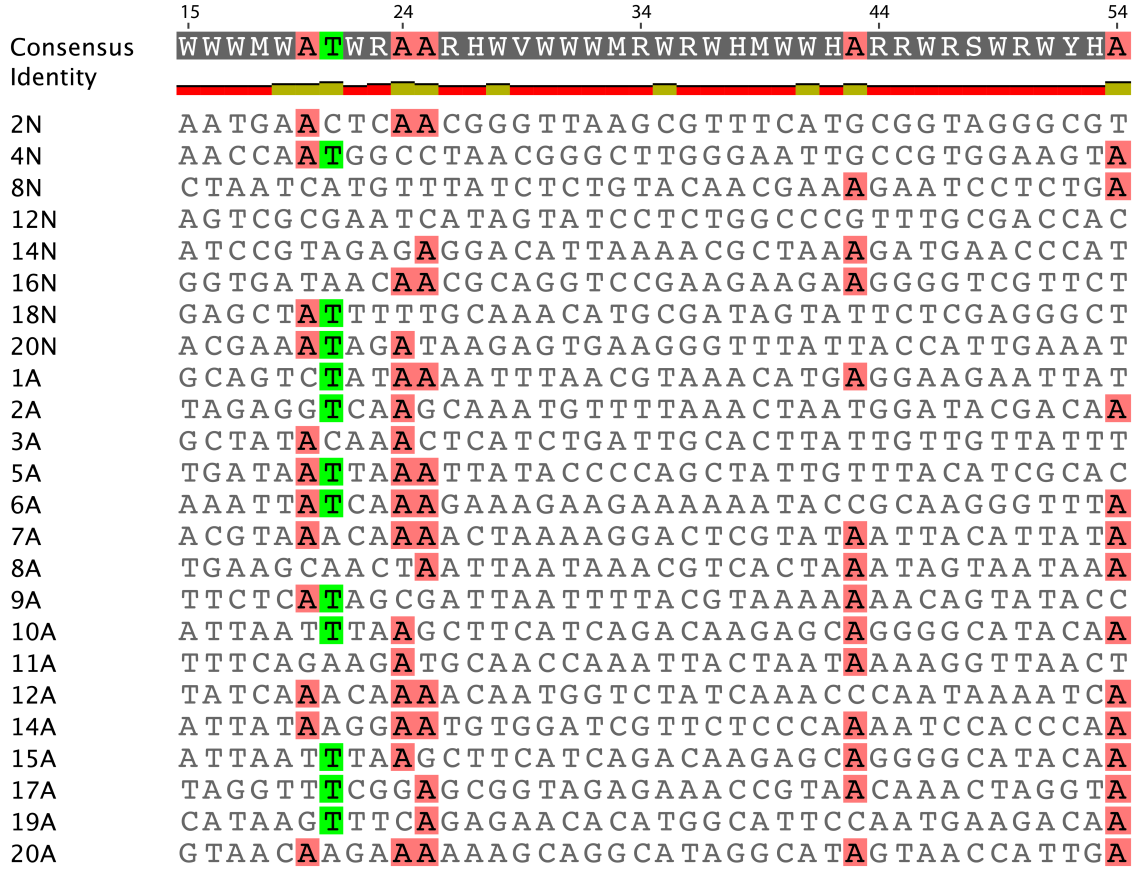

Figure 5.3.3. Multiple sequence alignment of the central variable base segments of AuNP-binding sequences identified from both the normal and A-rich random libraries indicated by the letters "N" and "A", respectively in the aptamer nomenclature in the left column. Highlighted bases indicated base positions found in at least 50% of all 24 sequences (base 20 = A in 12 sequences; base 21 = T in 12 sequences; base 24 = A in 15 sequences; base 25 =A in 13 sequences; base 43 = A in 13 sequences; base 54 = A in 13 sequences). The full-length or 69 base-long sequences include two constant segments (bases 1-14 and bases 55-69) intended to serve as primer hybridization sites and a central variable segment (40N): 5'-GGGACAGGGCTAGC(40N) GAGGCAAAGCTTCCG -3'. Alignment output generated with Geneious 7.1.2.

Pairwise comparisons were also conducted with all sequences in Geneious to create a distance matrix that yielded information on degrees of similarity between sequence pairs as shown in Figure 5.3.4.

	2N	4N	8N	12N	14N	16N	18N	20N	1A	2A	3A	5A	6A	7A	8A	9A	10A	11A	12A	14A	15A	17A	19A	20A
2N		27.5%	12.5%	22.5%	22.5%	30.0%	27.5%	35.0%	20.0%	25.0%	25.0%	25.0%	22.5%	25.0%	22.5%	10.0%	30.0%	22.5%	30.0%	27.5%	30.0%	25.0%	27.5%	20.0%
4N	27.5%		17.5%	25.0%	17.5%	20.0%	27.5%	32.5%	20.0%	25.0%	32.5%	22.5%	32.5%	15.0%	12.5%	27.5%	20.0%	22.5%	37.5%	22.5%	20.0%	25.0%	32.5%	22.5%
8N	12.5%	17.5%		17.5%	30.0%	20.0%	20.0%	12.5%	32.5%	37.5%	25.0%	15.0%	30.0%	25.0%	25.0%	27.5%	35.0%	27.5%	20.0%	37.5%	35.0%	32.5%	17.5%	42.5%
12N	22.5%	25.0%	17.5%		30.0%	20.0%	12.5%	10.0%	22.5%	20.0%	20.0%	27.5%	15.0%	25.0%	32.5%	17.5%	27.5%	15.0%	27.5%	35.0%	27.5%	12.5%	20.0%	30.0%
14N	22.5%	17.5%	30.0%	30.0%		30.0%	20.0%	20.0%	20.0%	32.5%	25.0%	27.5%	27.5%	27.5%	30.0%	25.0%	37.5%	30.0%	25.0%	45.0%	37.5%	27.5%	30.0%	27.5%
16N	30.0%	20.0%	20.0%	20.0%	30.0%		20.0%	22.5%	37.5%	30.0%	20.0%	17.5%	27.5%	17.5%	30.0%	22.5%	32.5%	30.0%	32.5%	25.0%	32.5%	17.5%	20.0%	30.0%
18N	27.5%	27.5%	20.0%	12.5%	20.0%	20.0%		27.5%	27.5%	25.0%	32.5%	35.0%	32.5%	22.5%	25.0%	25.0%	15.0%	30.0%	25.0%	20.0%	15.0%	32.5%	37.5%	10.0%
20N	35.0%	32.5%	12.5%	10.0%	20.0%	22.5%	27.5%		22.5%	30.0%	35.0%	25.0%	32.5%	35.0%	30.0%	37.5%	22.5%	40.0%	20.0%	22.5%	22.5%	20.0%	35.0%	22.5%
1A	20.0%	20.0%	32.5%	22.5%	20.0%	37.5%	27.5%	22.5%		32.5%	35.0%	25.0%	42.5%	30.0%	35.0%	25.0%	30.0%	25.0%	27.5%	30.0%	30.0%	37.5%	25.0%	37.5%
2A	25.0%	25.0%	37.5%	20.0%	32.5%	30.0%	25.0%	30.0%	32.5%		35.0%	27.5%	42.5%	20.0%	20.0%	22.5%	35.0%	25.0%	45.0%	22.5%	35.0%	30.0%	35.0%	27.5%
3A	25.0%	32.5%	25.0%	20.0%	25.0%	20.0%	32.5%	35.0%	35.0%	35.0%		32.5%	25.0%	22.5%	17.5%	17.5%	25.0%	32.5%	27.5%	27.5%	25.0%	22.5%	20.0%	22.5%
5A	25.0%	22.5%	15.0%	27.5%	27.5%	17.5%	35.0%	25.0%	25.0%	27.5%	32.5%		30.0%	25.0%	30.0%	27.5%	27.5%	17.5%	27.5%	27.5%	27.5%	20.0%	35.0%	25.0%
6A	22.5%	32.5%	30.0%	15.0%	27.5%	27.5%	32.5%	32.5%	42.5%	42.5%	25.0%	30.0%		45.0%	22.5%	25.0%	25.0%	25.0%	40.0%	20.0%	25.0%	35.0%	35.0%	45.0%
7A	25.0%	15.0%	25.0%	25.0%	27.5%	17.5%	22.5%	35.0%	30.0%	20.0%	22.5%	25.0%	45.0%		40.0%	35.0%	37.5%	32.5%	37.5%	35.0%	37.5%	32.5%	27.5%	45.0%
8A	22.5%	12.5%	25.0%	32.5%	30.0%	30.0%	25.0%	30.0%	35.0%	20.0%	17.5%	30.0%	22.5%	40.0%		37.5%	27.5%	32.5%	30.0%	27.5%	27.5%	25.0%	37.5%	30.0%
9A	10.0%	27.5%	27.5%	17.5%	25.0%	22.5%	25.0%	37.5%	25.0%	22.5%	17.5%	27.5%	25.0%	35.0%	37.5%		27.5%	35.0%	27.5%	25.0%	27.5%	25.0%	20.0%	25.0%
10A	30.0%	20.0%	35.0%	27.5%	37.5%	32.5%	15.0%	22.5%	30.0%	35.0%	25.0%	27.5%	25.0%	37.5%	27.5%	27.5%		27.5%	22.5%	32.5%	100%	22.5%	32.5%	27.5%
11A	22.5%	22.5%	27.5%	15.0%	30.0%	30.0%	30.0%	40.0%	25.0%	25.0%	32.5%	17.5%	25.0%	32.5%	32.5%	35.0%	27.5%		42.5%	25.0%	27.5%	27.5%	35.0%	27.5%
12A	30.0%	37.5%	20.0%	27.5%	25.0%	32.5%	25.0%	20.0%	27.5%	45.0%	27.5%	27.5%	40.0%	37.5%	30.0%	27.5%	22.5%	42.5%		22.5%	22.5%	35.0%	37.5%	35.0%
14A	27.5%	22.5%	37.5%	35.0%	45.0%	25.0%	20.0%	22.5%	30.0%	22.5%	27.5%	27.5%	20.0%	35.0%	27.5%	25.0%	32.5%	25.0%	22.5%		32.5%	30.0%	30.0%	35.0%
15A	30.0%	20.0%	35.0%	27.5%	37.5%	32.5%	15.0%	22.5%	30.0%	35.0%	25.0%	27.5%	25.0%	37.5%	27.5%	27.5%	100%	27.5%	22.5%	32.5%		22.5%	32.5%	27.5%
17A	25.0%	25.0%	32.5%	12.5%	27.5%	17.5%	32.5%	20.0%	37.5%	30.0%	22.5%	20.0%	35.0%	32.5%	25.0%	25.0%	22.5%	27.5%	35.0%	30.0%	22.5%		22.5%	30.0%
19A	27.5%	32.5%	17.5%	20.0%	30.0%	20.0%	37.5%	35.0%	25.0%	35.0%	20.0%	35.0%	35.0%	27.5%	37.5%	20.0%	32.5%	35.0%	37.5%	30.0%	32.5%	22.5%		10.0%
20A	20.0%	22.5%	42.5%	30.0%	27.5%	30.0%	10.0%	22.5%	37.5%	27.5%	22.5%	25.0%	45.0%	45.0%	30.0%	25.0%	27.5%	27.5%	35.0%	35.0%	27.5%	30.0%	10.0%	

Figure 5.3.4. Primary sequence pairwise distance matrix for all aptamer candidates. Generated with Geneious 7.1.2 created by Biomatters. Available from http://www.geneious.com.

This matrix revealed that sequences from clones **10A** and **15A** were identical. With the exception of these two identical sequences, the maximum percentage in base position consensus is 45% among 5 subgroups of sequences shown in Figure 5.3.5. Consensus motifs were also evaluated using MEME, however none of the identified motifs from this analysis resulting from CISL-based screening were statistically significant (in which E values were less than 0.01).[151]

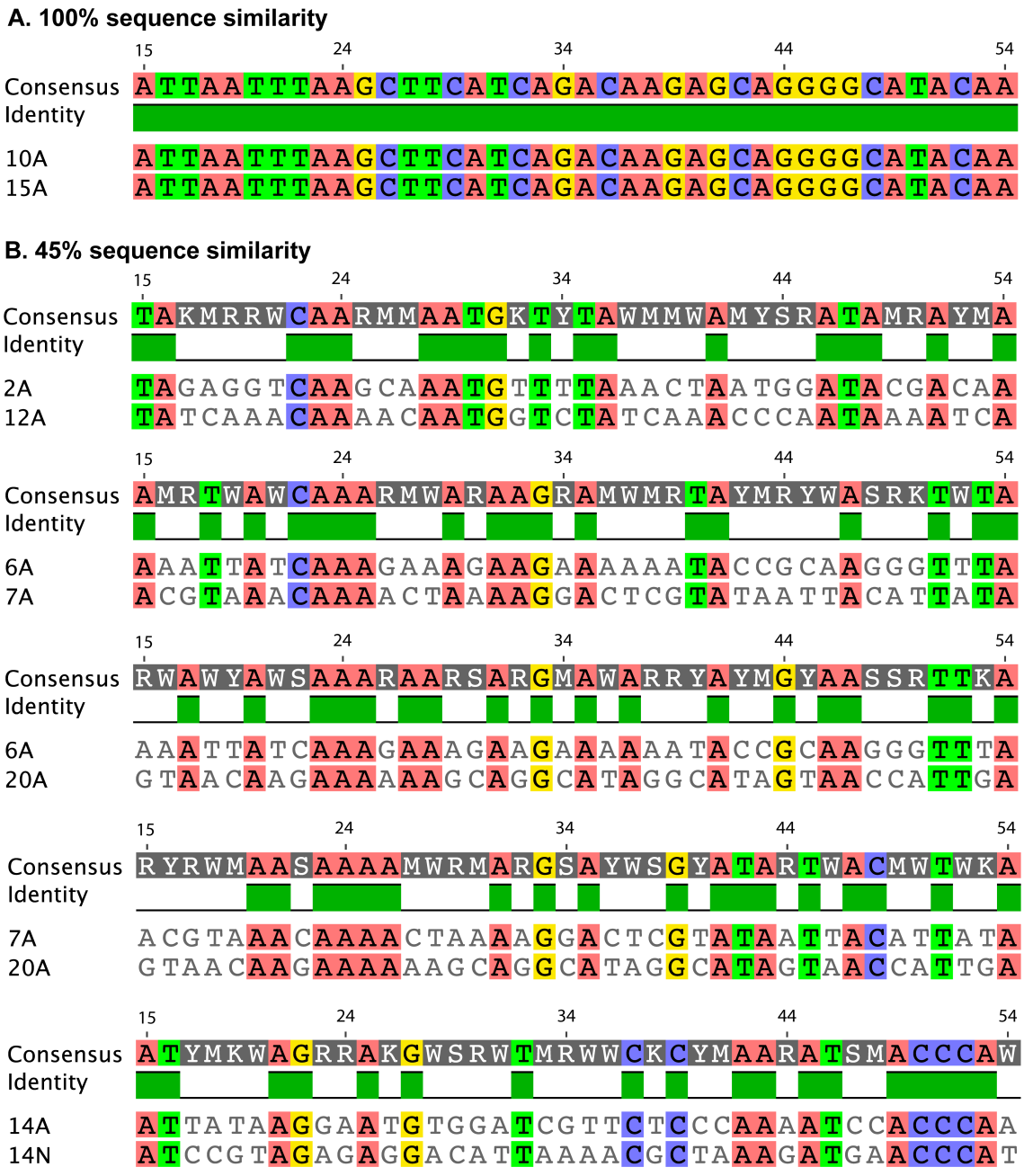

Figure 5.3.5. Pairwise sequence alignment of the central variable base segments of AuNP-binding sequences identified from both the normal and A-rich random libraries that exhibit (A) 100% sequence similarity and (B) 45% sequence similarity.

5.3.4 Predicted Secondary Structure Analysis of Aptamer Candidates

The 24 sequences were next analyzed to identify both position-dependent and position-independent similarities in base pairings that result in a variety of predicted secondary structures. The UNAFOLD server (also know by its older nomenclature as Mfold) was used to predict thermodynamically favorable secondary structures for all candidates under the same salt conditions used during selection rounds.[100] UNAFOLD predictions take into account Watson-Crick base-pair matches as well as occasional G-T wobble base pairs that are flanked by Watson-Crick base pair matches. The entire 69-base length of the sequences is included in UNAFOLD analysis since the primer binding segments can influence the overall secondary structure. The predicted secondary structures for all candidates with accompanying self-melt temperatures (T_m) and Gibbs free energy (dG) are shown in Figures 5.3.6 and 5.3.7.

Aptamer candidates selected from the normal library

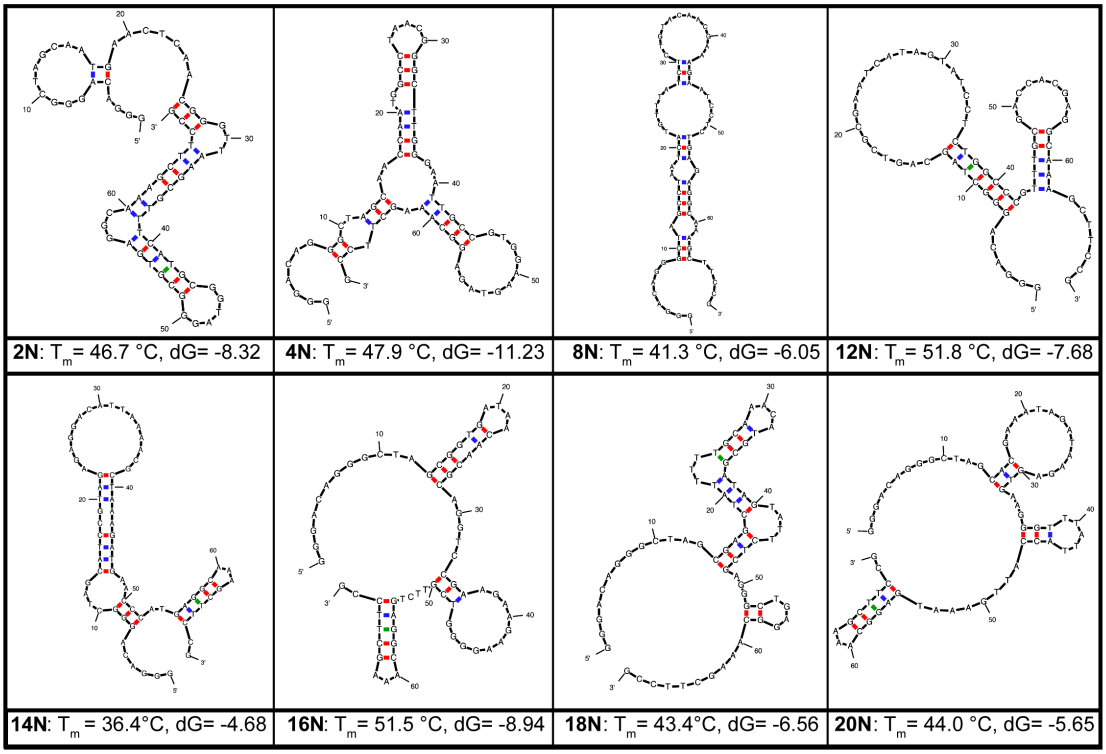

Figure 5.3.6. Thermodynamically favorable secondary structures of the 8 aptamer sequences selected from the normal random library (25% of each base) for AuNP. Predicted structures were generated using UNAFOLD (http://mfold.rna.albany.edu/?q=mfold/DNA-Folding-Form, access date: July 23, 2014) under the following solution conditions: T=23 °C, 152 mM [Na^{+}], 4 mM [Mg^{++}]. The position-specific (with base #1 at the 5' end and base #69 at the 3' end) base pairings are color-coded as follows: A-T and T-A (blue); G-C and C-G (red); G-T and T-G (green). The Gibbs free energy associated with self-hybridization, dG, is provided in units of kcal/mol.

Aptamer candidates selected from the A-rich library

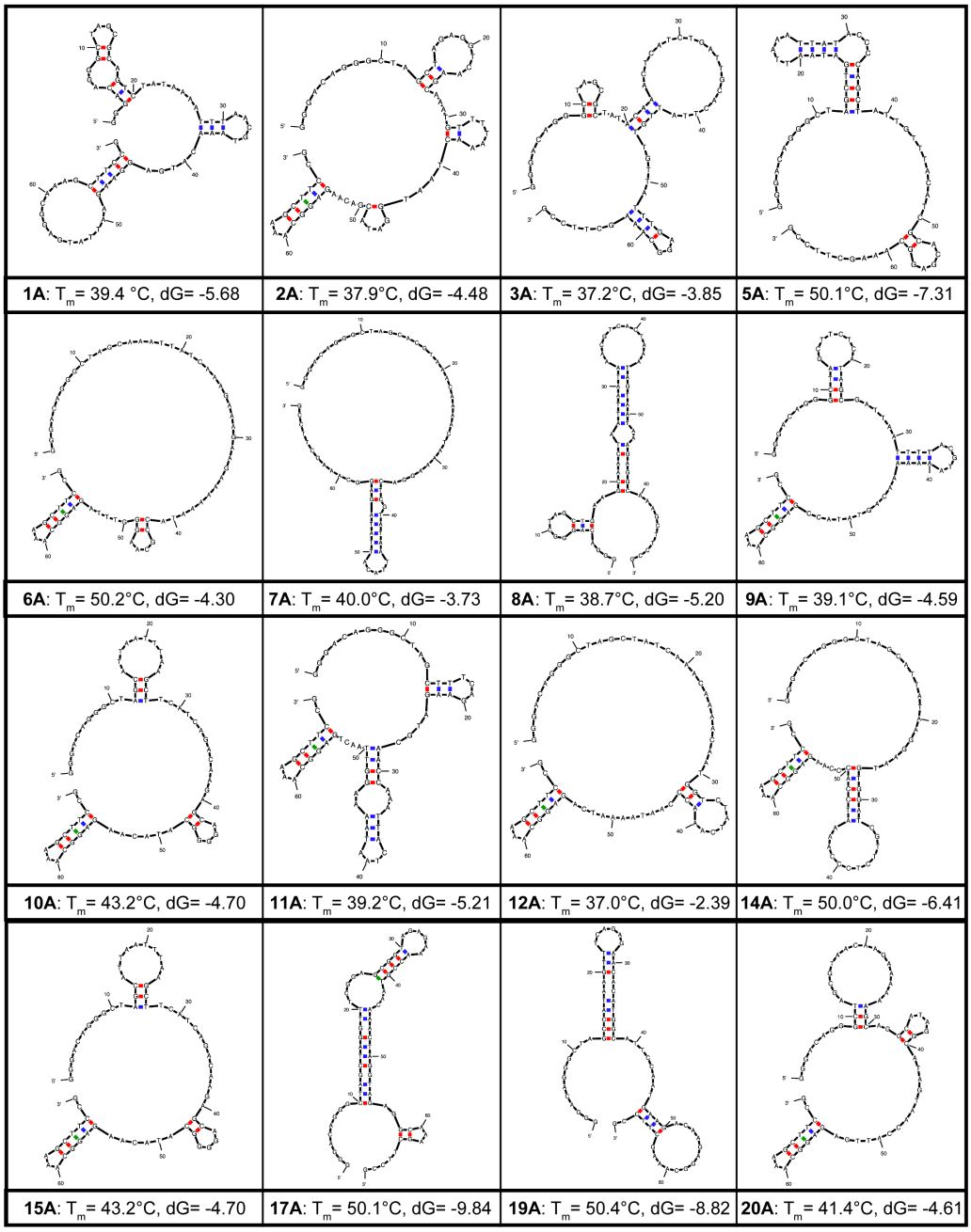

Figure 5.3.7. Thermodynamically favorable secondary structures of the 16 aptamer sequences selected from the A-rich random library (40% A, 20% each of C, T, G) for AuNP. Predicted structures were generated using UNAFOLD (http://mfold.rna.albany.edu/?q=mfold/DNA-Folding-Form, access date: July 23, 2014) under the following solution conditions: T=23 °C, 152 mM [Na^+], 4 mM [Mg^{++}]. The position-specific (with base #1 at the 5' end and base #69 at the 3' end) base pairings are color-coded as follows: A-T and T-A (blue); G-C and C-G (red); G-T and T-G (green). The Gibbs free energy associated with self-hybridization, dG, is provided in units of kcal/mol.

To specifically pinpoint conserved position-dependent base pairing at specific base positions due to self-hybridization, a base pairing map was then constructed using the 24 predicted secondary structures. As shown in Figure 5.3.8, the leftmost half of the map shows position-dependent base pairings that are located in two or more secondary structures to specifically highlight shared base pairings across all the candidate sequences while the bottom rightmost half shows all base pair interactions, both shared and unshared. Notably, many (62 in total) of the shared base-pairings in the leftmost half of the map correspond to conserved primer binding segments; however, as shown in the tabulated form of this base pairing map in Table 5.3.1, there are still numerous (20 in total) base pair interactions solely due to base pairing in the variable region and several (14 in total) base pairings involving both conserved and variable bases of the 24 sequences. As shown in Table 5.3.2, aptamer sequences **10A**, **14A** and **15A** each exhibited the maximum of 10 shared base pairings with at least 12 other aptamer sequences.

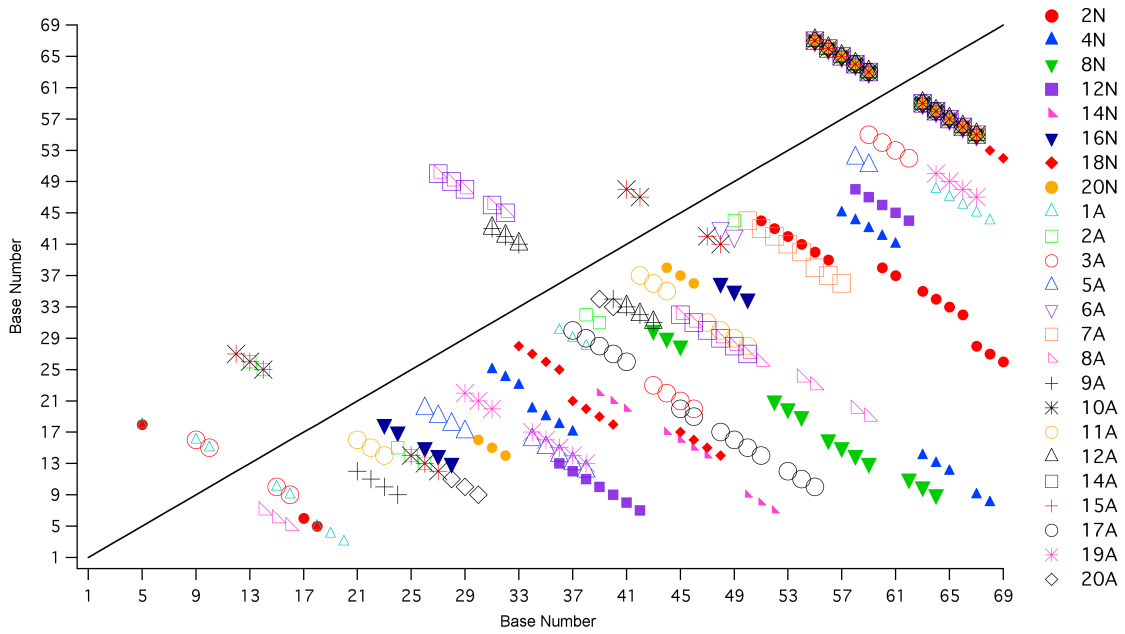

Figure 5.3.8. Base-pair map highlighting all base pair interactions for each aptamer candidate (below the line) and the shared base pair interactions between aptamer candidates (above the line). Detailed lists of all shared and unshared position-dependent base pair interactions for all 24 sequences are provided in Tables 5.3.1 and 5.3.2.

Table 5.3.1. List of the position-dependent identities of base pairs shared by two or more aptamer sequences. Base positions in red indicate positions within random variable region of the sequence.

Base Pair	Sequence (Pair Type)	Sequence (Pair Type)	Sequence (Pair Type)	Sequence (Pair Type)	Sequence (Pair Type)	Sequence (Pair Type)	Sequence (Pair Type)	Sequence (Pair Type)	Sequence (Pair Type)	Sequence (Pair Type)	Sequence (Pair Type)	Sequence (Pair Type)	Sequence (Pair Type)
5, 18	2N (C-G)	1A (C-G)											
9, 16	1A (G-C)	3A (G-C)											
10, 15	1A (C-G)	3A (C-G)											
12, 27	10A (A-T)	15A (A-T)											
13 ,26	2A (G-C)	10A (G-C)	15A (G-C)										
14, 25	2A (C-G)	10A (C-G)	15A (C-G)										
27, 50	8A (T-A)	14A (G-C)											
28, 49	8A (T-A)	14A (T-A)											
29, 48	8A (A-T)	14A (G-C)											
31, 43	9A (T-A)	12A (G-C)											
31, 46	8A (T-A)	14A (A-T)											
32, 42	9A (T-A)	12A (G-C)											
32, 45	8A (A-T)	14A (T-A)											
33,41	9A (T-A)	12A (T-A)											
41, 48	10A (G-C)	15A (G-C)											
42, 47	10A (C-G)	15A (C-G)											
55, 67	14N (G-C)	16N (G-C)	20N (G-C)	2A (G-C)	6A (G-C)	9A (G-C)	10A (G-C)	11A (G-C)	12A (G-C)	14A (G-C)	15A (G-C)	20A (G-C)	
56, 66	14N (C-G)	16N (C-G)	20N (C-G)	2A (C-G)	6A (C-G)	9A (C-G)	10A (C-G)	11A (C-G)	12A (C-G)	14A (C-G)	15A (C-G)	20A (C-G)	
57, 65	14N (T-G)	16N (T-G)	20N (T-G)	2A (T-G)	6A (T-G)	9A (T-G)	10A (T-G)	11A (T-G)	12A (T-G)	14A (T-G)	15A (T-G)	20A (T-G)	
58, 64	14N (T-A)	16N (T-A)	20N (T-A)	2A (T-A)	6A (T-A)	9A (T-A)	10A (T-A)	11A (T-A)	12A (T-A)	14A (T-A)	15A (T-A)	17A (T-A)	20A (T-A)
59, 63	14N (C-G)	16N (C-G)	20N (C-G)	2A (C-G)	6A (C-G)	9A (C-G)	10A (C-G)	11A (C-G)	12A (C-G)	14A (C-G)	15A (C-G)	17A (C-G)	20A (C-G)

Table 5.3.2. List of all aptamer sequences and the total number of position-dependent base pairs shared with other aptamer sequences as well as the total number and nomenclature of aptamer sequences with at least one shared base pairing for a given aptamer sequence.

Sequence	Total number of shared base pair positions	Number (and aptamer nomenclature) of sequences with at least one shared base pair
2N	1	1 (1A)
4N	0	0
8N	0	0
12N	0	0
14N	5	12 (16N, 20N, 2A, 6A, 9A, 10A, 11A, 12A, 14A, 15A, 17A, 20A)
16N	5	12 (14N, 20N, 2A, 6A, 9A, 10A, 11A, 12A, 14A, 15A, 17A, 20A)
18N	0	0
20N	5	12 (14N, 16N, 2A, 6A, 9A, 10A, 11A, 12A, 14A, 15A, 17A, 20A)
1A	3	2 (2N, 3A)
2A	7	12 (14N, 16N, 20N, 6A, 9A, 10A, 11A, 12A, 14A, 15A, 17A, 20A)
3A	2	1 (1A)
5A	0	0
6A	5	12 (14N, 16N, 20N, 2A, 9A, 10A, 11A, 12A, 14A, 15A, 17A, 20A)
7A	0	0
8A	5	1 (14A)
9A	8	12 (14N, 16N, 20N, 2A, 6A, 10A, 11A, 12A, 14A, 15A, 17A, 20A)
10A	10	12 (14N, 16N, 20N, 2A, 6A, 9A, 11A, 12A, 14A, 15A, 17A, 20A)
11A	5	12 (14N, 16N, 20N, 2A, 6A, 9A, 10A, 12A, 14A, 15A, 17A, 20A)
12A	8	12 (14N, 16N, 20N, 2A, 6A, 9A, 10A, 11A, 14A, 15A, 17A, 20A)
14A	10	13 (14N, 16N, 20N, 2A, 6A, 8A, 9A, 10A, 11A, 12A, 14A, 15A, 17A, 20A)
15A	10	12 (14N, 16N, 20N, 2A, 6A, 9A, 10A, 11A, 12A, 14A, 17A, 20A)
17A	2	12 (14N, 16N, 20N, 2A, 6A, 9A, 10A, 11A, 12A, 14A, 15A, 20A)
19A	0	0
20A	5	12 (14N, 16N, 20N, 2A, 6A, 9A, 10A, 11A, 12A, 14A, 15A, 17A)

To next investigate secondary structure similarity simply based on the presence of certain secondary structure features independent of base type or positioning, segments of the predicted secondary structures are classified according to the following features illustrated in Figure 5.3.9: single-stranded segments, duplex regions, hairpins, interior loops, bulges and multi-branched loops. Based on this classification of each sequence segment, the candidates are then arranged into subgroups that shared the same number of these six secondary structure features.

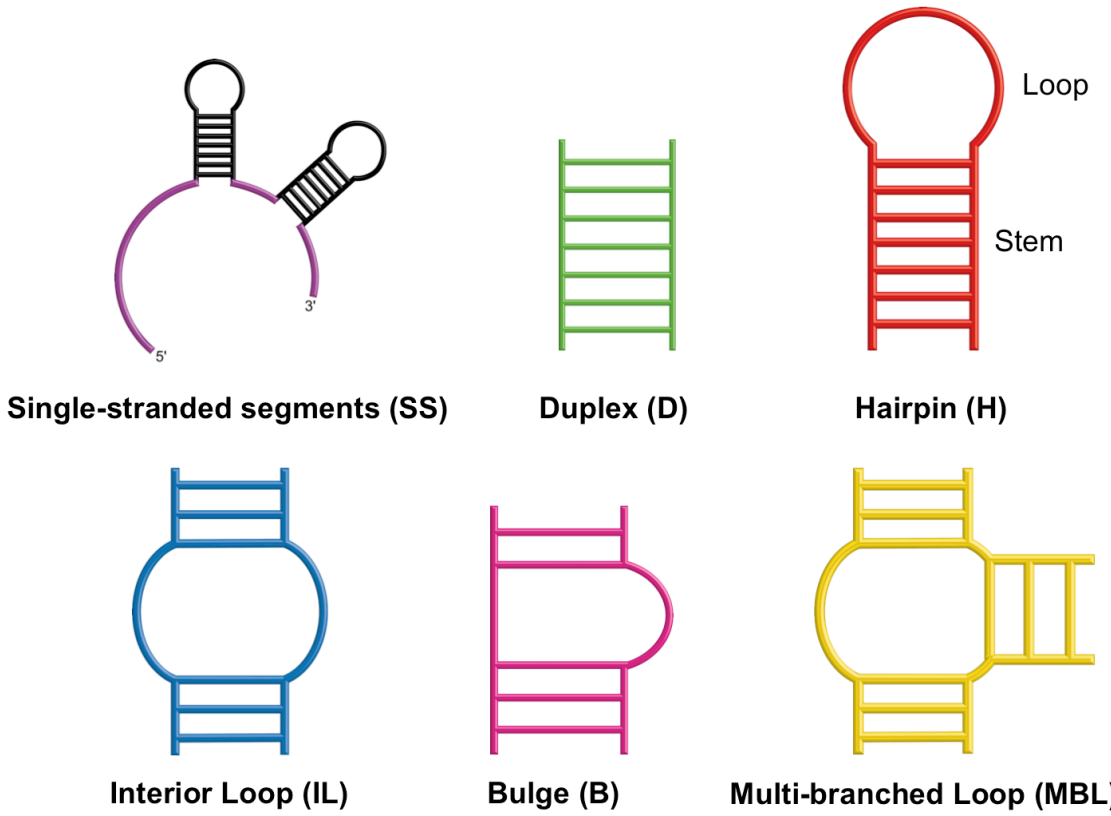

Figure 5.3.9. Schematic of secondary structure features to group aptamer sequences with identical or shared structural features.

As shown in Figure 5.3.10, this analysis revealed that the most populated subgroup is comprised of sequences exhibiting 3 hairpins and 4 single-stranded segments (notably, duplicate sequences **10A** and **15A** are present in this group), followed by a subgroup of sequences that have 2 hairpins and 3 single-stranded segments. It should also be noted that amongst all the sequences in Figure 5.3.10, an identical hairpin structure occurs in the primer-binding segment at the 3' end of the sequences in 8 out of the 12 secondary structures namely, **6A**, **10A**, **12A**, **14A**, **15A**, **20A**, **20N**. This information is easily verified by the tabulated, position-specific base pairing interactions in Table 5.3.1. As it relates to the pairwise primary sequence analysis discussed earlier (See Figure 5.3.4), in

the first subgroup of Figure 5, the highest percentage of primary sequence similarity is between sequences **20N** and **9A** at 37.5%. For the second subgroup, **6A** and **12A** exhibit 40% sequence similarity where in the third subgroup, **7A** and **8N** only shared 25% sequence similarity.

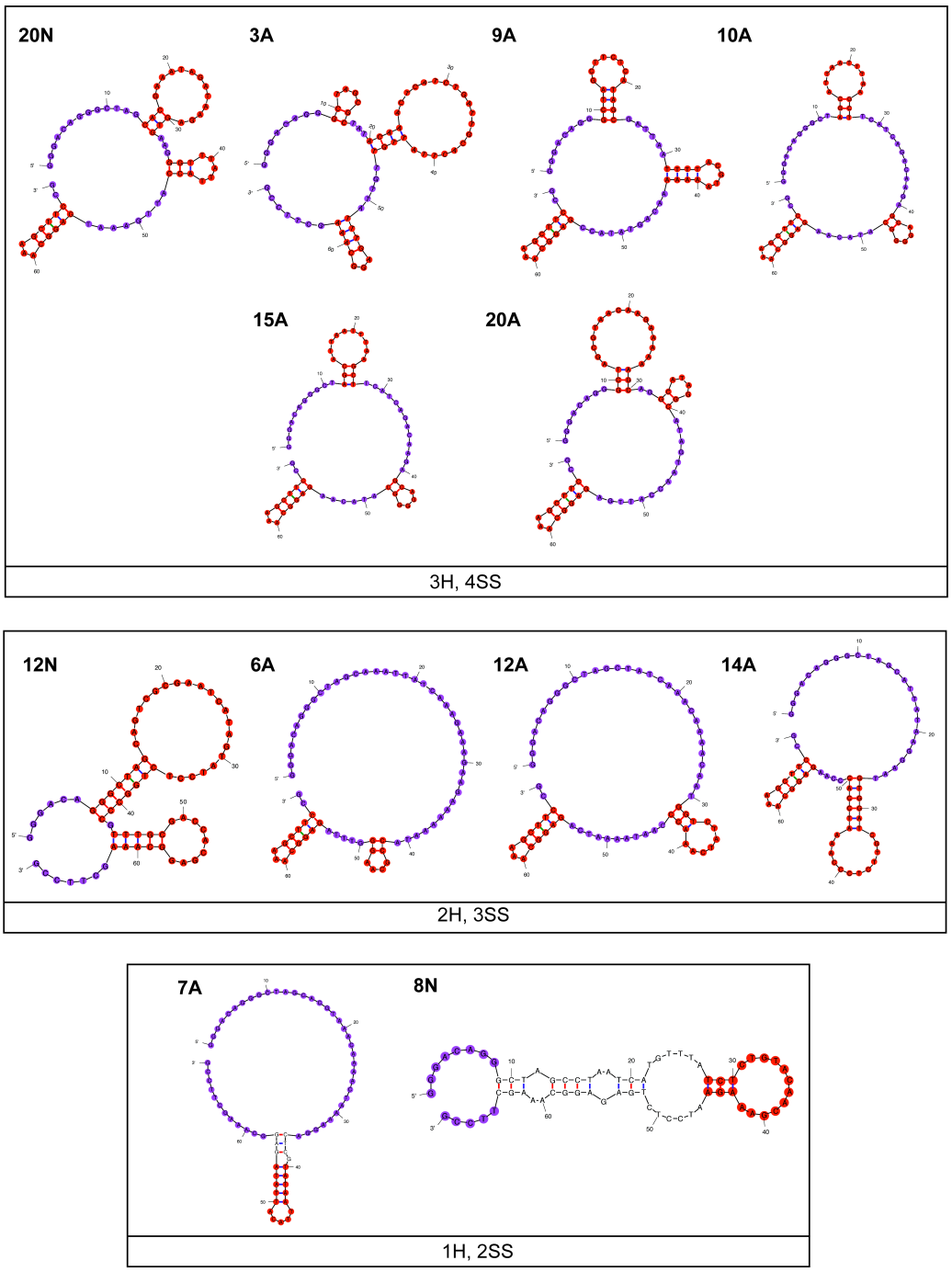

Figure 5.3.10. Three subgroups of aptamer candidates that share an identical number of types (hairpin (H) in red, single-stranded segment (SS) in purple) of secondary structure features. Any bases that are not part of the 1 hairpin or 2 single-stranded segments (seen in last subgroup) are not highlighted in color.

Other sets of smaller subgroupings of 2 or 3 sequences that shared identical 3 or even 4 structural features are shown in Figures 5.3.11 and 5.3.12. Notably, out of the 6 types of secondary structure features evaluated (Figure 5.3.9), the predicted secondary structures for all 24 sequences exhibited all features except for multi-branched loops (Table 5.3.3).

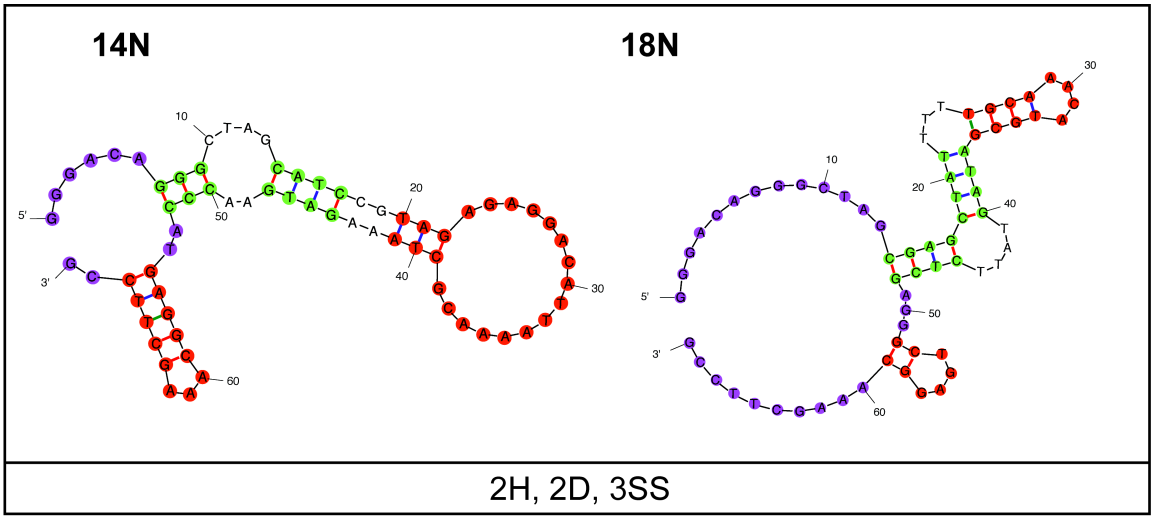

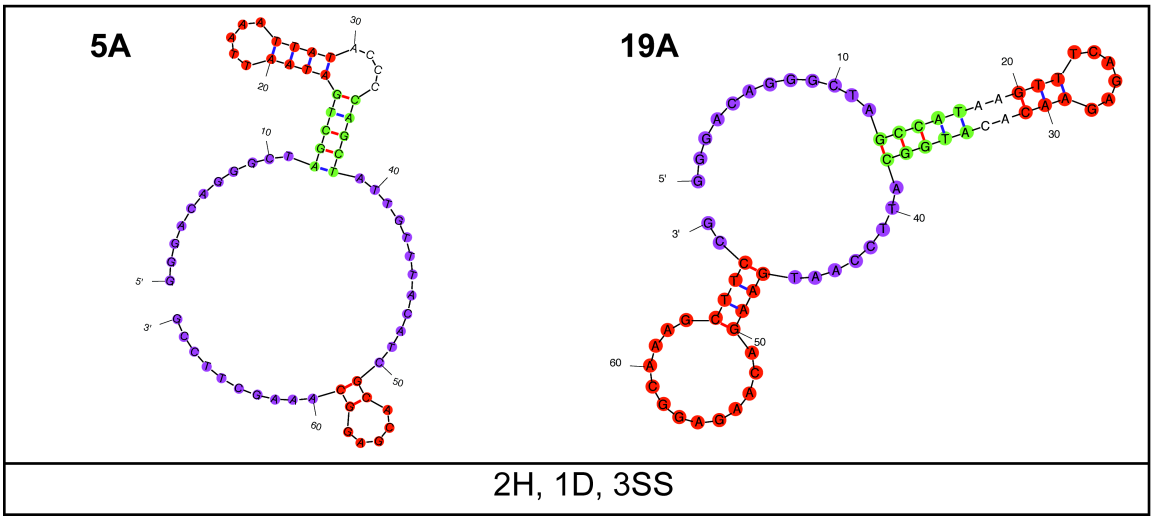

Figure 5.3.11. Two subgroups of aptamer candidates that share an identical number of types (hairpin (H) in red, duplex (D in green, single-stranded segments (SS) in purple) of secondary structural features. Any bases that are not part of the 2 hairpins, 1(or 2) duplex(es), or 3 single-stranded segments are not highlighted in color.

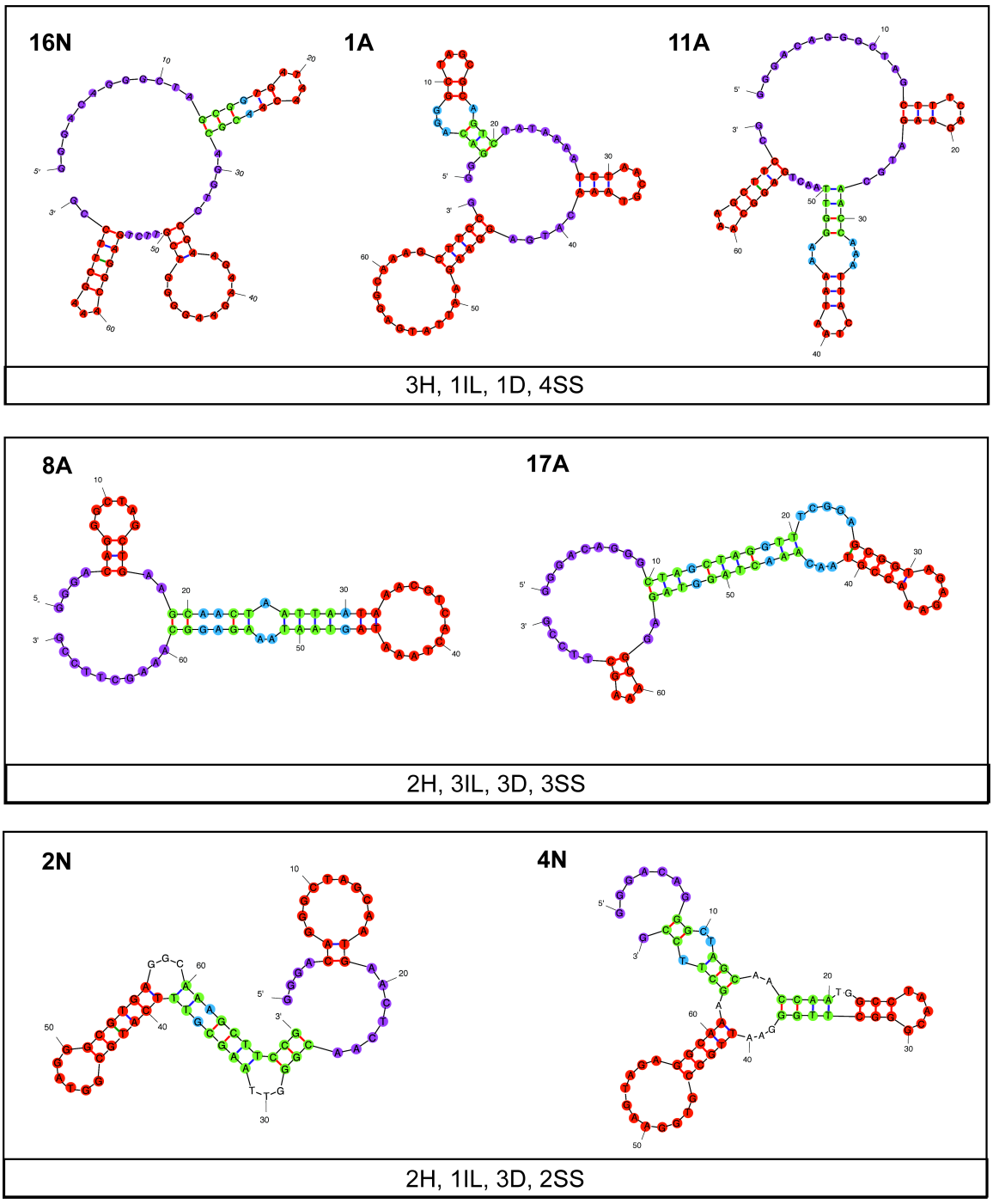

Figure 5.3.12. Three subgroups of aptamer candidates that share an identical number of types (hairpin (H) in red, interior loop (IL) in blue, duplex (D) in green, single-stranded segment (SS) in purple) of secondary structural features. Any bases that are not part of the 3(or 2) hairpins, 1(or 2) interior loops, 1(or 3) duplex(es), or 4(3 or 2) single-stranded segments are not highlighted in color.

Table 5.3.3. List of each aptamer sequence and the total number of hairpins (H), interior loops (IL), bulges (B), duplexes (D) and single-stranded segments (SS) found in its predicted secondary structure for AuNPs.

	Secondary Structure Features													
Sequence	1H	2H	3H	1IL	3IL	1B	2B	1D	2D	3D	2SS	3SS	4SS	Total
2N		X		X			X			X	X			5
4N		X		X		X				X	X			5
8N	X				X					X	X			4
12N		X										X		2
14N		X							X			X		3
16N			X	X				X					X	4
18N		X					X		X			X		4
20N			X										X	2
1A			X	X				X					X	4
2A														0
3A			X										X	2
5A		X				X		X				X		4
6A		X										X		2
7A	X					X		X			X			4
8A		X			X					X		X		4
9A			X										X	2
10A			X										X	2
11A			X	X				X					X	4
12A		X										X		2
14A		X										X		2
15A			X										X	2
17A		X			X					X		X		4
19A		X		X				X				X		4
20A			X										X	2
Total	2	12	9	6	3	3	2	6	2	5	4	10	9	
%	8.33	50.00	37.50	25.00	12.50	12.50	8.33	25.00	8.33	20.83	16.67	41.67	37.50	

5.3.4. Incubation of aptamer candidate (10A) with gold nanoparticle seed

Following primary and secondary structure analysis of aptamer candidates, one candidate was selected for an incubation study with gold nanoparticle seed to evaluate if the presence of the aptamer candidate during gold nanoparticle growth would affect resulting particle morphology and spectral properties. For these studies, the aptamer sequence **10A** was selected since it is a member of the most populated secondary structure subgroup family as shown in Figure 5.3.10 with each sequence member exhibiting three hairpins and four single-stranded segments. This sequence (**10A** or **15A**) also appears twice

following CISL screening and Sanger sequencing of randomly picked colonies after the aptamer screening process.

As shown in Figure 5.3.13, the UV-Vis spectra of the aging gold nanoparticle seeds in the presence or absence (controls) of the **10A** aptamer remains featureless at the 2 h incubation timepoint due to the relatively small gold nanoparticle seed size (~ 4 nm).[66] After a 7 d incubation period, a peak appears at 530 nm which is also consistent for the controls in this study. Due to the lack of differences observed in the UV-Vis spectra of the gold nanoparticle solution aged in the presence of the **10A** aptamer, it appears that the **10A** aptamer does not have a noticeable affect on the morphology and optical properties of gold nanoparticles during growth of a gold nanoparticle seed solution. Although the AuNP suspension incubated with **10A** remained stable during UV-Vis analysis, it was observed that the sample aggregated following centrifugation while preparing the sample for TEM, whereas the other control samples remained stable during preparation (See Figure 5.3.14). This result contrasts with our prior study in Chapter 4 where we observed that incubation of polyadenine and adenine-rich ssDNA sequences with gold nanoparticle seed at the same concentration instead induced aggregation of the gold nanoparticles during seeded growth which was observed in the UV-vis spectra of these samples.

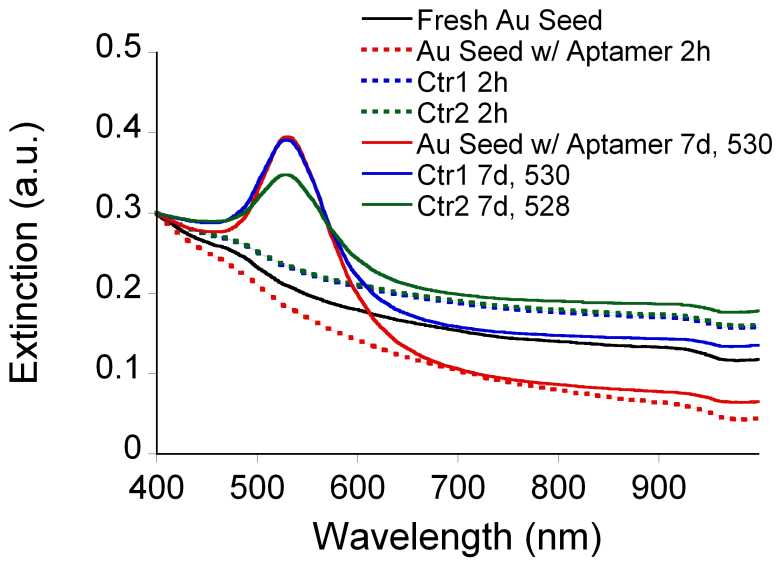

Figure 5.3.13. UV-Vis spectra of gold seed following incubation with aptamer candidate (**10A**) at 2 h and 7 d timepoints. Fresh Au seed refers to the as-synthesized gold nanoparticle seed solution. Controls involve a pure gold nanoparticle seed solution (**Ctr1**) or the addition of aptamer incubation buffer (AIB) to gold nanoparticle seed solution (**Ctr2**= 2 µL AIB) in the absence of DNA. The resulting peak wavelength values are included in the legend for each suspension.

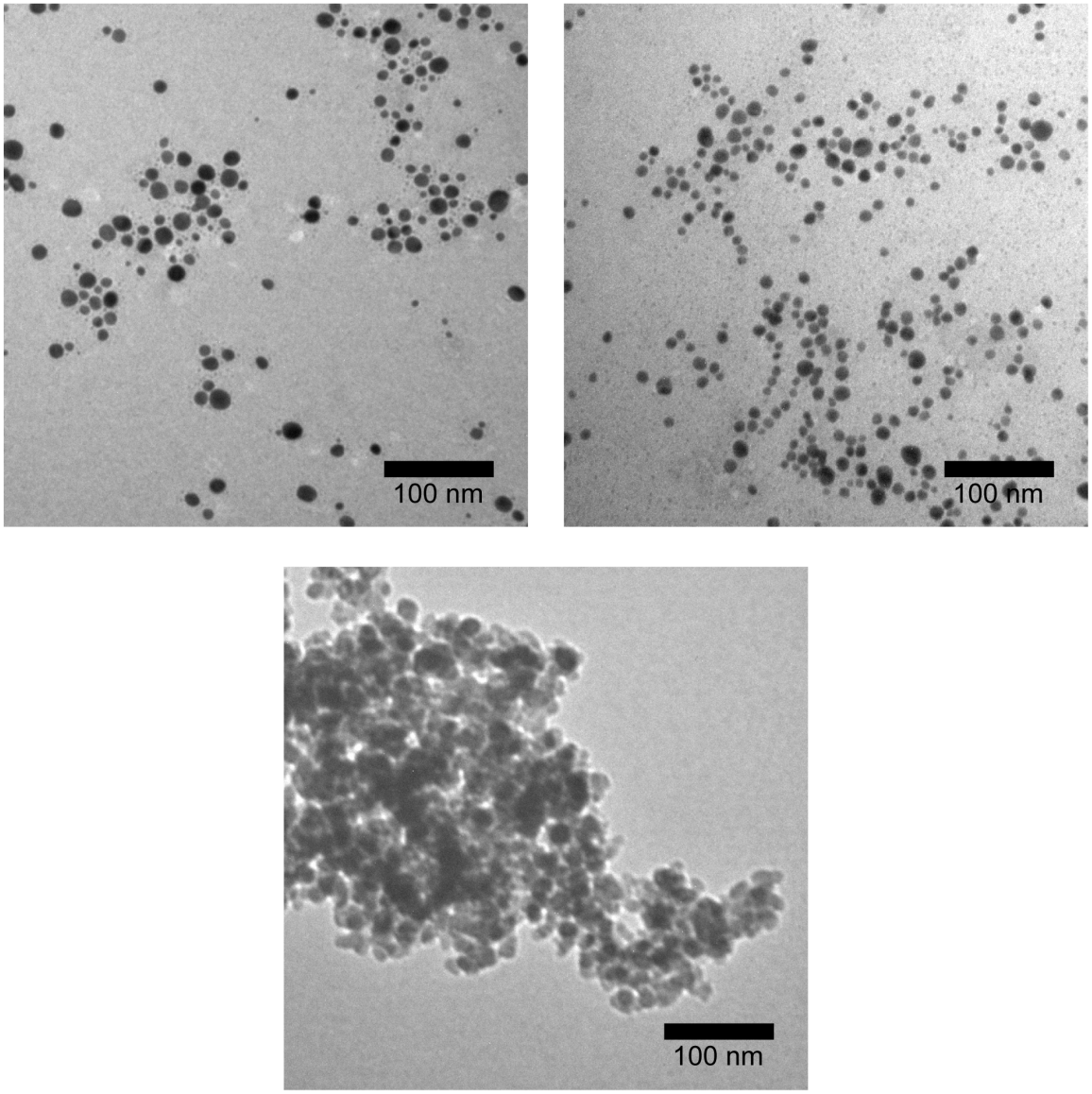

Figure 5.3.14. TEM micrographs of gold seed aged for 7 days with (a) no aptamer present (pure gold seed solution in nanopure water) (b) aptamer incubation buffer present (20 mM HEPES, 2 mM $MgCl_2$, 150 mM NaCl, 2 mM $CaCl_2$, 2 mM KCl at pH 7.4) (c) aptamer sequence **10A** (identical to **15A**) at 2 μM in aptamer incubation buffer.

5.4 CONCLUSIONS

The study presented in this chapter offers an alternative method for the identification of aptamers for a non-nucleotide target. This modified approach (i) shortens the selection process, (ii) promotes increased competition during selection rounds and (iii) reduces the likelihood of introducing PCR amplification-induced artifacts in the candidate sequence pool. This approach has the potential to be extended to other colloidal target systems, particularly if successful simultaneous elution and PCR amplification of remaining adsorbate sequences can be undertaken in the presence of the target as done here. Using this approach, 24 aptamer sequences were identified from random ssDNA libraries for AuNPs. Primary and secondary structural analysis indicates that although there were only six (out of 40) individual base positions conserved for 50% of all identified sequences, consensus motifs, common structural motifs in predicted secondary structures are found after grouping the structures according to the presented classification scheme. The most populated secondary structure subgroup consisted of aptamer candidates exhibiting three hairpins and four single-stranded regions. This analytical scheme will help to further elucidate the factors contributing to binding when paired with future binding affinity assays.

CHAPTER 6[3]

COMPETITION-INDUCED SELECTION OF LIGANDS TO SCREEN FOR SSDNA APTAMERS FOR PLANAR GOLD SURFACES

6.1 Introduction

In this chapter, the CISL approach was used to identify ssDNA aptamer candidates for a planar gold substrate. In contrast to the colloidal gold target study presented in Chapter 5, a planar gold substrate was of interest for this study in order to evaluate if face-specific aptamer candidates could potentially be identified. An additional difference between the AuNP and PlanarAu gold targets is the fact that the PlanarAu was not ever exposed to surface-stabilizing agents, such as CTAB. The gold substrates used in this study exhibit the (111) crystalline planes on their surface as indicated by XRD analysis. Identified aptamer sequences were analyzed to determine similarities in their primary structures and their predicted secondary structures in the same manner as described in Chapter 5. In addition to primary and secondary structure analysis, an incubation study with the 25 identified aptamer candidates and the planar gold substrate was conducted and accompanied with next generation sequencing analysis to reveal a potential indication of relative binding affinities. To the best of our knowledge, the work in this chapter is the first report of an aptamer screening process with a planar gold target.

6.2 Materials and Methods

6.2.1 Materials

The normal (25% A, 25% C, 25% T, 25% G) and A-rich (40% A, 20% C, 20% T, 20% G) random single-stranded DNA (ssDNA) template libraries were purchased from

[3] Manuscript in preparation for publication.

Integrated DNA Technologies. The ssDNA template strands were 69 bases in length and contained a central 40-base randomized region flanked on either end by primer binding regions (5'-GGG ACA GGG CTA GC-[40N]-GAG GCA AAG CTT CCG -3'). The random libraries were synthesized via hand mixing and were PAGE-purified. The reverse primer (5'-CGG AAG CTT TGC CTC-3'), phosphorylated reverse primer (5'-Phos-CGG AAG CTT TGC CTC-3') and forward primer (5'-GGG ACA GGG CTA GC-3') were purchased from Integrated DNA Technologies and were HPLC purified.

Dow Corning Sylgard 170 fast cure and Sylgard 164 were purchased from Ellsworth Adhesives (Germantown, WI). Gold-coated microscope slides (layer thickness 1000 Å, 99.999% (Au)) were purchased from Sigma Aldrich (St. Louis, MO). Characterization of the gold-coated microscope slides is provided in Chapter 3. GoTaq DNA polymerase and 5X colorless GoTaq reaction buffer were purchased from Promega (Madison, WI). The 10 mM dNTP mix, O'Generuler Low Range DNA ladder, phenol:chloroform:isoamyl alcohol (25:24:1), ethidium bromide, 1X PCR optimized Buffer A, TOPO TA Cloning Kit for Subcloning, One Shot TOP10 Chemically Competent E. coli and X-gal were purchased from Invitrogen (Grand Island, NY). (HEPES, $MgCl_2$, $CaCl_2$, and KCl were purchased from BDH Chemicals (VWR Scientific, Radnor, PA). Ethanol and Tris EDTA pH 7.4 were purchased from Fisher Scientific (Pittsburgh, PA). NaCl, hexadecyltrimethylammonium bromide (CTAB) hydrogen tetrachloroaurate (III) hydrate ($HAuCl_4 \bullet 3H_2O$), sodium borohydride ($NaBH_4$), ammonium persulfate (98%), tetramethylethylene diamine, ampicillin sodium salt, and dimethylformamide were purchased from Sigma Aldrich (St. Louis, MO). Glycogen, Acryl/Bis 29:1 40% w/v solution, Acryl/Bis 37.5:1 40% w/v solution, agar (bacteriological), LB broth (Luria-

Bertani) were purchased from Amresco (Solon, OH). Lambda exonuclease enzyme and 10X lambda exonuclease reaction buffer were purchased from New England Biolabs (Ipswich, MA). The MinElute PCR Purification Kit was purchased from Qiagen (Gaithersburg, MD). The aptamer incubation buffer (AIB) used for selection consisted of 20 mM HEPES, 2 mM $MgCl_2$, 150 mM NaCl, 2 mM $CaCl_2$, 2 mM KCl at pH 7.4 All buffers were prepared using 0.2 μM filtered water from a Barnstead Nanopure ultrapure water purification system (Barnstead, Thermo Fisher Scientific, Inc., USA).

6.2.2 Random Library Amplification and ssDNA Generation

Amplified libraries of random ssDNA 69-base long template strands were prepared via exponential PCR reactions. Normal and A-rich libraries were prepared separately using the following PCR reagent concentrations: 0.17 pM ssDNA template, 200 μM dNTPs, 60 nM forward primer, 60 nM phosphorylated reverse primer, 0.05 unit/μL GoTaq polymerase and 1X colorless GoTaq buffer. Twenty-five cycles of denaturation (95 °C, 30 s), annealing (47 °C, 30 s), and extension (72 °C, 30 s) were conducted to amplify the random ssDNA template libraries. Amplified PCR products in dsDNA form were purified via ethanol precipitation with glycogen and resuspended in Tris EDTA pH 7.4.

To generate ssDNA needed for aptamer selection, the purified dsDNA PCR products were digested with lambda exonuclease. Purified dsDNA PCR product was mixed with lambda exonuclease enzyme (10U lambda exonuclease/ 2 μg dsDNA) and lambda exonuclease reaction buffer to yield 1X from a 10X buffer stock. The mixed solution was then incubated at 37 °C for 1 h, followed by a 10 min incubation step at 80 °C to halt the enzymatic reaction. The digested ssDNA was then purified with a

phenol/chloroform/Isoamyl alcohol extraction followed by ethanol precipitation with glycogen. Purified ssDNA was resuspended in aptamer incubation buffer (20 mM HEPES, 2 mM $MgCl_2$, 150 mM NaCl, 2 mM $CaCl_2$, 2 mM KCl pH 7.4) to prepare for aptamer selection.

Generation of ssDNA products after lambda exonuclease digestion was confirmed by an exonuclease I (Exo I) digestion (See Chapter 3). Initial dsDNA PCR product and lambda exonuclease generated ssDNA product were mixed with Exo I (1U/1 μL DNA) and 1X Exo I reaction buffer. These mixtures were incubated at 37 °C for 30 min followed by a 20 min incubation step at 80 °C. Final products were analyzed on a 13 wt% polyacrylamide/bis gel stained with ethidium bromide and imaged using a UV transluminator (BioDoc-IT, UVP, Inc., Upland, CA).

6.2.3 Competition-Induced Selection of Ligands (CISL) for a Planar Gold Substrate

The CISL procedure outlined below was carried out for two separate screening procedures using the normal and A-rich random ssDNA libraries but the same procedure was followed for both cases and sequence results for both CISL screening sessions were combined for subsequent analysis. An incubation chamber was prepared on the gold-coated microscope slide by adhering an eppendorf vial to the slide using Sylgard adhesive and allowing it cure for 30 min at room temperature before use. The area of the gold substrate exposed to the amplified random ssDNA libraries during selection was estimated to be around 32.7 mm^2. X-ray diffraction analysis of the planar gold substrate used for aptamer selection indicated a strong tendency towards the <111> direction (See Chapter 3). In order to eliminate ssDNA sequences that may have had an affinity to the

Sylgard used to adhere the incubation chamber to the gold-coated slide, a counter-selection step was performed by incubating the entire amplified random ssDNA library in an eppendorf vial with cured Sylgard. Before the counter-selection step, the amplified library was first denatured (90 °C for 10 min, 4 °C for 15 min, 24 °C for 5 min) and then incubated in a vial containing cured Sylgard for 1 h under mixing (RT, 1200 rpm). After incubation, the supernatant was collected and separated into 10 aliquots to prepare for aptamer selection. Before the first selection round with the post counter-selection amplified library, a pre-incubation step was conducted by incubating 100 μL of a 2 μM dNTP mix with the planar gold substrate and allowing it to mix on a thermomixer for 30 min (RT, 1200 rpm). The dNTPs were intended to serve as temporary blocking agents to minimize nonspecific binding of ssDNA. After incubation, the dNTP solution was removed from the chamber.

Before each selection round, each random ssDNA library aliquot (100 μL) in AIB was denatured by heating to 90 °C for 10 min, 4 °C for 15 min and 24 °C for 5 min. Each aliquot was then immediately added to the incubation chamber and allowed to incubate at room temperature for 30 min on a shaking thermomixer (1200 rpm). The concentrations of amplified random ssDNA libraries used in each selection round were 3.5 μM for the normal library and 2.23 μM for the A-rich library. After incubation, the supernatant was removed and the gold substrate was washed 3 times with 200 μL incubation buffer. Following these wash steps, the next denatured random ssDNA library aliquot was added. This was repeated for a total of 10 selection rounds. After the 10^{th} round, the supernatant was removed and the substrate was washed four times with 100 μL of 1X PCR optimized Buffer A. After the wash steps, the area of the gold substrate that was exposed during

aptamer selection was crushed and placed in two PCR vials containing the following PCR reaction mix in order to amplify the bound ssDNA remaining on the gold substrate: 200 μM dNTPs, 60 nM forward primer, 60 nM reverse primer, 0.05 unit/μL GoTaq polymerase, 1X colorless GoTaq buffer. Twenty-five cycles of denaturation (95 °C, 30 s), annealing (47 °C, 30 s), and extension (72 °C, 30 s) were conducted. Final PCR product was purified using the Qiagen MinElute PCR Purification Kit with the manufacturer's protocol (Qiagen, Inc., Gaithersburg, MD).

6.2.4 Cloning and Sequencing of Aptamer Candidates

Aptamer candidates were identified by inserting purified PCR product from aptamer selection into *Escherichia coli* using the TOPO TA Cloning Kit (Invitrogen, Life Technologies, Grand Island, NY). Transformed bacteria were then plated on LB-agar medium supplemented with ampicillin and X-gal, followed by overnight growth in a 37 °C incubator. Sanger-based sequencing was then carried out as follows. Twenty positive bacterial colonies out of several hundred colonies from both aptamer selection cases (normal & A-rich random ssDNA libraries) were randomly picked and after plasmid purification, were sent to GENEWIZ Inc. for sequencing analysis (South Plainfield, NJ).

6.2.5 Primary and Secondary Structure Analysis of Aptamer Candidates

The primary sequences of identified aptamer candidates were analyzed and aligned using Geneious 7.1.2 (Biomatters Ltd., Auckland, New Zealand). A multiple sequence alignment of the 40 base variable regions (bases 15-54) of the candidates was performed using Geneious. This alignment was also used to generate a distance matrix to evaluate

pairwise similarity comparisons between sequences. Online software MEME 4.9.1 was used to identify sequence motifs that could occur at any position throughout the length of the 40 base variable region of the candidate sequences.[99, 151]

Thermodynamically favorable secondary structures of all aptamer candidates were generated using UNAFOLD (also known by its older nomenclature as Mfold)[100] software under the given salt conditions ($[Na^{+}]$ = 152 mM, $[Mg^{++}]$ = 4 mM). Base-pair maps were constructed by highlighting the base pair interactions indicated in the UNAFOLD-predicted secondary structures for each aptamer candidate. Aptamer candidates were also categorized by their secondary structure similarities by analyzing the appearance of specific secondary structural features in their predicted secondary structures: single-stranded segments, duplex regions (not associated with a hairpin), hairpins, interior loops, bulges and multi-branched loops. Structures sharing the same number of these specific features were grouped together.

6.2.6 Competitive Incubation of Aptamer Candidates with Next Generation Sequencing Analysis

A homogeneous mixture of all identified 25 aptamer candidates was created with an overall ssDNA concentration of 2.5 μM suspended in AIB. The pool of ssDNA aptamer candidates for planar gold was denatured (90 °C for 10 min, 4 °C for 15 min, 24 °C for 5 min) and then 100 μL of the 2.5 μM pool was incubated with the gold substrate for 1 h on a thermomixer (RT, 1200 rpm). After incubation, the substrate was washed three times with 200 μL AIB. The substrate was then washed four times with 100 μL of 1X PCR Optimized Buffer A. As described previously, the substrate was then crushed and put into

PCR vials for amplification of bound ssDNA. Final PCR product was purified using the Qiagen MinElute PCR Purification Kit. The purified sample was sent to GENEWIZ for next generation sequencing (NGS) analysis. GENEWIZ conducted around 6.9 million reads on an Illumina MiSeq platform. Bioinformatics analysis was also conducted by GENEWIZ, to identify the unique sequences and calculate their relative abundance.

To investigate potential non-preferential amplification of any of the 25 candidate sequences during PCR for the competitive incubation experiment, a separate PCR experiment was conducted where known, equimolar concentrations of all 25 candidate sequences were amplified via PCR without subsequent exposure to PlanarAu. The amplified dsDNA product was purified as described above and sent to GENEWIZ for NGS analysis. DNA libraries were prepared by GENEWIZ using an Illumina TruSeq kit and sequenced on the Illumina MiSeq with 2x75bp configuration with over 17.6 million reads.

6.3 Results and Discussion

6.3.1 Competition-Induced Selection of Ligands (CISL) for a Planar Gold Substrate

Aptamer selection was conducted for a planar gold substrate in two separate CISL-based screening sessions using normal and A-rich random libraries under otherwise identical conditions. For the same reason as described in Chapter 5, the choice of employing an A-rich library is based on the prior studies conducted in Chapter 4 that indicated adenine-rich ssDNA and pure polyadenine induced aggregation of gold nanoparticles during their seeded growth as well as after growth in the case of pure polyadenine. As detailed previously in Chapter 5, the key differences between the CISL approach and the

conventional SELEX process for the selection of aptamers stem are that CISL introduces a unique, unenriched pool of random ssDNA for each round of selection and also eliminates intermittent oligonucleotide PCR amplification steps between selection rounds.

As illustrated in Figure 6.3.1, the CISL process begins with the preparation of the amplified random ssDNA library, as described in detail in Chapter 3. Each library used for aptamer selection consisted of random ssDNA sequences that are 69 bases in length that contain a 40-base central randomized region flanked on both ends by primer binding regions. After generation of the amplified random ssDNA library (~10^7 copies of each unique template strand from starting library) as described previously in Chapter 3, an aliquot of the amplified random ssDNA library (3.5 μM normal library, 2.23 μM A-rich library) was incubated with the PlanarAu within the incubation chamber. This concentration of ssDNA was chosen in order to ensure an excess of ssDNA with a simple random coil conformation are available for monolayer coverage of the PlanarAu ($R_{g,69\ base\ ssDNA}$ ~ 3.32 nm) compared to the total surface area of the PlanarAu surface area exposed to the solution (total surface area ~ 32.7 mm^2).

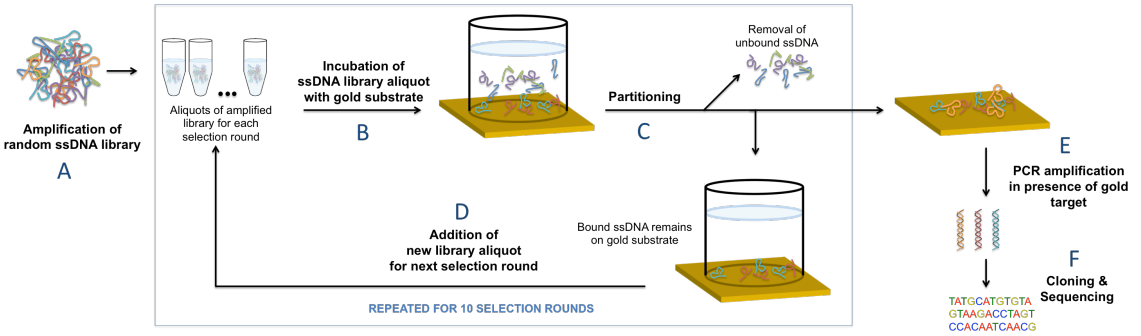

Figure 6.3.1. Schematic overview of the competition-induced selection of ligands (CISL) aptamer screening process that involves the following steps: (A) preparation of the random ssDNA library by PCR amplification and lambda exonuclease digestion; (B) incubation of the amplified random ssDNA library with the planar gold target; (C) removal of unbound ssDNA after incubation round; (D) addition of new aliquot of amplified random ssDNA library for the next selection round. After steps (A) - (C) have been repeated for a total of 10 rounds, then the next steps are (E) PCR amplification of bound ssDNA in presence of the planar gold target; and finally the sequences in the supernatant undergo (F) cloning and sequencing of identified aptamer candidates.

Following each incubation round, a partitioning step is conducted to remove non-binding ssDNA from the target surface and a new aliquot of unenriched random ssDNA library is added to the PlanarAu for the next selection round, while sequences that bound in the previous round remain present on the surface and are able to compete with sequences in the newly introduced library. A total of 10 incubation rounds are carried out and after the final round, non-binding sequences are removed and PCR amplification is performed in the presence of the PlanarAu substrate to amplify the sequences that remain bound to the surface. PCR amplification is followed by cloning and sequencing of the identified aptamer candidates. In total, 25 aptamer candidate sequences were identified from two CISL screening sessions using normal or A-rich random ssDNA libraries.

6.3.2 Primary structure analysis of aptamer candidates

The 25 sequences were analyzed to identify both position-dependent and position-independent similarities in their primary structures in the same manner as described in Chapter 4. Figure 6.3.2 shows the resulting multiple sequence alignment of the 40-base central variable region (bases 15-54) of the 25 sequences. The highlighted bases represent specific positions that are conserved in at least 50% of all 25 sequences. Despite the large number of sequences involved in the screening process (~ 10^{15}), Figure 6.3.2 reveals that there are still 6 base positions conserved in at least 50% of the 25 sequences.

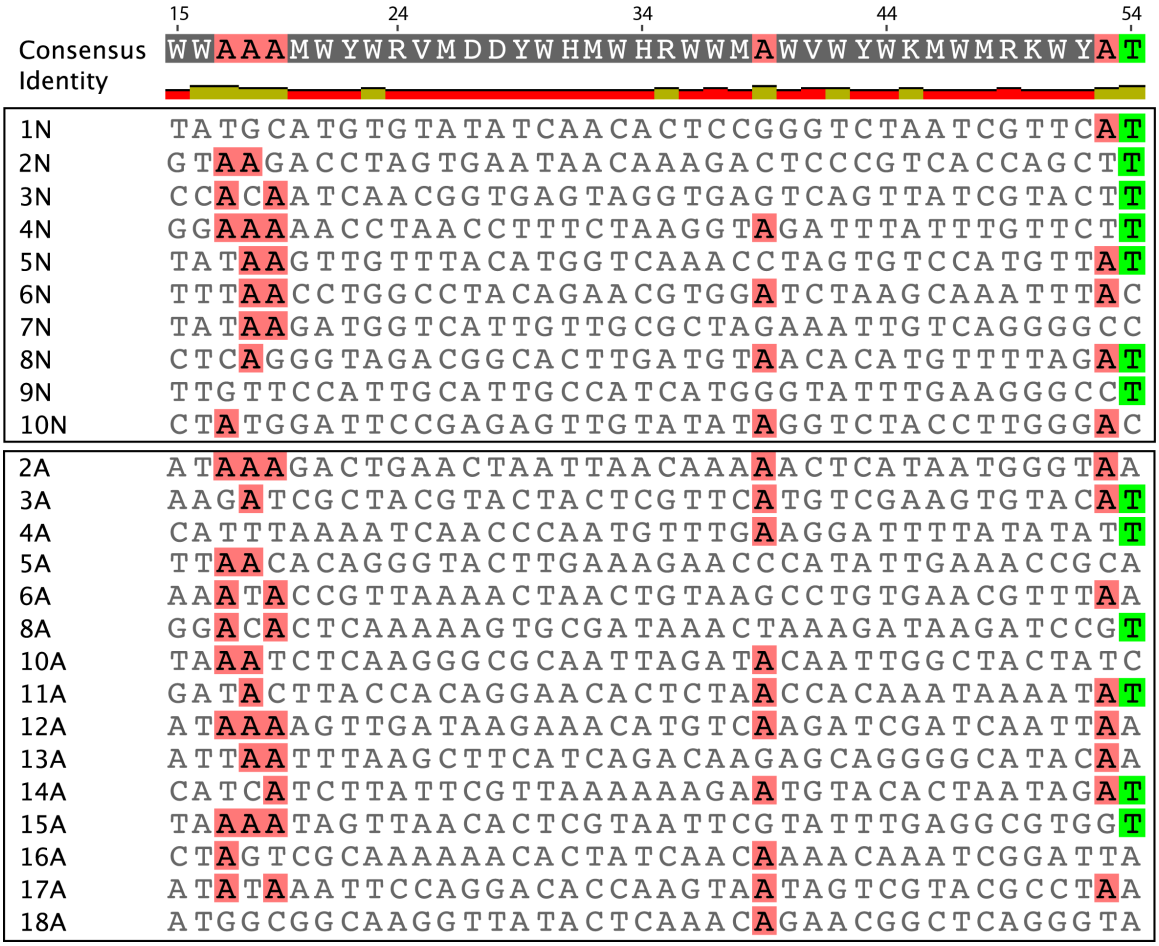

Figure 6.3.2. Multiple sequence alignment of the central variable base segments of AuNP-binding sequences identified from both the normal and A-rich random libraries indicated by the letters "N" and "A" respectively, in the aptamer nomenclature in the left column. Highlighted bases indicated base positions found in at least 50% of all 24 sequences (base 17 = A in 13 sequences; base 18 = A in 14 sequences; base 19 = A in 13 sequences; base 39 = A in 14 sequences; base 53 = A in 13 sequences; base 54 = T in 13 sequences). The full-length or 69 base-long sequences include two constant segments (bases 1-14 and bases 55-69) intended to serve as primer hybridization sites and a central variable segment (40N): 5'-GGGACAGGGCTAGC(40N) GAGGCAAAGCTTCCG -3'. Alignment output generated with Geneious 7.1.2.

In addition to the multiple sequence alignment, pairwise comparisons were also made across all sequences in Geneious in order to generate a distance matrix that provided information on degrees of primary sequence similarity between all sequence pairings as shown in Figure 6.3.3.

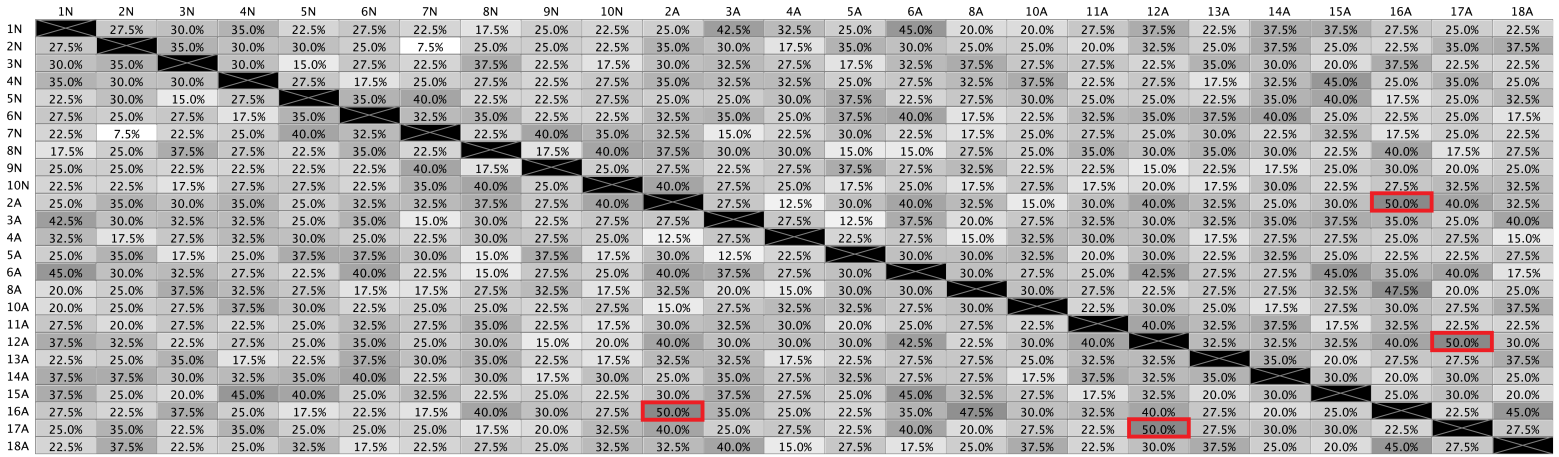

	1N	2N	3N	4N	5N	6N	7N	8N	9N	10N	2A	3A	4A	5A	6A	8A	10A	11A	12A	13A	14A	15A	16A	17A	18A
1N		27.5%	30.0%	35.0%	22.5%	27.5%	22.5%	17.5%	25.0%	22.5%	25.0%	42.5%	32.5%	25.0%	45.0%	20.0%	20.0%	27.5%	37.5%	22.5%	37.5%	37.5%	27.5%	25.0%	22.5%
2N	27.5%		35.0%	30.0%	30.0%	25.0%	7.5%	25.0%	25.0%	22.5%	35.0%	30.0%	17.5%	35.0%	30.0%	25.0%	25.0%	20.0%	32.5%	25.0%	37.5%	25.0%	22.5%	35.0%	37.5%
3N	30.0%	35.0%		30.0%	15.0%	27.5%	22.5%	37.5%	22.5%	17.5%	30.0%	32.5%	27.5%	17.5%	32.5%	37.5%	27.5%	27.5%	22.5%	35.0%	30.0%	20.0%	37.5%	22.5%	22.5%
4N	35.0%	30.0%	30.0%		27.5%	17.5%	25.0%	27.5%	22.5%	27.5%	35.0%	32.5%	32.5%	25.0%	27.5%	32.5%	37.5%	22.5%	27.5%	17.5%	32.5%	45.0%	25.0%	35.0%	25.0%
5N	22.5%	30.0%	15.0%	27.5%		35.0%	40.0%	22.5%	22.5%	27.5%	25.0%	25.0%	30.0%	37.5%	22.5%	27.5%	30.0%	25.0%	25.0%	22.5%	35.0%	40.0%	17.5%	25.0%	32.5%
6N	27.5%	25.0%	27.5%	17.5%	35.0%		32.5%	35.0%	22.5%	22.5%	32.5%	35.0%	25.0%	37.5%	40.0%	17.5%	22.5%	32.5%	35.0%	37.5%	40.0%	25.0%	22.5%	25.0%	17.5%
7N	22.5%	7.5%	22.5%	25.0%	40.0%	32.5%		22.5%	40.0%	35.0%	32.5%	15.0%	22.5%	30.0%	22.5%	17.5%	25.0%	27.5%	25.0%	30.0%	22.5%	32.5%	17.5%	25.0%	22.5%
8N	17.5%	25.0%	37.5%	27.5%	22.5%	35.0%	22.5%		17.5%	40.0%	37.5%	30.0%	30.0%	15.0%	15.0%	27.5%	25.0%	35.0%	30.0%	35.0%	30.0%	22.5%	40.0%	17.5%	27.5%
9N	25.0%	25.0%	22.5%	22.5%	22.5%	22.5%	40.0%	17.5%		25.0%	27.5%	22.5%	27.5%	37.5%	27.5%	32.5%	22.5%	22.5%	15.0%	22.5%	17.5%	25.0%	30.0%	20.0%	25.0%
10N	22.5%	22.5%	17.5%	27.5%	27.5%	22.5%	35.0%	40.0%	25.0%		40.0%	27.5%	25.0%	17.5%	25.0%	17.5%	27.5%	17.5%	20.0%	17.5%	30.0%	22.5%	27.5%	32.5%	32.5%
2A	25.0%	35.0%	30.0%	35.0%	25.0%	32.5%	32.5%	37.5%	27.5%	40.0%		27.5%	12.5%	30.0%	40.0%	32.5%	15.0%	30.0%	40.0%	32.5%	25.0%	30.0%	50.0%	40.0%	32.5%
3A	42.5%	30.0%	32.5%	32.5%	25.0%	35.0%	15.0%	30.0%	22.5%	27.5%	27.5%		27.5%	12.5%	37.5%	20.0%	27.5%	32.5%	30.0%	32.5%	35.0%	37.5%	35.0%	25.0%	40.0%
4A	32.5%	17.5%	27.5%	32.5%	30.0%	25.0%	22.5%	30.0%	27.5%	25.0%	12.5%	27.5%		22.5%	27.5%	15.0%	32.5%	30.0%	30.0%	17.5%	27.5%	27.5%	25.0%	27.5%	15.0%
5A	25.0%	35.0%	17.5%	25.0%	37.5%	37.5%	30.0%	15.0%	37.5%	17.5%	30.0%	12.5%	22.5%		30.0%	30.0%	32.5%	20.0%	30.0%	22.5%	32.5%	25.0%	22.5%	22.5%	27.5%
6A	45.0%	30.0%	32.5%	27.5%	22.5%	40.0%	22.5%	15.0%	27.5%	25.0%	40.0%	37.5%	27.5%	30.0%		30.0%	27.5%	25.0%	42.5%	27.5%	27.5%	45.0%	35.0%	40.0%	17.5%
8A	20.0%	25.0%	37.5%	32.5%	27.5%	17.5%	17.5%	27.5%	32.5%	17.5%	32.5%	20.0%	15.0%	30.0%	30.0%		30.0%	27.5%	22.5%	27.5%	27.5%	32.5%	47.5%	20.0%	25.0%
10A	20.0%	25.0%	27.5%	37.5%	30.0%	22.5%	25.0%	25.0%	22.5%	27.5%	15.0%	27.5%	32.5%	32.5%	27.5%	30.0%		22.5%	30.0%	25.0%	17.5%	27.5%	30.0%	27.5%	37.5%
11A	27.5%	20.0%	27.5%	22.5%	25.0%	32.5%	27.5%	35.0%	22.5%	17.5%	30.0%	32.5%	30.0%	20.0%	25.0%	27.5%	22.5%		40.0%	32.5%	37.5%	17.5%	32.5%	22.5%	22.5%
12A	37.5%	32.5%	22.5%	27.5%	25.0%	35.0%	25.0%	30.0%	15.0%	20.0%	40.0%	30.0%	30.0%	30.0%	42.5%	22.5%	30.0%	40.0%		32.5%	32.5%	32.5%	40.0%	50.0%	30.0%
13A	22.5%	25.0%	35.0%	17.5%	22.5%	37.5%	30.0%	35.0%	22.5%	17.5%	32.5%	32.5%	17.5%	22.5%	27.5%	27.5%	25.0%	32.5%	32.5%		35.0%	20.0%	27.5%	27.5%	37.5%
14A	37.5%	37.5%	30.0%	32.5%	35.0%	40.0%	22.5%	30.0%	17.5%	30.0%	25.0%	35.0%	27.5%	32.5%	27.5%	27.5%	17.5%	37.5%	32.5%	35.0%		30.0%	20.0%	30.0%	25.0%
15A	37.5%	25.0%	20.0%	45.0%	40.0%	25.0%	32.5%	22.5%	25.0%	22.5%	30.0%	37.5%	27.5%	25.0%	45.0%	32.5%	27.5%	17.5%	32.5%	20.0%	30.0%		25.0%	30.0%	20.0%
16A	27.5%	22.5%	37.5%	25.0%	17.5%	22.5%	17.5%	40.0%	30.0%	27.5%	50.0%	35.0%	25.0%	22.5%	35.0%	47.5%	30.0%	32.5%	40.0%	27.5%	20.0%	25.0%		22.5%	45.0%
17A	25.0%	35.0%	22.5%	35.0%	25.0%	25.0%	25.0%	17.5%	20.0%	32.5%	40.0%	25.0%	27.5%	22.5%	40.0%	20.0%	27.5%	22.5%	50.0%	27.5%	30.0%	30.0%	22.5%		27.5%
18A	22.5%	37.5%	22.5%	25.0%	32.5%	17.5%	22.5%	27.5%	25.0%	32.5%	32.5%	40.0%	15.0%	27.5%	17.5%	25.0%	37.5%	22.5%	30.0%	37.5%	25.0%	20.0%	45.0%	27.5%	

Figure 6.3.3. Primary sequence pairwise distance matrix for all aptamer candidates. Generated with Geneious 7.1.2 created by Biomatters. Available from http://www.geneious.com.

This matrix revealed that the maximum percentage in overall primary sequence similarity is 50% and is exhibited by 2 pairs of sequences (**2A** and **16A**, **12A** and **17A**) shown in Figure 6.3.4. Consensus motifs were also evaluated using MEME, however none of the identified motifs from this analysis resulting from CISL-based screening were statistically significant (having E values less than 0.01).

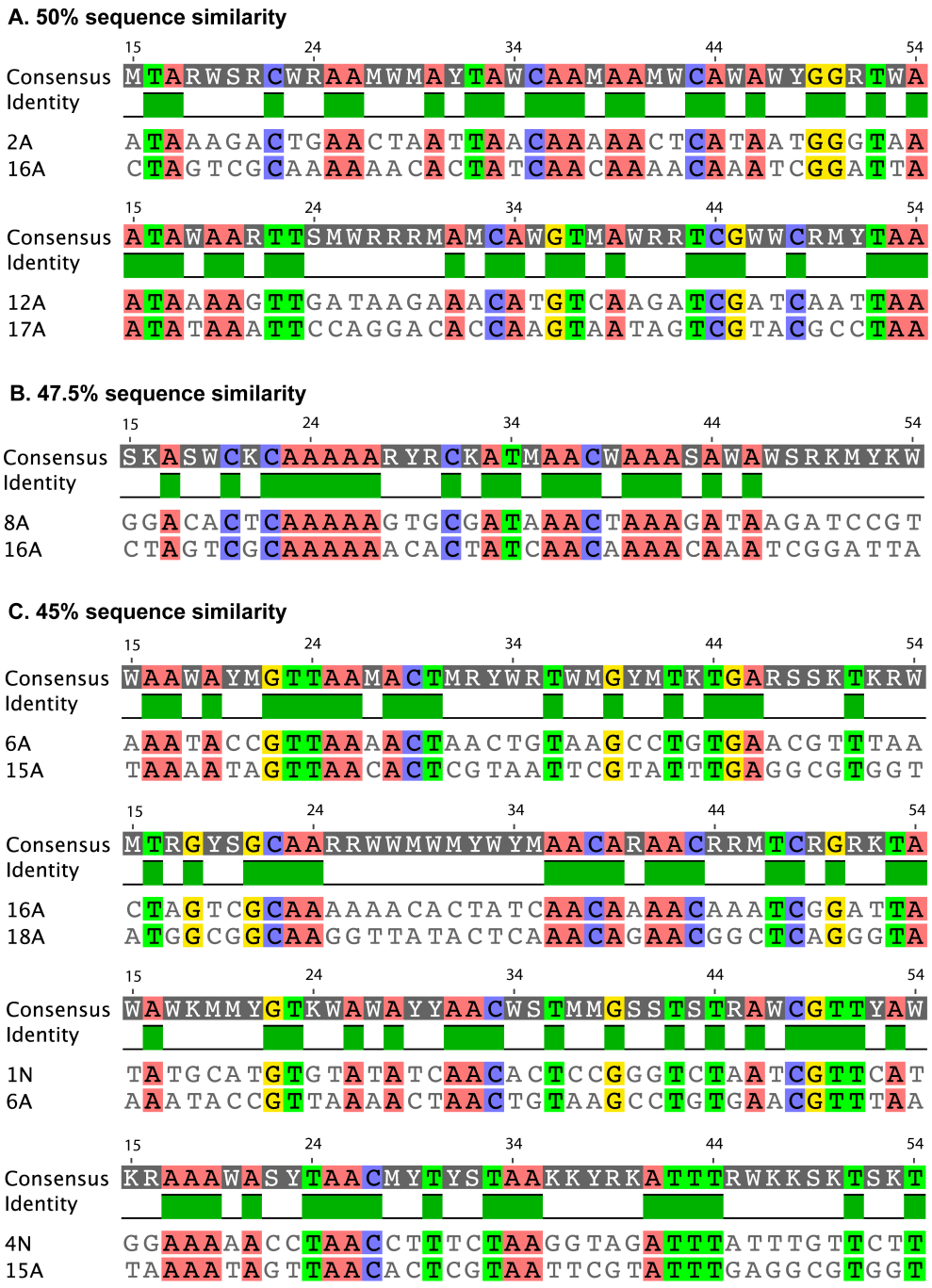

Figure 6.3.4. Pairwise sequence alignment of the central variable base segments of PlanarAu-binding sequences identified from both the normal and A-rich random libraries that exhibit (A) 100% sequence similarity (B) 47.5% sequence similarity and (C) 45 % sequence similarity.

6.3.3 Secondary structure analysis of aptamer candidates

The 25 sequences were next analyzed to identify both position-dependent and position-independent similarities in base pairings that result from predicted secondary structures. The UNAFOLD server was used to predict thermodynamically favorable secondary structures under the same salt conditions that were used during aptamer selection rounds. The entire length of the sequences (69 bases) is included in the UNAFOLD analysis as the primer binding regions can influence the formation of the predicted secondary structure. All predicted secondary structures with corresponding self-melt temperatures (T_m) and Gibbs free energy (dG) is shown in Figures 6.3.5 and 6.3.6.

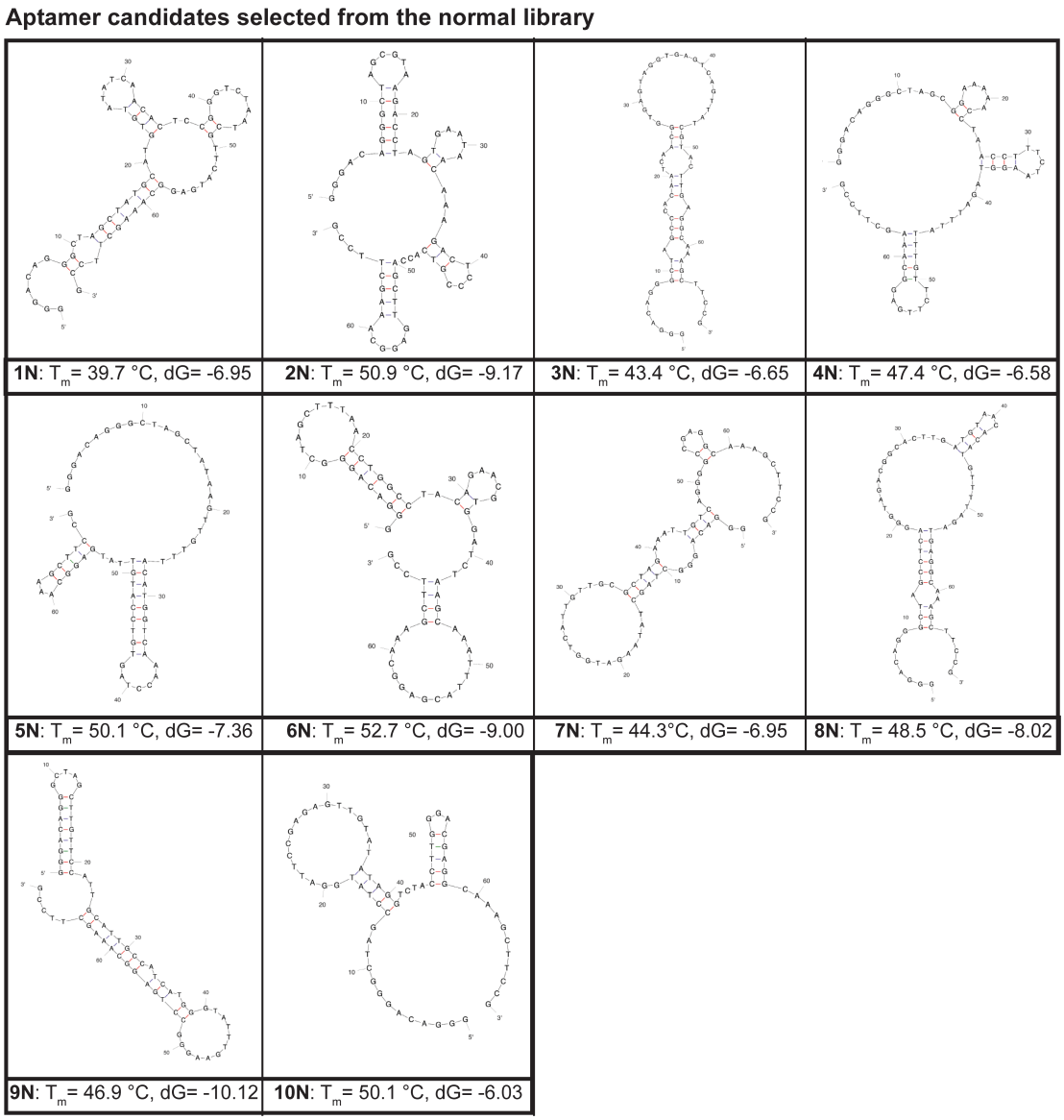

Figure 6.3.5. Thermodynamically favorable secondary structures of the 10 aptamer sequences selected from the normal random library (25% of each base) for PlanarAu. Predicted structures were generated using UNAFOLD (http://mfold.rna.albany.edu/?q=mfold/DNA-Folding-Form, access date: July 23, 2014) under the following solution conditions: T=23 °C, 152 mM [Na^{+}], 4 mM [Mg^{++}]. The position-specific (with base #1 at the 5' end and base #69 at the 3' end) base pairings are color-coded as follows: A-T and T-A (blue); G-C and C-G (red); G-T and T-G (green). The Gibbs free energy associated with self-hybridization, dG, is provided in units of kcal/mol.

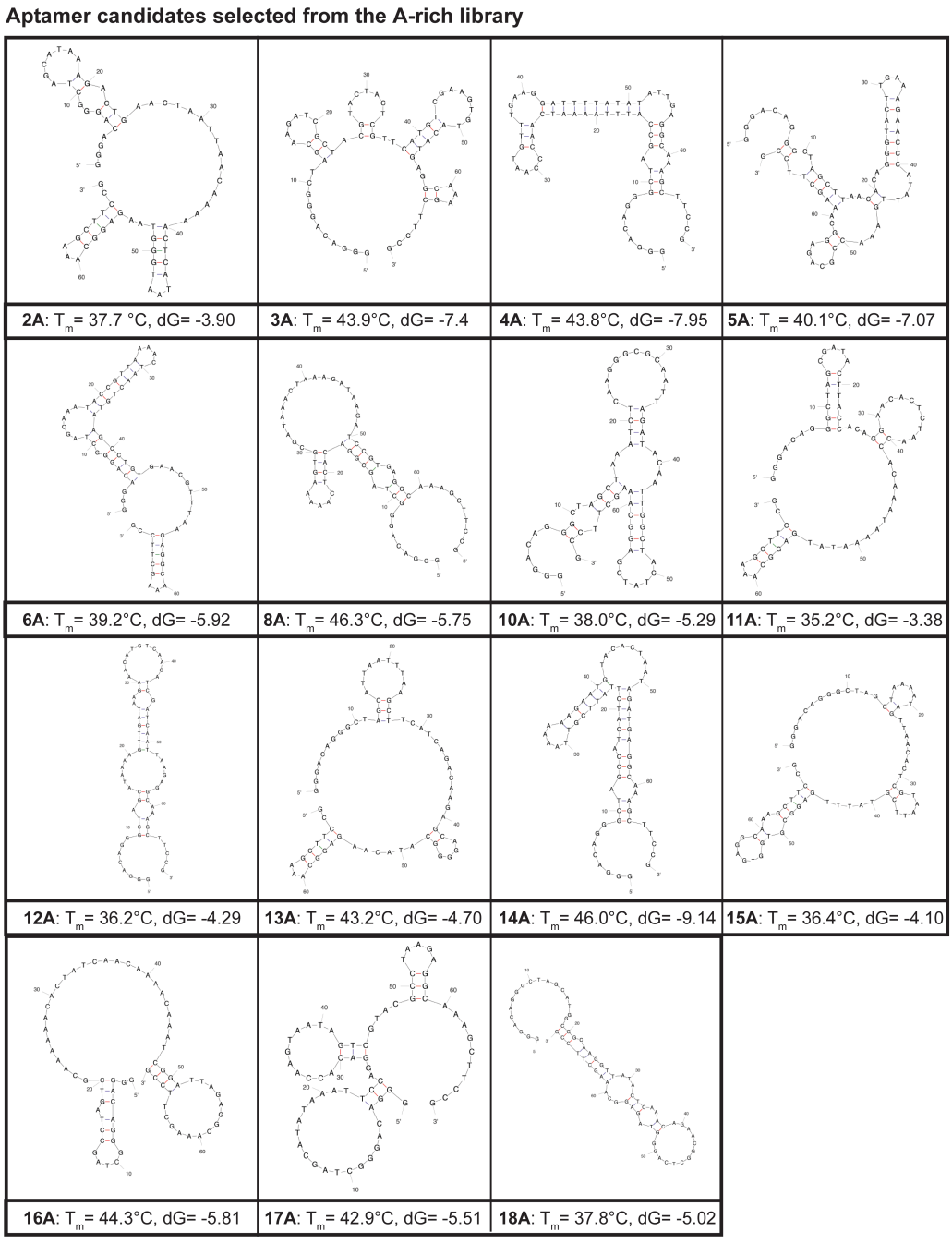

Figure 6.3.6. Thermodynamically favorable secondary structures of the 15 aptamer sequences selected from the A-rich random library (40% A, 20% each of C, T, G) for PlanarAu. Predicted structures were generated using UNAFOLD (http://mfold.rna.albany.edu/?q=mfold/DNA-Folding-Form, access date: July 23, 2014) under the following solution conditions: T=23 °C, 152 mM [Na^{+}], 4 mM [Mg^{++}]. The position-specific (with base #1 at the 5' end and base #69 at the 3' end) base pairings are color-coded as follows: A-T and T-A (blue); G-C and C-G (red); G-T and T-G (green). The Gibbs free energy associated with self-hybridization, dG, is provided in units of kcal/mol.

To identify conserved position-dependent base pairings due to self-hybridization, a base pairing map was then constructed based on the predicted secondary structures of the 25 candidate sequences. As shown in Figure 6.3.7, the leftmost half of the map shows position-dependent base pairings that are located in two or more secondary structures to specifically highlight shared base pairings across all the candidate sequences while the bottom rightmost half shows all base pair interactions, both shared and unshared.

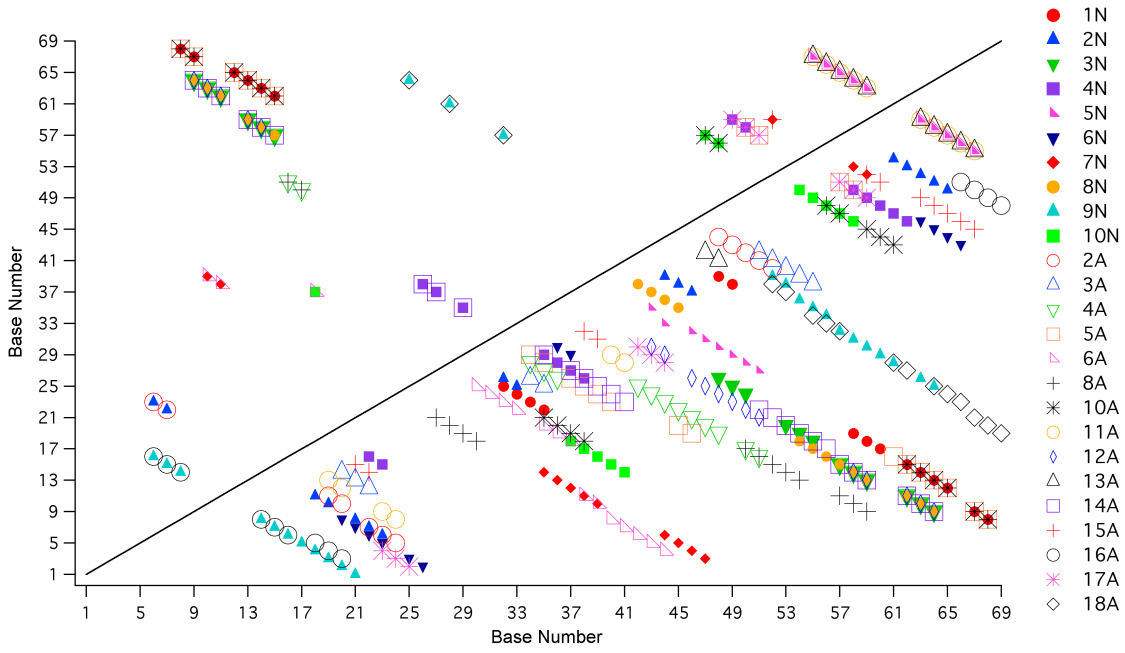

Figure 6.3.7. Base-pair map highlighting all base pair interactions for each aptamer candidate (below the line) and the shared base pair interactions between aptamer candidates (above the line) for PlanarAu. Detailed lists of all shared and unshared position-dependent base pair interactions for all 25 sequences are provided in Tables 6.3.1 and 6.3.2.

Notably, many (69 in total) of the shared base-pairings in the leftmost half of the map correspond to base pair interactions that occur in the conserved primer binding segments (bases 1-14, 55-69); however, as shown in the tabulated form of this base pairing map in

Table 6.3.1, there are still several (10 in total) base pair interactions solely due to base pairing in the variable region (bases 15-54) as well as numerous (38 in total) base pairings that involve both conserved and variable bases of the 25 sequences. As shown in Table 6.3.2, aptamer sequence **14A** exhibited the maximum of 9 shared base pairings that were present in 5 other aptamer sequences.

Table 6.3.1. List of the position-dependent identities of base pairs shared by two or more aptamer sequences for PlanarAu. Base positions in red indicate positions within random variable region of the sequence.

Base Pair	Sequence (Pair Type)	Sequence (Pair Type)	Sequence (Pair Type)	Sequence (Pair Type)	Sequence (Pair Type)	Sequence (Pair Type)
6, 16	9N (A-T)	16A (A-T)				
6, 23	2N (A-T)	2A (A-T)				
7, 15	9N (G-T)	16A (G-C)				
7, 22	2N (G-C)	2A (G-C)				
8, 14	9N (G-C)	16A (G-C)				
8, 68	1N (G-C)	5A (G-C)	10A (G-C)			
9, 64	3N (G-C)	8N (G-C)	4A (G-C)	12A (G-C)	14A (G-C)	
9, 67	1N (G-C)	5A (G-C)	10A (G-C)			
10, 39	7N (C-G)	6A (C-G)				
10, 63	3N (C-G)	8N (C-G)	4A (C-G)	12A (C-G)	14A (C-G)	
11, 38	7N (T-A)	6A (T-A)				
11, 62	3N (T-A)	8N (T-A)	4A (T-A)	12A (T-A)	14A (T-A)	
12, 65	1N (A-T)	5A (A-T)	10A (A-T)			
13, 59	3N (G-C)	8N (G-C)	4A (G-C)	12A (G-C)	14A (G-C)	
13, 64	1N (G-C)	5A (G-C)	10A (G-C)			
14, 58	3N (C-G)	8N (C-G)	4A (C-G)	12A (C-G)	14A (C-G)	
14, 63	1N (C-G)	5A (C-G)	10A (C-G)			
15, 57	3N (C-G)	8N (C-G)	4A (C-G)	14A (C-G)		
15, 62	1N (T-A)	5A (T-A)	10A (T-A)			
16, 51	4A (A-T)	8A (G-C)				
17, 50	4A (T-A)	8A (A-T)				
18, 37	10N (T-A)	6A (T-A)				
25, 64	9N (G-C)	18A (G-C)				
26, 38	4N (A-T)	14A (T-A)				
27, 37	4N (C-G)	14A (C-G)				
28, 61	9N (T-A)	18A (T-A)				
29, 35	4N (T-A)	14A (T-A)				
32, 57	9N (C-G)	18A (C-G)				
47, 57	10N (C-G)	10A (C-G)				
48, 56	10N (T-A)	10A (T-A)				
49, 59	4N (G-C)	17A (G-C)				
50, 58	4N (T-G)	5A (C-G)	17A (C-G)			
51, 57	5A (C-G)	17A (C-G)				
52, 59	7N (G-C)	15A (G-C)				
55, 67	5N (G-C)	2A (G-C)	6A (G-C)	11A (G-C)	13A (G-C)	
56, 66	5N (A-T)	2A (A-T)	6A (A-T)	11A (A-T)	13A (A-T)	
57, 65	5N (G-T)	2A (G-T)	6A (G-T)	11A (G-T)	13A (G-T)	
58, 64	5N (G-C)	2A (G-C)	3A (G-C)	6A (G-C)	11A (G-C)	13A (G-C)
59, 63	5N (C-G)	2A (C-G)	3A (C-G)	6A (C-G)	11A (C-G)	13A (C-G)

Table 6.3.2. List of all aptamer sequences and the total number of position-dependent base pairs shared with other aptamer sequences as well as the total number and nomenclature of aptamer sequences with at least one shared base pairing for a given aptamer sequence for PlanarAu.

Sequence	Total number of shared base pair positions	Number (and aptamer nomenclature) of sequences with at least one shared base pair
1N	6	2 (5A, 10A)
2N	2	1 (2A)
3N	6	4 (8N, 4A, 12A, 14A)
4N	5	3 (5A, 14A, 17A)
5N	5	5 (2A, 3A, 6A, 11A, 13A)
6N	0	0
7N	3	3 (6A, 15A, 16A)
8N	6	4 (3N, 4A, 12A, 14A)
9N	6	2 (16A, 18A)
10N	3	2 (6A, 10A)
2A	6	5 (2N, 5N, 6A, 11A, 13A)
3A	2	5 (5N, 2A, 6A, 11A, 13A)
4A	8	5 (3N, 8N, 12A, 14A, 8A)
5A	8	4 (1N, 4N, 10A, 17A)
6A	8	7 (5N, 7N, 10N, 2A, 3A, 11A, 13A)
8A	2	1 (4A)
10A	8	3 (1N, 10N, 5A)
11A	5	5 (5N, 2A, 3A, 6A, 13A)
12A	5	4 (3N, 8N, 4A, 14A)
13A	5	5 (5N, 2A, 3A, 6A, 11A)
14A	9	5 (3N, 4N, 8N, 4A, 12A)
15A	1	1 (7N)
16A	3	1 (9N)
17A	3	2 (4N, 5A)
18A	3	1 (9N)

Secondary structure similarity was investigated next simply based on the presence of secondary structure features independent of base type or positioning. For this analysis, segments of the predicted secondary structures are classified in the same manner as described in Chapter 5 according to the following features: single-stranded segments, duplex regions, hairpins, interior loops, bulges and multi-branched loops. Based on this classification of each sequence segment, the candidates are then arranged into subgroups that share the same number of these six secondary structure features.

As shown in Figure 6.3.8, this analysis revealed that the most populated subgroup is comprised of sequences exhibiting 3 hairpins, 1 interior loop, 1 duplex region and 4 single-stranded segments. It should be noted that two of the sequences (**2A** and **11A**) in this particular subgroup exhibit an identical hairpin structure that occurs in the primer-binding segment at the 3' end of the sequences. This information is by the tabulated, position-specific base pairing interactions in Table 6.3.1. As it relates to the pairwise primary sequence analysis discussed earlier (See Figure 6.3.3), in the first subgroup of Figure 6.3.8, the highest percentage of primary sequence similarity is between two pairs of sequences (**6N** and **2A**, **6N** and **11A**) at 32.5%. For the second subgroup, **9N** and **16A** exhibit only 27.5% sequence similarity. In the third subgroup, **5N** and **7N** share 40% sequence similarity and in the fourth subgroup, **3N** and **12A** share only 22.5% sequence similarity. Other sets of smaller subgroupings of 2 or 3 sequences that shared 2, 3 or even 5 identical structural features are shown in Figures 6.3.9, 6.3.10 and 6.3.11. A complete listing of all secondary structure features identified are shown in Table 6.3.3.

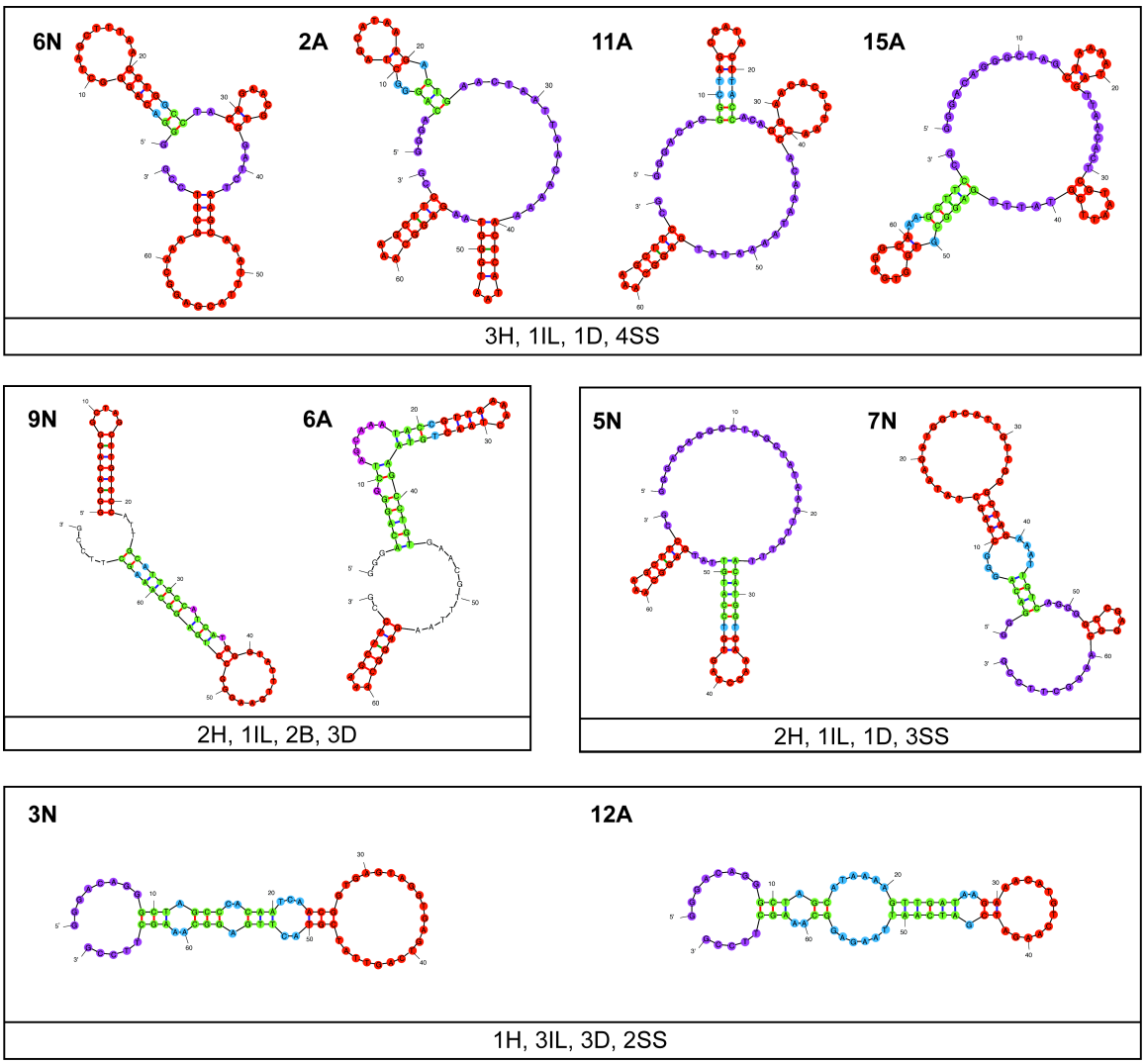

Figure 6.3.8. Four subgroups of aptamer candidates that share an identical number of types (hairpin (H) in red, interior loop (IL) in blue, bulge (B) in pink, duplex regions (D) in green and single-stranded segments (SS) in purple) of secondary structural features. For **9N** and **6A**, any bases that are not part of the shared 2 hairpins, 1interior loop, 2 bulges or 3 duplex segments are not highlighted in color.

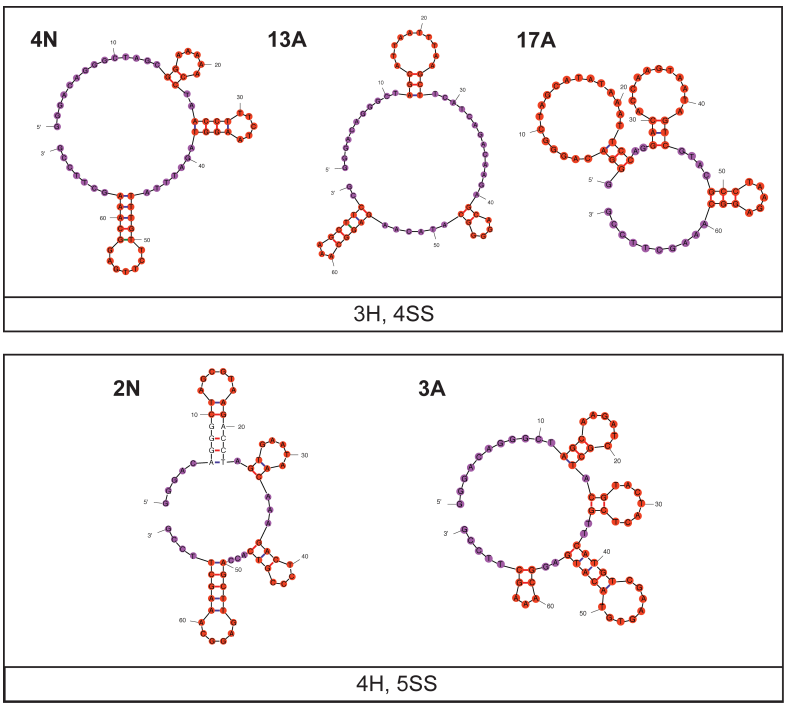

Figure 6.3.9. Two subgroups of aptamer candidates that share an identical number of types (hairpin (H) in red and single-stranded segments (SS) in purple) of secondary structural features. For **2N** and **3A**, any bases that are not part of the shared 4 hairpins, or 5 single-stranded segments are not highlighted in color.

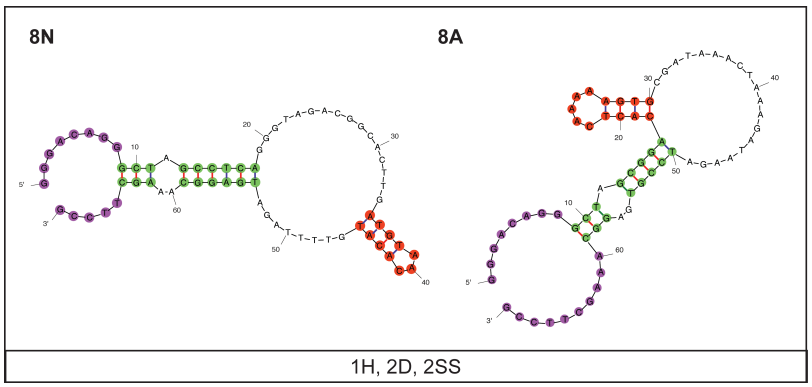

Figure 6.3.10. One pair of aptamer candidates that share an identical number of types (hairpin (H) in red, duplex regions (D) in green and single-stranded segments (SS) in purple) of secondary structural features. Any bases that are not part of the shared 1 hairpin, 2 duplex regions or 2 single-stranded segments are not highlighted in color.

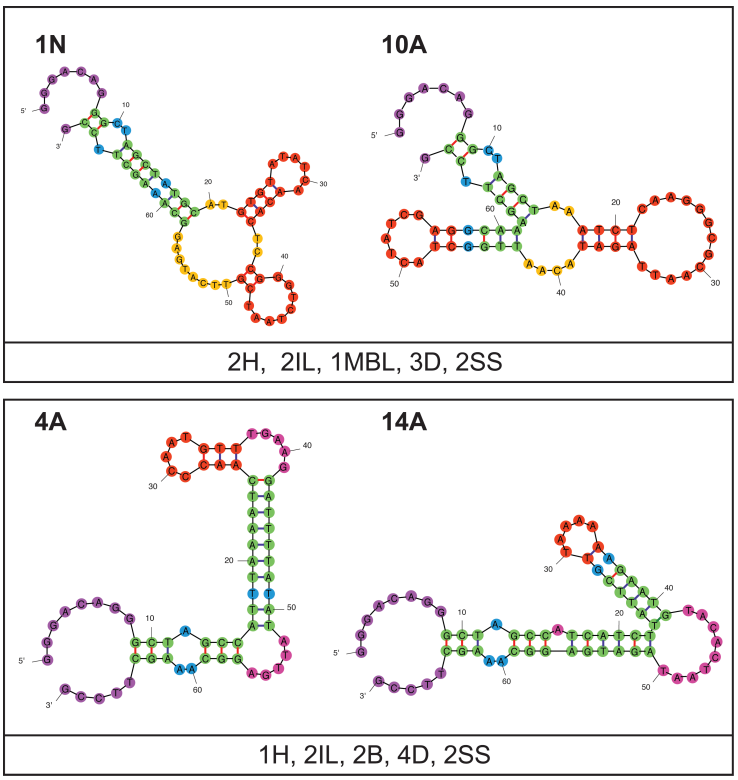

Figure 6.3.11. Two subgroups of aptamer candidates that share an identical number of types (hairpin (H) in red, interior loop (IL) in blue, bulge (B) in pink, duplex regions (D) in green and single-stranded segments (SS) in purple) of secondary structural features.

Table 6.3.3. List of each aptamer sequence and the total number of hairpins (H), interior loops (IL), multi-branched loops (MBL), bulges (B), duplexes (D) and single-stranded segments (SS) found in its predicted secondary structure. The total number of the 6 types of structural features observed for each sequence (right) as well as across all sequences (bottom) is provided.

	Secondary Structure Features																		
Sequence	1H	2H	3H	4H	1IL	2IL	3IL	1MBL	1B	2B	1D	2D	3D	4D	2SS	3SS	4SS	5SS	Total
1N		X				X		X					X		X				5
2N				X	X						X							X	4
3N	X						X						X		X				4
4N			X														X		2
5N		X			X						X					X			4
6N			X		X						X						X		4
7N		X			X						X					X			4
8N	X					X						X			X				4
9N		X			X					X			X		X				5
10N		X														X			2
2A			X		X						X						X		4
3A				X														X	2
4A	X					X				X				X	X				5
5A		X					X	X						X	X				5
6A		X			X					X			X			X			5
8A	X				X				X			X			X				5
10A		X				X		X					X		X				5
11A			X		X						X						X		4
12A	X						X						X		X				4
13A			X														X		2
14A	X					X				X				X	X				5
15A			X		X						X						X		4
16A		X							X		X				X				4
17A			X														X		2
18A	X						X		X					X					4
Total	7	9	7	2	10	5	4	3	3	4	8	2	6	4	11	4	7	2	
%	28	36	28	8	40	20	16	12	12	16	32	8	24	16	44	16	28	8	

6.3.4. Competitive Incubation of Aptamer Sequences with Next Generation Sequencing Analysis

In order to investigate the relative binding strengths of the 25 identified aptamer sequences, all 25 sequences were incubated with the planar gold substrate at equimolar concentrations. Following incubation, unbound sequences were removed from the target surface and PCR was carried out in the presence of the substrate in order to amplify bound sequences. The amplified PCR product was then analyzed via next generation sequencing (NGS) conducted by GENEWIZ, allowing for the identification of the unique

sequences and their relative abundance. It is hypothesized that sequences found to be in high abundance as reported by NGS results, corresponds to those sequences having a higher relative binding strength compared to the other candidate sequences in solution. NGS results shown in Figure 6.3.12 revealed that sequence **1N** ranked highest in terms of total counts (1,996,301) while the second highest-ranking sequence, **18A** had total counts (317,207 counts) that were an order of magnitude lower than that of **1N**. It would appear from this data that **1N** exhibiting the highest count number could potentially correlate to it also having the highest relative binding affinity, however, this would need to be confirmed by additional binding assays. The reported counts for all 25 aptamer candidates can be seen in Table 6.3.4.

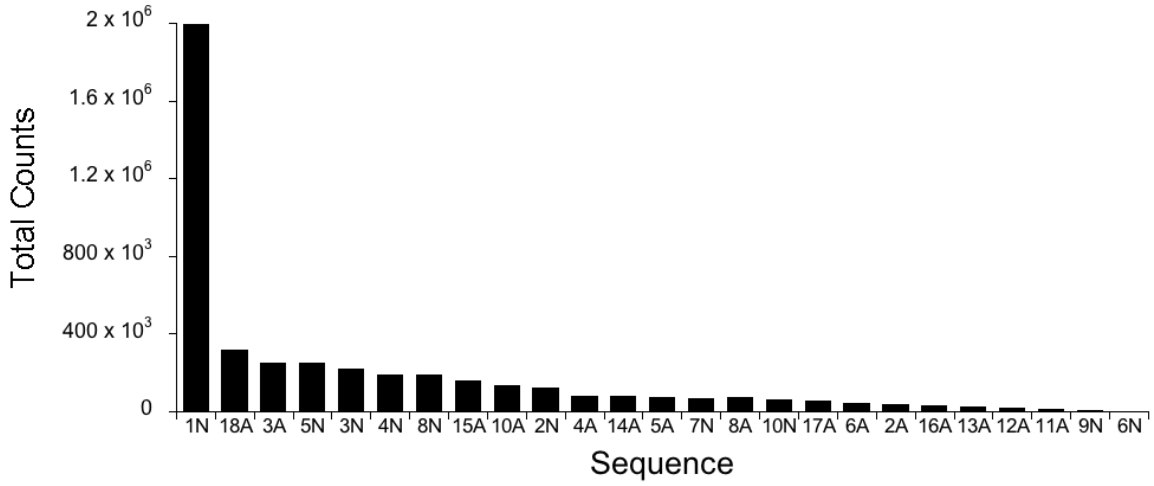

Figure 6.3.12. Next generation sequencing counts of all 25 aptamer candidates following competitive incubation experiment (variance=$1.51E^{11}$, range=$1.99E^{6}$).

Table 6.3.4. Next generation sequencing total results indicating total counts for each sequence from the competitive incubation experiment.

Sequence	Counts
1N	1996301
18A	317207
3A	252778
5N	250933
3N	217421
4N	190936
8N	190576
15A	156707
10A	132273
2N	124560
14A	79563
4A	79009
5A	75681
8A	71678
7N	70012
10N	64301
17A	56157
6A	42935
2A	36582
16A	33145
13A	24256
12A	17994
11A	12895
9N	3799
6N	3287

In order to evaluate if there was any non-preferential amplification during PCR following incubation with the gold substrate that led to the distinct differences in NGS total counts as shown in Figure 6.3.12, a separate PCR amplification was conducted with equimolar concentrations of all 25 aptamer candidate sequences and also evaluated with NGS in the absence of PlanarAu. The reported counts for all 25 aptamer candidates can be seen in Table 6.3.5. The results from this study as shown in Figure 6.3.13 indicate that there appears to be some variation in the amplification of the sequences due to the large variance in the data set ($2.99E^{10}$). However, it should be noted that the highest number of

counts in this study (Figure 6.3.13) is attributed to sequence **4N** (918,668) and not **1N**, which was the case for the competitive incubation experiment (Figure 6.3.12). The variance for the NGS competitive incubation experiment is also an order of a magnitude higher ($1.51E^{11}$) leading to the possibility that the differences seen in sequence counts can be partially attributed to differences in relative binding affinities.

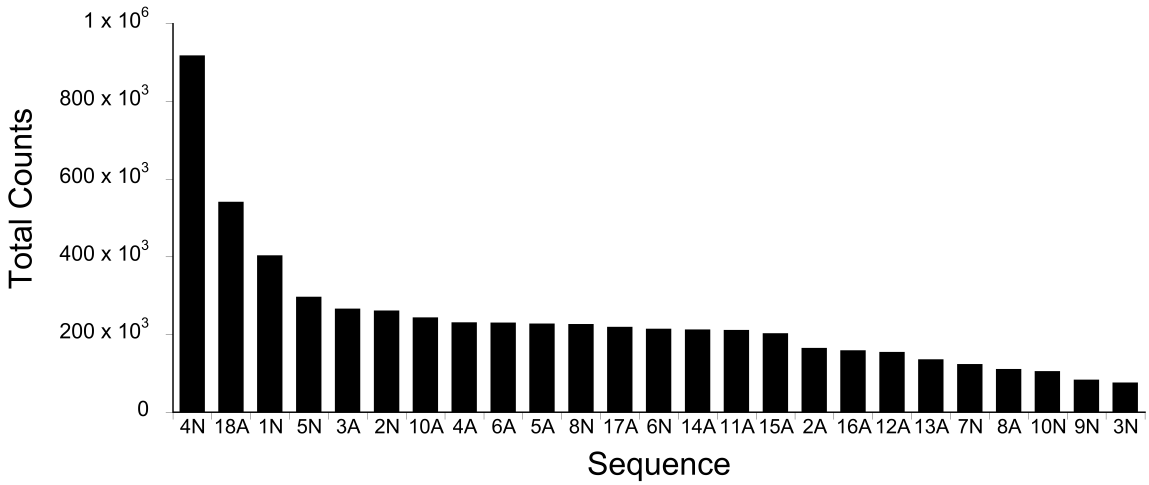

Figure 6.3.13. Next generation sequencing counts of all 25 aptamer candidates following exponential PCR amplification experiment (variance=$2.99E^{10}$, range=$8.42E^{5}$).

Table 6.3.5. Next generation sequencing total results indicating total counts for each sequence from the PCR evaluation experiment for non-preferential amplification.

Sequence	Counts
4N	918668
18A	541945
1N	404100
5N	297199
3A	266530
2N	262160
10A	243906
4A	231423
6A	230761
5A	228221
8N	227101
17A	220007
6N	214786
14A	213021
11A	211803
15A	203253
2A	165388
16A	159568
12A	155370
13A	136055
7N	123896
8A	111019
10N	105848
9N	83547
3N	76288

In a separate incubation study with **1N**, AFM analysis indicates that **1N** does bind to the gold planar surface, even after subsequent wash steps following incubation (See Figure 6.3.14).

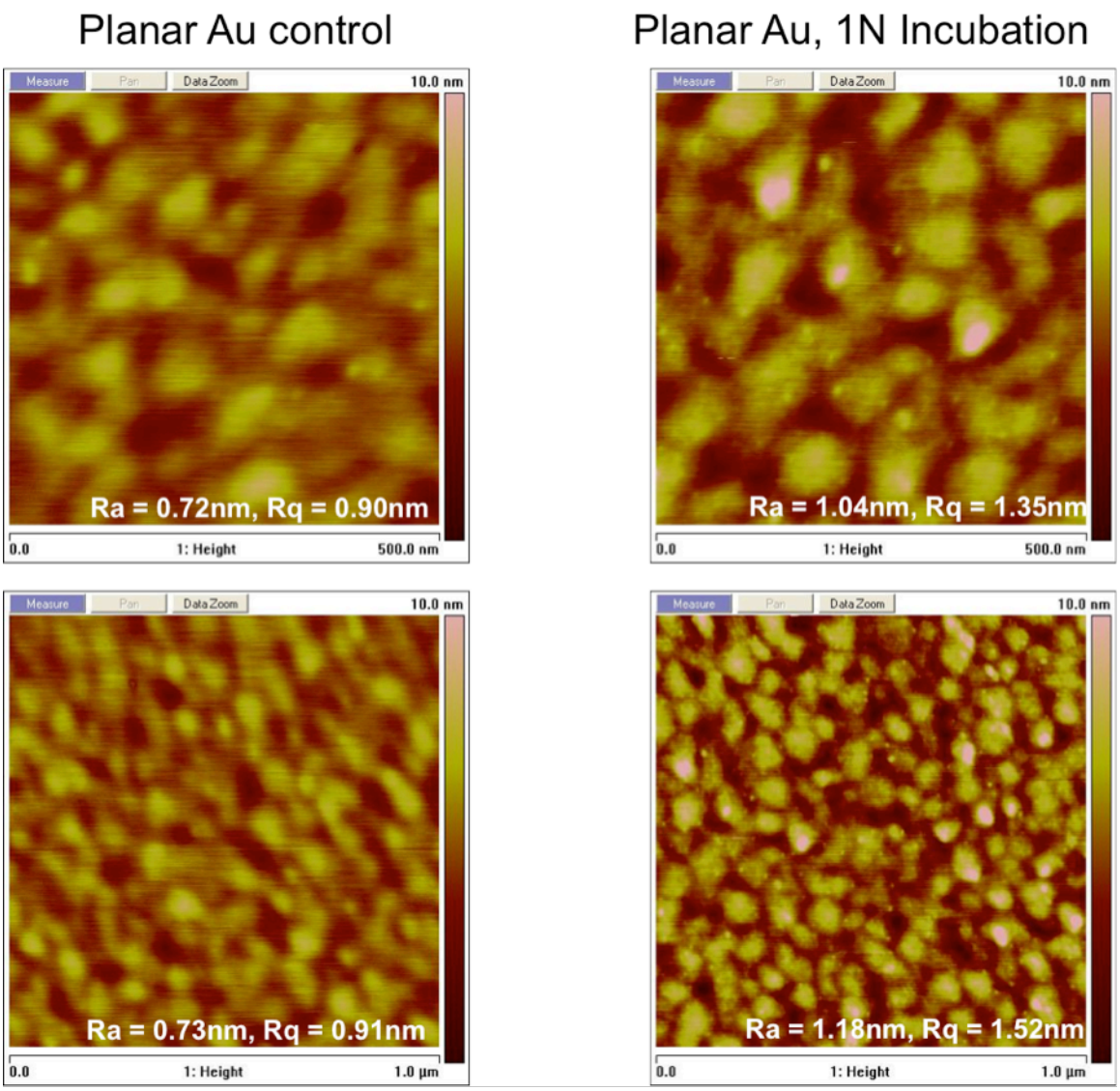

Figure 6.3.14. AFM image of 1N aptamer candidate sequences bound to a planar gold substrate following incubation and wash steps. 1N was incubated at 2 µM (100 µL) in aptamer incubation buffer (AIB) with the planar gold substrate for 1 hour. Immediately after incubation, the substrate was washed three times with 200 µL of AIB. R_a =average roughness and R_q=root mean square roughness. Images were acquired using a Bruker Dimension 3100 AFM equipped with a NanoScope V controller operated in Tapping Mode using PPP-NCHR probes from NanoAndMore, 29 September 2014 by Kristi Singh (*POC: Rajesh Naik, Air Force Research Laboratory Materials and Manufacturing Directorate*)

6.4 Conclusions

In this chapter, the CISL aptamer screening process was used to identify 25 ssDNA aptamer candidates for planar gold substrates. Primary and secondary structural analysis indicates that although unenriched random ssDNA libraries were used during selection, some sequences still shared similarities in primary sequence and secondary structure features. The most populated secondary structure group consisted of aptamer candidates exhibiting 3 hairpins, 1 interior loop, 3 duplex regions and 2 single-stranded segments. Characterizing aptamer candidates with respect to their shared similarities in primary and secondary structure is one step towards further understanding the nature of aptamer-target interactions. The presented strategy can also be modified for other planar target systems with potential benefits such as a shortened selection process, increased competition between sequences during selection rounds and the reduction of errors introduced into the final library used in selection and ultimately winning aptamer candidates by eliminating intermittent PCR amplification steps.

CHAPTER 7

GENERAL CONCLUSIONS AND FUTURE WORK

7.1 General Conclusions and Discussion

This dissertation details the development and use of Competition-Induced Selection of Ligands (CISL) for the identification of single-stranded DNA aptamer candidates for both a colloidal gold and planar gold target. The effects of various nucleic acid additions during the seed-mediated growth of gold nanoparticles is also explored in efforts to better understand the interactions of DNA with gold surfaces. To date, few studies have attempted to identify aptamers for non-biological or non-molecular targets. This study is the first in attempting to identify oligonucleotide sequences from a random library that bind to gold substrates. Initial incubation studies with gold nanoparticle seed revealed that polyadenine and adenine-rich single-stranded sequences induced aggregation of gold nanoparticles during growth, pointing to a specific interaction with the surface that induced particle-particle bridging. This observed phenomenon guided the decision to use both a normal and an A-rich library during the aptamer screening process for both gold targets. Through primary and secondary structure analysis of identified sequences from the screening process, it was observed that with the respect to primary structure, the identified aptamer candidates were diverse. Although the sequences in each of the studies did not share many conserved base positions or exhibit shared sequence motifs, there were notable similarities in the predicted secondary structures that were revealed using the developed secondary structure feature classification system. There is the potential for this work to be extended in the area of binding affinity assays to determine the actual strengths of binding and also studies that systematically probe the aptamer structure to

reveal how the structure changes in the presence of the target through analysis techniques such as NMR and circular dichroism.[17, 152, 153]

7.2 Significance and Future Work

The CISL approach presents an alternative to the traditional SELEX approach and offers benefits including a reduction in overall time and resources for the aptamer screening process, potentially increased competition between sequences during incubation and reduces the risk of introducing errors into the library and/or identified aptamer candidates due to repeated PCR amplification steps between each selection round. This approach can also be adapted for the identification of aptamers for other colloidal or planar targets provided PCR amplification is successful in the presence of the target. If that proves difficult, an elution step can be added after the final selection round to prepare for PCR amplification.

The thorough and systematic investigation of primary and secondary structure similarities described in this study is readily applicable for the analysis of identified aptamer candidates for any target. Although many software programs exist for evaluating primary sequence similarities, there is a need for more powerful analysis platforms that can classify structures by shared secondary structure similarities that are not necessarily base-position dependent but can occur anywhere throughout the structure, similar to the identification of sequence motifs using MEME. The secondary structure feature analysis presented here could serve as a great starting point for that manner of analysis or be

incorporated into already existing tools such as Aptamotif, which currently focuses on characterizing RNA secondary structure motifs.[154]

There is also room to further optimize the CISL selection procedure with respect to the amplification of the random ssDNA library to identify a global maximum for the process. Additional PCR reagent concentrations, temperature ranges and cycle numbers can be explored to further increase the yield of desired PCR product while minimizing the formation of undesired byproducts as shown in Figure 3.4.2 in Chapter 3. Yield can be quantitatively evaluated by using quantitative PCR to monitor the progress and final products of the amplification reaction.

There were notable differences between the aptamer candidates identified for the gold nanoparticles in comparison to those identified for the planar gold surfaces specifically in relation to the conserved secondary structure features. To further elucidate why these differences occurred, it would be beneficial to conduct high resolution TEM on the gold nanoparticles to identify which crystalline facets are exposed on the surface and if they differ from the (111) crystalline planes that are dominant on the planar gold surfaces used in this study. Differences in the orientation of exposed crystalline planes could potentially explain the differences in the identified aptamer candidates as certain sequences could have different relative binding affinities for specific crystallographic planes. Functionalizing identified aptamer sequences with electron-dense dyes could also serve as a method for determining where the sequences are binding with respect to orientation on the gold substrates. In these studies, the gold nanoparticles used in the aptamer

screening process were stabilized with CTAB while the planar gold surfaces did not have CTAB present. To further evaluate potential differences in the identified aptamer candidates, additional aptamer screening studies could be performed with planar gold surfaces that have CTAB added to the surface in order to compare to the CTAB-stabilized gold nanoparticles. Despite the challenges that still remain in understanding the mechanism behind the observed affinity of these single-stranded DNA sequences to gold surfaces, the identified aptamer candidates can be further investigated for potential use as shape or face-specific functionalization tools in the development of novel systems such as advanced nanoassemblies and potentially in the directed deposition or precipitation of complex materials.

REFERENCES

1. Ciesiolka, J.; Gorski, J.; Yarus, M., Selection of an RNA domain that binds Zn2+. *RNA* **1995,** 1, (5), 538-550.

2. Hofmann, H. P.; Limmer, S.; Hornung, V.; Sprinzl, M., Ni2+-binding RNA motifs with an asymmetric purine-rich internal loop and a G-A base pair. *RNA* **1997,** 3, (11), 1289-1300.

3. Jo, M.; Ahn, J.-Y.; Lee, J.; Lee, S.; Hong, S. W.; Yoo, J.-W.; Kang, J.; Dua, P.; Lee, D.-k.; Hong, S.; Kim, S., Development of single-stranded DNA aptamers for specific bisphenol A detection. *Oligonucleotides* **2011,** 21, (2), 85-91.

4. Mann, D.; Reinemann, C.; Stoltenburg, R.; Strehlitz, B., In vitro selection of DNA aptamers binding ethanolamine. *Biochemical and Biophysical Research Communications* **2005,** 338, (4), 1928-1934.

5. Mallikaratchy, P. R.; Ruggiero, A.; Gardner, J. R.; Kuryavyi, V.; Maguire, W. F.; Heaney, M. L.; McDevitt, M. R.; Patel, D. J.; Scheinberg, D. A., A multivalent DNA aptamer specific for the B-cell receptor on human lymphoma and leukemia. *Nucleic Acids Res.* **2011,** 39, (6), 2458-2469.

6. Liu, J.; You, M.; Pu, Y.; Liu, H.; Ye, M.; Tan, W., Recent developments in protein and cell-targeted aptamer selection and applications. *Curr. Med. Chem.* **2011,** 18, (27), 4117-4125.

7. Radom, F.; Jurek, P. M.; Mazurek, M. P.; Otlewski, J.; Jeleń, F., Aptamers: Molecules of great potential. *Biotechnology Advances* **2013**, 1-15.

8. Martínez, O.; Bellard, E.; Golzio, M.; Mechiche-Alami, S.; Rols, M.-P.; Teissié, J.; Ecochard, V.; Paquereau, L., Direct Validation of Aptamers as Powerful Tools to Image Solid Tumor. *Nucleic Acid Therapeutics* **2014,** 24, (3), 217-225.

9. Jayasena, S. D., Aptamers: an emerging class of molecules that rival antibodies in diagnostics. *Clin. Chem.* **1999,** 45, (9), 1628-1650.

10. Syed, M. A.; Pervaiz, S., Advances in Aptamers. *Oligonucleotides* **2010,** 20, (5), 215-224.

11. Ng, E. W. M.; Shima, D. T.; Calias, P.; Cunningham, E. T.; Guyer, D. R.; Adamis, A. P., Pegaptanib, a targeted anti-VEGF aptamer for ocular vascular disease. *Nat Rev Drug Discov* **2006,** 5, (2), 123-132.

12. Bouchard, P. R.; Hutabarat, R. M.; Thompson, K. M., Discovery and development of therapeutic aptamers. *Annu. Rev. Pharmacol. Toxicol.* **2010,** 50, (1), 237-257.

13. Cheng, C.; Chen, Y. H.; Lennox, K. A.; Behlke, M. A.; Davidson, B. L., In vivo SELEX for Identification of Brain-penetrating Aptamers. *Mol Ther Nucleic Acids* **2013,** 2, (1), e67.

14. Šmuc, T.; Ahn, I.-Y.; Ulrich, H., Nucleic acid aptamers as high affinity ligands in biotechnology and biosensorics. *Journal of Pharmaceutical and Biomedical Analysis* **2013,** 81-82, 210-217.

15. Banerjee, J.; Nilsen-Hamilton, M., Aptamers: multifunctional molecules for biomedical research. *J. Mol. Med.* **2013,** 91, (12), 1333-1342.

16. Cekan, P.; Jonsson, E. O.; Sigurdsson, S. T., Folding of the cocaine aptamer studied by EPR and fluorescence spectroscopies using the bifunctional spectroscopic probe C. *Nucleic Acids Res.* **2009,** 37, (12), 3990-3995.

17. Neves, M. A. D.; Reinstein, O.; Johnson, P. E., Defining a Stem Length-Dependent Binding Mechanism for the Cocaine-Binding Aptamer. A Combined NMR and Calorimetry Study. *Biochemistry* **2010,** 49, (39), 8478-8487.

18. Hermann, T., Adaptive Recognition by Nucleic Acid Aptamers. *Science* **2000,** 287, (5454), 820-825.

19. Lee, S. W.; Zhao, L.; Pardi, A.; Xia, T., Ultrafast Dynamics Show That the Theophylline and 3-Methylxanthine Aptamers Employ a Conformational Capture Mechanism for Binding Their Ligands. *Biochemistry* **2010,** 49, (13), 2943-2951.

20. Yang, Y.; Yang, D.; Schluesener, H. J.; Zhang, Z., Advances in SELEX and application of aptamers in the central nervous system. *Biomolecular Engineering* **2007,** 24, (6), 583-592.

21. Bunka, D. H.; Platonova, O.; Stockley, P. G., Development of aptamer therapeutics. *Current Opinion in Pharmacology* **2010,** 10, (5), 557-562.

22. Robertson, D. L.; Joyce, G. F., Selection in vitro of an RNA enzyme that specifically cleaves single-stranded DNA. *Nature* **1990,** 344, (6265), 467-468.

23. Tuerk, C.; Gold, L., Systematic evolution of ligands by exponential enrichment: RNA ligands to bacteriophage T4 DNA polymerase. *Science* **1990,** 249, (4968), 505-510.

24. Ellington, A. D.; Szostak, J. W., In vitro selection of RNA molecules that bind specific ligands. *Nature* **1990,** 346, (6287), 818-822.

25. Mencin, N.; Šmuc, T.; Vraničar, M.; Mavri, J.; Hren, M.; Galeša, K.; Krkoč, P.; Ulrich, H.; Šolar, B., Optimization of SELEX: Comparison of different methods for

monitoring the progress of in vitro selection of aptamers. *Journal of Pharmaceutical and Biomedical Analysis* **2014,** 91, 151-159.

26. Hamula, C.; Guthrie, J.; Zhang, H.; Li, X.; Le, X., Selection and analytical applications of aptamers. *TrAC Trends in Analytical Chemistry* **2006,** 25, (7), 681-691.

27. Ulrich, H.; Trujillo, C. A.; Nery, A. A.; Alves, J. M.; Majumder, P.; Resende, R. R.; Martins, A. H., DNA and RNA aptamers: from tools for basic research towards therapeutic applications. *Comb. Chem. High Throughput Screen.* **2006,** 9, (8), 619-632.

28. Wilson, D. S.; Szostak, J. W., In vitro selection of functional nucleic acids. *Annu. Rev. Biochem.* **1999,** 68, 611-647.

29. Keefe, A. D.; Cload, S. T., SELEX with modified nucleotides. *Current Opinion in Chemical Biology* **2008,** 12, (4), 448-456.

30. Kuwahara, M.; Sugimoto, N., Molecular Evolution of Functional Nucleic Acids with Chemical Modifications. *Molecules* **2010,** 15, (8), 5423-5444.

31. Sefah, K.; Yang, Z.; Bradley, K. M.; Hoshika, S.; Jimenez, E.; Zhang, L.; Zhu, G.; Shanker, S.; Yu, F.; Turek, D.; Tan, W.; Benner, S. A., In vitro selection with artificial expanded genetic information systems. *Proceedings of the National Academy of Sciences* **2014,** 111, (4), 1449-1454.

32. Berezovski, M.; Musheev, M.; Drabovich, A.; Krylov, S. N., Non-SELEX Selection of Aptamers. *J. Am. Chem. Soc.* **2006,** 128, (5), 1410-1411.

33. Tok, J.; Lai, J.; Leung, T.; Li, S. F. Y., Selection of aptamers for signal transduction proteins by capillary electrophoresis. *Electrophoresis* **2010,** 31, (12), 2055-2062.

34. Ashley, J.; Ji, K.; Li, S. F. Y., Selection of bovine catalase aptamers using non-SELEX. *Electrophoresis* **2012,** 33, (17), 2783-2789.

35. Berti, L.; Burley, G. A., Nucleic acid and nucleotide-mediated synthesis of inorganic nanoparticles. *Nature Publishing Group* **2008,** 3, (2), 81-87.

36. Gmeiner, W. H.; Walberer, B. J., Base Pairing in DNA: Unusual Patterns. *Encyclopedia of Life Sciences* **2001**.

37. Jana, N.; Gearheart, L., Seed‐mediated growth approach for shape‐controlled synthesis of spheroidal and rod‐like gold nanoparticles using a surfactant template. *Adv. Mater.* **2001**.

38. Liu, X.; Atwater, M.; Wang, J.; Huo, Q., Extinction coefficient of gold nanoparticles with different sizes and different capping ligands. *Colloids and Surfaces B: Biointerfaces* **2007,** 58, (1), 3-7.

39. Murphy, C. J.; Thompson, L. B.; Alkilany, A. M.; Sisco, P. N.; Boulos, S. P.; Sivapalan, S. T.; Yang, J. A.; Chernak, D. J.; Huang, J., The Many Faces of Gold Nanorods. *J. Phys. Chem. Lett.* **2010,** 1, (19), 2867-2875.

40. Jain, P. K.; Lee, K. S.; El-Sayed, I. H.; El-Sayed, M. A., Calculated Absorption and Scattering Properties of Gold Nanoparticles of Different Size, Shape, and Composition: Applications in Biological Imaging and Biomedicine. *J. Phys. Chem. B* **2006,** 110, (14), 7238-7248.

41. Hurst, S. J.; Hill, H. D.; Macfarlane, R. J.; Wu, J.; Dravid, V. P.; Mirkin, C. A., Synthetically Programmable DNA Binding Domains in Aggregates of DNA-Functionalized Gold Nanoparticles. *Small* **2009,** 5, (19), 2156-2161.

42. Xia, F.; Zuo, X.; Yang, R.; Xiao, Y.; Kang, D.; Vallée-Bélisle, A.; Gong, X.; Yuen, J. D.; Hsu, B. B. Y.; Heeger, A. J., Colorimetric detection of DNA, small molecules, proteins, and ions using unmodified gold nanoparticles and conjugated polyelectrolytes. *Proc. Natl. Acad. Sci. U.S.A.* **2010,** 107, (24), 10837-10841.

43. Taton, T. A., Scanometric DNA Array Detection with Nanoparticle Probes. *Science* **2000,** 289, (5485), 1757-1760.

44. Jain, P. K.; Huang, X.; El-Sayed, I. H.; El-Sayed, M. A., Noble Metals on the Nanoscale: Optical and Photothermal Properties and Some Applications in Imaging, Sensing, Biology, and Medicine. *Acc. Chem. Res.* **2008,** 41, (12), 1578-1586.

45. Storhoff, J. J.; Elghanian, R.; Mucic, R. C.; Mirkin, C. A.; Letsinger, R. L., One-Pot Colorimetric Differentiation of Polynucleotides with Single Base Imperfections Using Gold Nanoparticle Probes. *J. Am. Chem. Soc.* **1998,** 120, (9), 1959-1964.

46. Sandström, P.; Boncheva, M.; Åkerman, B., Nonspecific and Thiol-Specific Binding of DNA to Gold Nanoparticles. *Langmuir* **2003,** 19, (18), 7537-7543.

47. Balasubramanian, S. K.; Yang, L.; Yung, L.-Y. L.; Ong, C.-N.; Ong, W.-Y.; Yu, L. E., Characterization, purification, and stability of gold nanoparticles. *Biomaterials* **2010,** 31, (34), 9023-9030.

48. Giljohann, D. A.; Seferos, D. S.; Daniel, W. L.; Massich, M. D.; Patel, P. C.; Mirkin, C. A., Gold Nanoparticles for Biology and Medicine. *Angew. Chem. Int. Ed.* **2010,** 49, (19), 3280-3294.

49. Pylaev, T. E.; Khanadeev, V. A.; Khlebtsov, B. N.; Dykman, L. A.; Bogatyrev, V. A.; Khlebtsov, N. G., Colorimetric and dynamic light scattering detection of DNA sequences by using positively charged gold nanospheres: a comparative study with gold nanorods. *Nanotechnology* **2011,** 22, (28), 285501.

50. Elghanian, R.; Storhoff, J.; Mucic, R.; Letsinger, R., Selective colorimetric detection of polynucleotides based on the distance-dependent optical properties of gold nanoparticles. *Science* **1997**.

51. Li, H.; Rothberg, L., Colorimetric detection of DNA sequences based on electrostatic interactions with unmodified gold nanoparticles. *Proc. Natl. Acad. Sci. U.S.A.* **2004,** 101, (39), 14036-14039.

52. Li, H.; Nelson, E.; Pentland, A.; Buskirk, J.; Rothberg, L., Assays Based on Differential Adsorption of Single-stranded and Double-stranded DNA on Unfunctionalized Gold Nanoparticles in a Colloidal Suspension. *Plasmonics* **2007,** 2, (4), 165-171.

53. Huang, Y.-F.; Lin, Y.-W.; Lin, Z.-H.; Chang, H.-T., Aptamer-modified gold nanoparticles for targeting breast cancer cells through light scattering. *J Nanopart Res* **2008,** 11, (4), 775-783.

54. Lalander, C. H.; Zheng, Y.; Dhuey, S.; Cabrini, S.; Bach, U., DNA-Directed Self-Assembly of Gold Nanoparticles onto Nanopatterned Surfaces: Controlled Placement of Individual Nanoparticles into Regular Arrays. *ACS Nano* **2010,** 4, (10), 6153-6161.

55. Jones, M. R.; Macfarlane, R. J.; Lee, B.; Zhang, J.; Young, K. L.; Senesi, A. J.; Mirkin, C. A., DNA-nanoparticle superlattices formed from anisotropic building blocks. *Nature Materials* **2010,** 9, (11), 913-917.

56. Mirkin, C. A., The Polyvalent Gold Nanoparticle Conjugate—Materials Synthesis, Biodiagnostics, and Intracellular Gene Regulation. *MRS bulletin* **2010,** 35, (07), 532-539.

57. Gearheart, L. A.; Ploehn, H. J.; Murphy, C. J., Oligonucleotide Adsorption to Gold Nanoparticles: A Surface-Enhanced Raman Spectroscopy Study of Intrinsically Bent DNA. *J. Phys. Chem. B* **2001,** 105, (50), 12609-12615.

58. Demers, L. M.; Östblom, M.; Zhang, H.; Jang, N.-H.; Liedberg, B.; Mirkin, C. A., Thermal Desorption Behavior and Binding Properties of DNA Bases and Nucleosides on Gold. *J. Am. Chem. Soc.* **2002,** 124, (38), 11248-11249.

59. Kimura-Suda, H.; Petrovykh, D. Y.; Tarlov, M. J.; Whitman, L. J., Base-Dependent Competitive Adsorption of Single-Stranded DNA on Gold. *J. Am. Chem. Soc.* **2003,** 125, (30), 9014-9015.

60. Nelson, E. M., The Adsorption of DNA onto Unmodified Gold Nanoparticles. **2009**, 1-128.

61. Long, N. N.; Vu, L. V.; Kiem, C. D.; Doanh, S. C.; Nguyet, C. T.; Hang, P. T.; Thien, N. D.; Quynh, L. M., Synthesis and optical properties of colloidal gold nanoparticles. *J. Phys.: Conf. Ser.* **2009,** 187, 012026.

62. Polte, J.; Ahner, T. T.; Delissen, F.; Sokolov, S.; Emmerling, F.; Thünemann, A. F.; Kraehnert, R., Mechanism of Gold Nanoparticle Formation in the Classical Citrate Synthesis Method Derived from Coupled In Situ XANES and SAXS Evaluation. *J. Am. Chem. Soc.* **2010,** 132, (4), 1296-1301.

63. Cai, M.; Li, F.; Zhang, Y.; Wang, Q., One-pot polymerase chain reaction with gold nanoparticles for rapid and ultrasensitive DNA detection. *Nano Research* **2010,** 3, (8), 557-563.

64. Turkevich, J.; Stevenson, P. C.; Hillier, J., A study of the nucleation and growth processes in the synthesis of colloidal gold. *Discuss. Faraday Soc.* **1951,** 11, 55.

65. Frens, G., Particle size and sol stability in metal colloids. *Kolloid-Zeitschrift und Zeitschrift für Polymere* **1972**.

66. Nikoobakht, B.; El-Sayed, M. A., Preparation and Growth Mechanism of Gold Nanorods (NRs) Using Seed-Mediated Growth Method. *Chemistry of Materials* **2003,** 15, (10), 1957-1962.

67. Grzelczak, M.; Pérez-Juste, J.; Mulvaney, P.; Liz-Marzán, L. M., Shape control in gold nanoparticle synthesis. *Chem. Soc. Rev.* **2008,** 37, (9), 1783.

68. Alkilany, A. M.; Nagaria, P. K.; Wyatt, M. D.; Murphy, C. J., Cation Exchange on the Surface of Gold Nanorods with a Polymerizable Surfactant: Polymerization, Stability, and Toxicity Evaluation. *Langmuir* **2010,** 26, (12), 9328-9333.

69. Sutton, A.; Franc, G.; Kakkar, A., Silver metal nanoparticles: Facile dendrimer‐assisted size‐controlled synthesis and selective catalytic reduction of chloronitrobenzenes. *Journal of Polymer Science Part A …* **2009**.

70. Carter, C. J.; Ackerson, C. J.; Feldheim, D. L., Unusual reactivity of a silver mineralizing peptide. *ACS Nano* **2010,** 4, (7), 3883-3888.

71. Carter, C. J.; Dolska, M.; Owczarek, A.; Ackerson, C. J.; Eaton, B. E.; Feldheim, D. L., In vitro selection of RNA sequences capable of mediating the formation of iron oxide nanoparticles. *J. Mater. Chem.* **2009,** 19, (44), 8320.

72. Feldheim, D. L.; Eaton, B. E., Selection of Biomolecules Capable of Mediating the Formation of Nanocrystals. *ACS Nano* **2007,** 1, (3), 154-159.

73. Dickerson, M. B.; Sandhage, K. H.; Naik, R. R., Protein- and Peptide-Directed Syntheses of Inorganic Materials. *Chem. Rev.* **2008,** 108, (11), 4935-4978.

74. Ahmad, G.; Dickerson, M. B.; Church, B. C.; Cai, Y.; Jones, S. E.; Naik, R. R.; King, J. S.; Summers, C. J.; Kröger, N.; Sandhage, K. H., Rapid, Room-Temperature Formation of Crystalline Calcium Molybdate Phosphor Microparticles via Peptide-Induced Precipitation. *Adv. Mater.* **2006,** 18, (13), 1759-1763.

75. Dickerson, M. B.; Naik, R. R.; Stone, M. O.; Cai, Y.; Sandhage, K. H., Identification of peptides that promote the rapid precipitation of germania nanoparticle networks via use of a peptide display library. *Chem. Commun.* **2004**, (15), 1776.

76. Rouge, J. L.; Ackerson, C. J.; Feldheim, D. L.; Eaton, B. E., Cooperativity between two selected RNA Pdases in the synthesis of Pd nanoparticles. *J. Mater. Chem.* **2010,** 20, (38), 8394.

77. Ma, N.; Dooley, C. J.; Kelley, S. O., RNA-Templated Semiconductor Nanocrystals. *J. Am. Chem. Soc.* **2006,** 128, (39), 12598-12599.

78. Sewell, S. L.; Wright, D. W., Biomimetic Synthesis of Titanium Dioxide Utilizing the R5 Peptide Derived from Cylindrothecafusiformis. *Chemistry of Materials* **2006,** 18, (13), 3108-3113.

79. Fang, Y.; Poulsen, N.; Dickerson, M. B.; Cai, Y.; Jones, S. E.; Naik, R. R.; Kröger, N.; Sandhage, K. H., Identification of peptides capable of inducing the formation of titania but not silica via a subtractive bacteriophage display approach. *J. Mater. Chem.* **2008,** 18, (32), 3871.

80. Naik, R. R.; Jones, S. E.; Murray, C. J.; McAuliffe, J. C.; Vaia, R. A.; Stone, M. O., Peptide Templates for Nanoparticle Synthesis Derived from Polymerase Chain Reaction-Driven Phage Display. *Adv. Funct. Mater.* **2004,** 14, (1), 25-30.

81. Spoerke, E. D.; Voigt, J. A., Influence of Engineered Peptides Cadmium Sulfide Nanocrystals. *Adv. Funct. Mater.* **2007,** 17, (13), 2031-2037.

82. Gugliotti, L. A., RNA-Mediated Metal-Metal Bond Formation in the Synthesis of Hexagonal Palladium Nanoparticles. *Science* **2004,** 304, (5672), 850-852.

83. Bawazer, L. A.; Newman, A. M.; Gu, Q.; Ibish, A.; Arcila, M.; Cooper, J. B.; Meldrum, F. C.; Morse, D. E., Efficient Selection of Biomineralizing DNA Aptamers Using Deep Sequencing and Population Clustering. *ACS Nano* **2014,** 8, (1), 387-395.

84. Zinchenko, A. A.; Yoshikawa, K.; Baigl, D., DNA-Templated Silver Nanorings. *Adv. Mater.* **2005,** 17, (23), 2820-2823.

85. Sun, L.; Song, Y.; Wang, L.; Sun, Y.; Guo, C.; Liu, Z.; Li, Z., DNA-templated gold nanoparticles formation. *J Nanosci Nanotechnol* **2008,** 8, (9), 4415-4423.

86. Zhou, Z.; Du, Y.; Dong, S., Double-Strand DNA-Templated Formation of Copper Nanoparticles as Fluorescent Probe for Label-Free Aptamer Sensor. *Anal. Chem.* **2011,** 83, (13), 5122-5127.

87. Gugliotti, L. A.; Feldheim, D. L.; Eaton, B. E., RNA-Mediated Control of Metal Nanoparticle Shape. *J. Am. Chem. Soc.* **2005,** 127, (50), 17814-17818.

88. Liu, D.; Gugliotti, L. A.; Wu, T.; Dolska, M.; Tkachenko, A. G.; Shipton, M. K.; Eaton, B. E.; Feldheim, D. L., RNA-Mediated Synthesis of Palladium Nanoparticles on Au Surfaces. *Langmuir* **2006,** 22, (13), 5862-5866.

89. Dooley, C. J.; Rouge, J.; Ma, N.; Invernale, M.; Kelley, S. O., Nucleotide-stabilized cadmium sulfide nanoparticles. *J. Mater. Chem.* **2007,** 17, (17), 1687.

90. Kumar, A.; Jakhmola, A., RNA-Mediated Fluorescent Q-PbS Nanoparticles. *Langmuir* **2007,** 23, (6), 2915-2918.

91. Wang, Z.; Zhang, J.; Ekman, J. M.; Kenis, P. J. A.; Lu, Y., DNA-Mediated Control of Metal Nanoparticle Shape: One-Pot Synthesis and Cellular Uptake of Highly Stable and Functional Gold Nanoflowers. *Nano Lett.* **2010,** 10, (5), 1886-1891.

92. Wang, Z.; Tang, L.; Tan, L. H.; Li, J.; Lu, Y., Discovery of the DNA genetic code for abiological gold nanoparticle morphologies. *Angew. Chem. Int. Ed. Engl.* **2012,** 51, (36), 9078-9082.

93. Hinds, S.; Taft, B. J.; Levina, L.; Sukhovatkin, V.; Dooley, C. J.; Roy, M. D.; MacNeil, D. D.; Sargent, E. H.; Kelley, S. O., Nucleotide-directed growth of semiconductor nanocrystals. *J. Am. Chem. Soc.* **2006,** 128, (1), 64-65.

94. Cushing, B. L.; Kolesnichenko, V. L.; O'Connor, C. J., Recent advances in the liquid-phase syntheses of inorganic nanoparticles. *Chem. Rev.* **2004,** 104, (9), 3893-3946.

95. Amendola, V.; Meneghetti, M., Size Evaluation of Gold Nanoparticles by UV−vis Spectroscopy. *J. Phys. Chem. C* **2009,** 113, (11), 4277-4285.

96. Gallagher, S. R., Quantitation of DNA and RNA with absorption and fluorescence spectroscopy. In *Current Protocols in Molecular Biology*, Ausubel, F. A.; Brent, R.; Kingston, R. E.; Moore, D. D.; Seidman, J. G.; Smith, J. A.; Struhl, K., Eds. John Wiley & Sons: New York, 1989; pp A.3.9-A.3.15.

97. Takeda, Y.; Kondow, T.; Mafune, F., Hybridization of ssDNA with a Complementary DNA Probe Tethered to a Gold Nanoparticle-Effect of Steric Hindrance Caused by Conformation. *J. Phys. Chem. C* **2008,** 112, (1), 89-94.

98. Murphy, M. C.; Rasnik, I.; Cheng, W.; Lohman, T. M.; Ha, T., Probing Single-Stranded DNA Conformational Flexibility Using Fluorescence Spectroscopy. *Biophysical Journal* **2004,** 86, (4), 2530-2537.

99. Bailey, T. L.; Boden, M.; Buske, F. A.; Frith, M.; Grant, C. E.; Clementi, L.; Ren, J.; Li, W. W.; Noble, W. S., MEME SUITE: tools for motif discovery and searching. *Nucleic Acids Res.* **2009,** 37, (Web Server), W202-W208.

100. Zuker, M., Mfold web server for nucleic acid folding and hybridization prediction. *Nucleic Acids Res.* **2003,** 31, (13), 3406-3415.

101. Musheev, M.; Krylov, S., Selection of aptamers by systematic evolution of ligands by exponential enrichment: Addressing the polymerase chain reaction issue. *Analytica Chimica Acta* **2006,** 564, (1), 91-96.

102. Citartan, M.; Tang, T.-H.; Tan, S.-C.; Gopinath, S. C. B., Conditions optimized for the preparation of single-stranded DNA (ssDNA) employing lambda exonuclease digestion in generating DNA aptamer. *World J Microbiol Biotechnol* **2010,** 27, (5), 1167-1173.

103. Marimuthu, C.; Tang, T.-H.; Tominaga, J.; Tan, S.-C.; Gopinath, S. C. B., Single-stranded DNA (ssDNA) production in DNA aptamer generation. *Analyst* **2012,** 137, (6), 1307.

104. Lehman, I. R.; Nussbaum, A. L., The deoxyribonucleases of Escherichia coli. *J. biol. Chem* **1964,** 239, 2628-2636.

105. Cho, M.; Xiao, Y.; Nie, J.; Stewart, R.; Csordas, A. T.; Oh, S. S.; Thomson, J. A.; Soh, H. T., Quantitative selection of DNA aptamers through microfluidic selection and high-throughput sequencing. *Proceedings of the National Academy of Sciences* **2010,** 107, (35), 15373-15378.

106. Lohse, S. E.; Murphy, C. J., The Quest for Shape Control: A History of Gold Nanorod Synthesis. *Chemistry of Materials* **2013,** 25, (8), 1250-1261.

107. Pu, Y.; Zhu, Z.; Liu, H.; Zhang, J.; Liu, J.; Tan, W., Using aptamers to visualize and capture cancer cells. *Anal Bioanal Chem* **2010,** 397, (8), 3225-3233.

108. Mirkin, C. A.; Letsinger, R. L.; Mucic, R. C.; Storhoff, J. J., A DNA-based method for rationally assembling nanoparticles into macroscopic materials. *Nature* **1996,** 382, 607-609.

109. Gupta, M. K.; König, T.; Near, R.; Nepal, D.; Drummy, L. F.; Biswas, S.; Naik, S.; Vaia, R. A.; El-Sayed, M. A.; Tsukruk, V. V., Surface Assembly and Plasmonic Properties in Strongly Coupled Segmented Gold Nanorods. *Small* **2013,** 9, (17), 2979-2990.

110. Huang, X.; El-Sayed, I. H.; Qian, W.; El-Sayed, M. A., Cancer Cell Imaging and Photothermal Therapy in the Near-Infrared Region by Using Gold Nanorods. *J. Am. Chem. Soc.* **2006,** 128, (6), 2115-2120.

111. Bedford, E. E.; Spadavecchia, J.; Pradier, C.-M.; Gu, F. X., Surface Plasmon Resonance Biosensors Incorporating Gold Nanoparticles. *Macromol. Biosci.* **2012,** 12, (6), 724-739.

112. Huang, X.; Neretina, S.; El-Sayed, M. A., Gold Nanorods: From Synthesis and Properties to Biological and Biomedical Applications. *Adv. Mater.* **2009,** 21, (48), 4880-4910.

113. Hubert, F.; Testard, F.; Rizza, G.; Spalla, O., Nanorods versus Nanospheres: A Bifurcation Mechanism Revealed by Principal Component TEM Analysis. *Langmuir* **2010,** 26, (10), 6887-6891.

114. Gole, A.; Murphy, C. J., Seed-Mediated Synthesis of Gold Nanorods: Role of the Size and Nature of the Seed. *Chemistry of Materials* **2004,** 16, (19), 3633-3640.

115. Jiang, X. C.; Pileni, M. P., Gold nanorods: Influence of various parameters as seeds, solvent, surfactant on shape control. *Colloids and Surfaces A: Physicochemical and Engineering Aspects* **2007,** 295, (1-3), 228-232.

116. Ofir, Y.; Samanta, B.; Rotello, V. M., Polymer and biopolymer mediated self-assembly of gold nanoparticles. *Chem. Soc. Rev.* **2008,** 37, (9), 1814.

117. Ghosh, S. K.; Pal, T., Interparticle Coupling Effect on the Surface Plasmon Resonance of Gold Nanoparticles: From Theory to Applications. *Chem. Rev.* **2007,** 107, (11), 4797-4862.

118. Rosi, N. L.; Mirkin, C. A., Nanostructures in Biodiagnostics. *Chem. Rev.* **2005,** 105, (4), 1547-1562.

119. Geerts, N.; Eiser, E., DNA-functionalized colloids: Physical properties and applications. *Soft Matter* **2010,** 6, (19), 4647.

120. Shin, J.; Zhang, X.; Liu, J., DNA-Functionalized Gold Nanoparticles in Macromolecularly Crowded Polymer Solutions. *J. Phys. Chem. B* **2012,** 116, (45), 13396-13402.

121. Smith, B. D.; Dave, N.; Huang, P.-J. J.; Liu, J., Assembly of DNA-Functionalized Gold Nanoparticles with Gaps and Overhangs in Linker DNA. *J. Phys. Chem. C* **2011,** 115, (16), 7851-7857.

122. Kim, J.; Rheem, Y.; Yoo, B.; Chong, Y.; Bozhilov, K. N.; Kim, D.; Sadowsky, M. J.; Hur, H.-G.; Myung, N. V., Peptide-mediated shape- and size-tunable synthesis of gold nanostructures. *Acta Biomaterialia* **2010,** 6, (7), 2681-2689.

123. Brown, K. R.; Lyon, L. A.; Fox, A. P.; Reiss, B. D.; Natan, M. J., Hydroxylamine Seeding of Colloidal Au Nanoparticles. 3. Controlled Formation of Conductive Au Films. *Chemistry of Materials* **2000,** 12, (2), 314-323.

124. Kumar, S. A.; Peter, Y.-A.; Nadeau, J. L., Facile biosynthesis, separation and conjugation of gold nanoparticles to doxorubicin. *Nanotechnology* **2008,** 19, (49), 495101.

125. Gardea-Torresdey, J. L.; Parsons, J. G.; Gomez, E.; Peralta-Videa, J.; Troiani, H. E.; Santiago, P.; Yacaman, M. J., Formation and Growth of Au Nanoparticles inside Live Alfalfa Plants. *Nano Lett.* **2002,** 2, (4), 397-401.

126. Radloff, C.; Vaia, R. A.; Brunton, J.; Bouwer, G. T.; Ward, V. K., Metal Nanoshell Assembly on a Virus Bioscaffold. *Nano Lett.* **2005,** 5, (6), 1187-1191.

127. Bigham, S. R.; Coffer, J. L., The influence of adenine content on the properties of Q-CdS clusters stabilized by polynucleotides. *Colloids and Surfaces A: Physicochemical and Engineering Aspects* **1995,** 95, (2), 211-219.

128. Lin, Y.; Yin, M.; Pu, F.; Ren, J.; Qu, X., DNA-Templated Silver Nanoparticles as a Platform for Highly Sensitive and Selective Fluorescence Turn-On Detection of Dopamine. *Small* **2011,** 7, (11), 1557-1561.

129. Wolf, L. K.; Gao, Y.; Georgiadis, R. M., Sequence-dependent DNA immobilization: specific versus nonspecific contributions. *Langmuir* **2004,** 20, (8), 3357-3361.

130. Liu, J., Adsorption of DNA onto gold nanoparticles and graphene oxide: surface science and applications. *Phys. Chem. Chem. Phys.* **2012,** 14, (30), 10485.

131. Storhoff, J. J.; Elghanian, R.; Mirkin, C. A.; Letsinger, R. L., Sequence-Dependent Stability of DNA-Modified Gold Nanoparticles. *Langmuir* **2002,** 18, (17), 6666-6670.

132. Murphy, C. J.; Thompson, L. B.; Chernak, D. J.; Yang, J. A.; Sivapalan, S. T.; Boulos, S. P.; Huang, J.; Alkilany, A. M.; Sisco, P. N., Gold nanorod crystal growth: From seed-mediated synthesis to nanoscale sculpting. *Current Opinion in Colloid & Interface Science* **2011,** 16, (2), 128-134.

133. Hardin, J. O.; Milam, V. T., Measuring in Situ Primary and Competitive DNA Hybridization Activity on Microspheres. *Biomacromolecules* **2013,** 14, (4), 986-992.

134. Nikoobakht, B.; El-Sayed, M. A., Evidence for Bilayer Assembly of Cationic Surfactants on the Surface of Gold Nanorods. *Langmuir* **2001,** 17, (20), 6368-6374.

135. Nykypanchuk, D.; Maye, M. M.; van der Lelie, D.; Gang, O., DNA-guided crystallization of colloidal nanoparticles. *Nature* **2008,** 451, (7178), 549-552.

136. Stoltenburg, R.; Reinemann, C.; Strehlitz, B., SELEX—A (r)evolutionary method to generate high-affinity nucleic acid ligands. *Biomolecular Engineering* **2007,** 24, (4), 381-403.

137. Kupakuwana, G. V.; Crill, J. E.; McPike, M. P.; Borer, P. N., Acyclic Identification of Aptamers for Human alpha-Thrombin Using Over-Represented Libraries and Deep Sequencing. *PLoS ONE* **2011,** 6, (5), e19395.

138. Yang, J.; Bowser, M. T., Capillary Electrophoresis–SELEX Selection of Catalytic DNA Aptamers for a Small-Molecule Porphyrin Target. *Anal. Chem.* **2013,** 85, (3), 1525-1530.

139. Ruff, P.; Pai, R. B.; Storici, F., Real-Time PCR-Coupled CE-SELEX for DNA Aptamer Selection. *ISRN Molecular Biology* **2012,** 2012, (4968), 1-9.

140. Oh, S. S.; Ahmad, K. M.; Cho, M.; Kim, S.; Xiao, Y.; Soh, H. T., Improving Aptamer Selection Efficiency through Volume Dilution, Magnetic Concentration, and Continuous Washing in Microfluidic Channels. *Anal. Chem.* **2011,** 83, (17), 6883-6889.

141. Forster, U.; Weigand, J. E.; Trojanowski, P.; Suess, B.; Wachtveitl, J., Conformational dynamics of the tetracycline-binding aptamer. *Nucleic Acids Res.* **2012,** 40, (4), 1807-1817.

142. Stojanovic, M. N.; de Prada, P.; Landry, D. W., Fluorescent Sensors Based on Aptamer Self-Assembly. *J. Am. Chem. Soc.* **2000,** 122, (46), 11547-11548.

143. Bock, L. C.; Griffin, L. C.; Latham, J. A.; Vermaas, E. H.; Toole, J. J., Selection of single-stranded DNA molecules that bind and inhibit human thrombin. *Nature* **1992,** 355, (6360), 564-566.

144. Potty, A. S. R.; Kourentzi, K.; Fang, H.; Jackson, G. W.; Zhang, X.; Legge, G. B.; Willson, R. C., Biophysical characterization of DNA aptamer interactions with vascular endothelial growth factor. *Biopolymers* **2009,** 91, (2), 145-156.

145. Waybrant, B.; Pearce, T. R.; Wang, P.; Sreevatsan, S.; Kokkoli, E., Development and characterization of an aptamer binding ligand of fractalkine using domain targeted SELEX. *Chem. Commun.* **2012,** 48, (80), 10043.

146. Li, W.-M.; Bing, T.; Wei, J.-Y.; Chen, Z.-Z.; Shangguan, D.-H.; Fang, J., Cell-SELEX-based selection of aptamers that recognize distinct targets on metastatic colorectal cancer cells. *Biomaterials* **2014,** 35, (25), 6998-7007.

147. Howes, P. D.; Chandrawati, R.; Stevens, M. M., Colloidal nanoparticles as advanced biological sensors. *Science* **2014,** 346, (6205), 1247390-1247390.

148. Murphy, C. J.; Gole, A. M.; Stone, J. W.; Sisco, P. N.; Alkilany, A. M.; Goldsmith, E. C.; Baxter, S. C., Gold Nanoparticles in Biology: Beyond Toxicity to Cellular Imaging. *Acc. Chem. Res.* **2008,** 41, (12), 1721-1730.

149. Wolf, L. K.; Gao, Y.; Georgiadis, R. M., SI: Sequence-dependent DNA immobilization: specific versus nonspecific contributions. *Langmuir* **2004,** 20, (8), 3357-3361.

150. Bailey, T. L.; Elkan, C., Fitting a mixture model by expectation maximization to discover motifs in biopolymers. *Proc Int Conf Intell Syst Mol Biol* **1994,** 2, 28-36.

151. Bailey, T. L.; Williams, N.; Misleh, C.; Li, W. W., MEME: discovering and analyzing DNA and protein sequence motifs. *Nucleic Acids Res.* **2006,** 34, (Web Server), W369-W373.

152. Eissa, S.; Ng, A.; Siaj, M.; Tavares, A. C.; Zourob, M., Selection and Identification of DNA Aptamers against Okadaic Acid for Biosensing Application. *Anal. Chem.* **2013,** 85, (24), 11794-11801.

153. Lin, P.-H.; Chen, R.-H.; Lee, C.-H.; Chang, Y.; Chen, C.-S.; Chen, W.-Y., Studies of the binding mechanism between aptamers and thrombin by circular dichroism, surface plasmon resonance and isothermal titration calorimetry. *Colloids and Surfaces B: Biointerfaces* **2011,** 88, (2), 552-558.

154. Hoinka, J.; Zotenko, E.; Friedman, A.; Sauna, Z. E.; Przytycka, T. M., Identification of sequence-structure RNA binding motifs for SELEX-derived aptamers. *Bioinformatics* **2012,** 28, (12), i215-i223.